Design and Analysis of a Constant Beamwidth Beamformer

Oren Rosen

Design and Analysis of a Constant Beamwidth Beamformer

Research Thesis

As Partial Fulfilment of the Requirements for
the Degree of Master of Science in Electrical Engineering

Oren Rosen

Submitted to the Senate of the Technion—Israel Institute of Technology

5776 Haifa February 2016

Acknowledgement

The Research Thesis Was Done Under The Supervision of Professor Israel Cohen in the Department of Electrical Engineering.

I would like to express my gratitude to my advisor, Professor Israel Cohen for his guidance and support throughout all research stages.

I would like to thank Professor David Malah for his substantial aid in the writing of this thesis.

Finally, I would like to thank my father Avi and wife Natalie for their support and patience during all stages of my research.

The Generous Financial Help Of The Technion Is Gratefully Acknowledged.

This work is dedicated to the memory of my late mother, Ilana.

Contents

List of Figures

List of Tables

List of Publications

1. O. Rosen, I. Cohen and D. Malah, "FIR-Based Symmetrical Acoustic Beamformer With a Constant Beamwidth". Submitted to Signal Processing.

2. O. Rosen, S. Mousazadeh and I. Cohen, "Voice Activity Detection In Presence Of Transients Using Spectral Clustering and Diffusion Kernels", in Proc. 28th IEEE Convention of the Electrical and Electronics Engineering in Israel 2014, Eilat, Israel.

Abstract

Beamforming algorithms are widely used in many real world applications such as radar, sonars, medical diagnosis, teleconferencing and seismic sensing. They are utilized to solve several problems in the areas of signal processing and communications. To name a few, for example, they can provide significant spatial filtering by suppressing both interference signals and noise signals while perfectly recovering the desired signals. Beamformers can be also used for direction of arrival and localization applications, dereverberation, and more.

In the literature, several approaches were proposed for the design of a constant beamwidth beamformer. Some of these approaches suffer from performance degradation in some aspects like poor sidelobe attenuation, reduced interference signal attenuation and sensitivity to model mismatch. Other approaches suffer from high computational complexity which make them infeasible in some applications involving large arrays or strict hardware limitations. Although some design methods provide fairly robust beamformer performance, the challenge of designing a constant beamwidth beamformer with noise robustness and reduced sensitivity to parameters mismatch is still a challenging task.

In this thesis, we introduce a new approach for designing a constant beamwidth beamformer. The proposed approach utilizes custom-tailored finite impulse response filters for each microphone channel, manipulating the beampattern beamwidth. The manipulated beampattern has approximately a constant beamwidth over a wide frequency band. By exploiting the physical microphone array configuration and attributes, we shape accordingly the frequency response of the finite impulse response filters and control the beamformer beamwidth. The proposed approach demonstrates low computational complexity as well as improved array response results in various scenarios, compared to other methods in the field. This approach could be used for beam steering in teleconferencing or speaker track-

ing devices. Beamformer steering is directing the beamformer's main beam to a desired direction by adding appropriate delays or phase shifts. This ability is required especially in applications where not only the location of the source is needed but also the ability to know when the source was active, as in teleconferencing and automatic video tracking.

As a part of this thesis, we also develop a voice activity detection algorithm based on spectral clustering and diffusion kernels. The proposed method is based on obtaining a low dimensional representation from feature vectors, which are viewed as a cloud of points. Then, we incorporate this representation in a Gaussian Mixture Model in order to build a statistical model for labeling data as speech or non-speech. Simulation results demonstrate improved performance of the proposed algorithm compared to a recent VAD algorithm in presence of environmental noise. This approach could be useful for teleconferencing and speaker tracking devices as well to further improve the speaker localization. For example, a teleconferencing device may achieve improved energy efficiency by only processing sequences where speech is present.

Notation

Notations for Chapter 3

c	velocity of sound propagation in air
d	inter-microphone spacing
$D(\omega, \theta)$	beampattern
$\mathbf{f}(t, \mathbf{x})$	set of signals sampled by the microphone
f_0	minimal frequency to achieve a desired beamwidth
f_h	higher boundary of a selected frequency range
f_l	lower boundary of a selected frequency range
f_max	maximal frequency to achieve a desired beamwidth
f_p	minimal frequency to achieve a desired beamwidth for M_p effective microphones
$f_\omega(t, x)$	propogating plane wave
k	bin index of the DFT
L	number of frequency bins in the lower band
m	microphone index
M	number of microphones in an array
M_min	minimal number of participating microphones in an array
M_p	number of effective participating microphones in an array
N	number of FIR filter coefficients
$P(\omega, \theta)$	beamformer response
T_s	delay between adjacent filter elements
$\mathbf{v}_s(\omega, \theta)$	stacked array manifold vector
$\mathbf{v}(\kappa)$	array manifold vector
$\mathbf{w}$	complex weighting vector
$\mathbf{W}$	filter array matrix
$\mathbf{W}_H$	magnitude response of $\mathbf{W}$ of the filters in the upper band
$\tilde{w}_k$	samples of the normalization filter frequency response
$\mathbf{W}_L$	magnitude response of $\mathbf{W}$ of the filters in the lower band
w_m	complex weighting of a microphone
$w^*_{m,n}$	a complex coefficient of the FIR filter

$W_m\left(\exp\left(j\omega T_s\right)\right)$	DTFT of $w_{m,n}$
$\mathbf{w}_s$	composite stacked weight vector
x_m	microphone positioning
$y(t)$	beamformer output
θ	direction of arrival
θ_{BW}	desired beamwidth
κ	wavenumber for plane waves in a locally homogeneous medium
λ	wavelength
τ_m	propogation delay of an incoming signal
ω	temporal frequency

Notations for Chapter 4

$\boldsymbol{C}_{\mathrm{t}}^{\ell}$	indicator matrix for a speech containing frame
$\boldsymbol{D}$	diagonal matrix whose i-th diagonal element equals to $\sum_{j=1}^{N} \boldsymbol{W}(i,j)$
$\mathbb{E}$	expected value of a matrix
$f(\cdot;\mathcal{H}_0)$	probability density function corresponding to speech absence frames
$f(\cdot;\mathcal{H}_1)$	probability density function corresponding to speech presence frames
$\mathcal{H}_0$	speech absence hypotheses
$\mathcal{H}_1$	speech presence hypotheses
i	desired number of samples per frame
j	frame index
k	current iteration index
K_m	MFCC coefficients frequency bins
K_s	STFT coefficients frequency bins
m	number of MFCCs
M	size of moving window
N	number of signal frames
$\boldsymbol{S}$	diagonal matrix made by $\boldsymbol{\Sigma}\boldsymbol{\Sigma}^T$ and $\boldsymbol{\Sigma}^T\boldsymbol{\Sigma}$
t	time frame
T_h	threshold of tradeoff between probability of detection and false alarm
$\boldsymbol{U}_\ell$	a matrix made of $\boldsymbol{D}^{\ell-1/2}\boldsymbol{W}^{\boldsymbol{\ell}}\boldsymbol{D}^{\ell-1/2}$
$\tilde{\boldsymbol{U}}(t,:)$	new representation of the unlabeled data
$\boldsymbol{V}$	orthogonal matrix, its columns are the eigenvectors of $\boldsymbol{\Sigma}^T\boldsymbol{\Sigma}$
VA_t	decision rule for an unlabeled time frame
w_M	moving window of size M
$\boldsymbol{W}_{\boldsymbol{\theta}^{opt}}^{\ell}$	similarity matrix of the ℓ-th training sequence
$x_{\mathrm{sp}}(n)$	speech signal
$x_{\mathrm{st}}(n)$	additive interfering stationary noise signals
$x_{\mathrm{tr}}(n)$	additive interfering transient noise signals
$\boldsymbol{X}_m^j$	size $m \times i$ matrix of MFCCs of the j-th frame
$y(n)$	VAD microphone input signal

$\hat{y}_j(n-k)$	generated sample cloud of the j-th frame (out of N)
$\boldsymbol{Y}_m(t,k)$	absolute value of the MFCC in a given time frame
$\boldsymbol{Y}_s(t,k)$	absolute value of the STFT coefficients in a given time frame
$\gamma_k(t)$	a-posteriori SNR
$\Gamma_{\mathrm{t}}^{\mathrm{train}}$	likelihood ratio for a labeled frame t
$\boldsymbol{\Delta}$	orthogonal matrix of size $3 \times N$
ϵ	kernel width obtained during the training stage
$\boldsymbol{\theta}$	a vector of system parameters
Λ_{t}	arithmetic mean of the log-likelihood ratios for frame t
$\lambda_s(t,k)$	variance of speech signal in the k-th frequency bin of the t-th frame
$\lambda_N(t,k)$	variance of stationary noise in t-th time frame and k-th frequency bin
$\Lambda_{\mathrm{i}}^{\ell}$	arithmetic mean of the log-likelihood ratio
$\boldsymbol{\Sigma}_{\mathrm{i}}^{\ell}$	covariance matrix of the i-th frame in the ℓ-th sequence
$\boldsymbol{\Sigma}$	covariance matrix for the j-th frame
$\boldsymbol{\Upsilon}$	approximate orthonormal basis of $\boldsymbol{D}^{-1/2}\boldsymbol{W}\boldsymbol{D}^{-1/2}$
$\xi_k(t)$	a-priori SNR

Abbreviations

DOA	Direction of arrival
DFT	Discrete Fourier transform
DTFT	Discrete-time Fourier transform
FIR	Finite impulse response
GMM	Gaussian mixture model
GSM	Global system for mobile communication
LCMV	Linearly constrained minimum variance
LRT	Likelihood Ratio Test
LS	Least squares
MAE	Mean absolute error
MCRA	Minima Controlled Recursive Averaging
MFCC	Mel-frequency cepstrum coefficient
MMSE	Minimum mean square error
MVDR	Minimum variance distortion-less response
SNR	Signal-to-noise ration
SV	Spatial variation
SVD	Singular vector decomposition
TASI	Time assignment speech interpolation
ULA	Uniform linear array
VAD	Voice activity detection

Chapter 1

Introduction

1.1 Motivation and Overview

Speech enhancement is used in many applications in communication and signals processing such as mobile devices, hearing aids, speech recognition and conferencing equipment [1–3]. Speech enhancement refers to the process of quality improvement of a speech signal by using digital signal processing algorithms. The main goal of speech enhancement is the improvement in intelligibility, a measure of comprehensibility assessment of the signal to the human ears [4, 5]. The main difficulties in implementing effective speech enhancement systems is the presence of additive acoustic noise, especially noticeable environmental noise. Traditional speech enhancement methods are based on simple features such as signal energy levels and zero-crossing rate [6–8]. These standards demonstrate fairly good performance and are therefore widely used in communication. Nevertheless, their performances degrade in presence of environmental noise, even for relatively high SNR values.

One of the most prominent methods introduced to overcome this problem is the presence of directional noise, i.e., noise originating from various ambient sources. Directional noise may cause speech signals not to be acquired and processed in a clean, desirable manner. Similarly to other environmental noises, directional noise degrades speech quality and intelligibility. Thus, there is a need to clean the microphone signal and spatially filter it before it is processed. One of the possible ways to obtain spatial filtering is the utilization of directional microphones, i.e., microphones that their mechanical and electrical charac-

teristics enable enhancing signals from specific directions while suppressing signals from other undesired directions, such as the cardioid and shut-gun microphones [9, 10]. Other traditioanl speech enhancement methods utilize a single, omnidirectional microphone. In the single-channel scenario, the microphone input is modelled as a superposition of the speech and noise signals. The main drawback of these methods is that they distort the desired speech signal. Thus, it has been proposed to utilized microphone arrays in order to tackle this problem [11, 12]. These methods are also referred to as beamforming, since the main-lobe (beam) is directed at the desired location. Basic beamforming techniques such as the delay and sum [13] utilize a single weight for the entire frequency spectrum. This makes them effective only for narrowband signals and ineffective when dealing with wideband signals that are composed of various frequency components. To overcome this problem, constant beamwidth beamformers have been introduced. Constant beamwidth beamformers are beamformers that have a constant main-lobe width over a range of frequencies in a wideband. A constant beamwidth is desirable in wideband applications such as speech processing with microphone arrays and multiple user conferencing. Traditional beamformer design approaches did not provide sufficient performance in terms of beamwidth constancy and other performance criteria. Therefore, numerous contemporary approaches to robust beamformer designs were proposed. The minimum variance distortion-less response (MVDR) [14,15], linearly constrained minimum variance (LCMV) [16] and least-squares [17, 18] are several widely used beamforming design techniques developed for improving the traditional methods. The least squares (LS) approach is a popular design method [18]. It can provide a closed-form solution to the problem and is more computationally efficient compared with the convex optimization method. Nevertheless, most contemporary LS methods are utilized for the design of general broadband beamformers and not necessarily for designing constant beamwidth beamformers. The task of beamforming and constant beamwidth beamforming in particular remains unsolved as beamformer design is based on balancing trade-offs between various performance criteria and physical constraints. One of the popular beamformer design approaches is the FIR based beamformer [19–23]. FIR beamformers perform temporal filtering that results in a frequency dependent response. The filtering is performed in order to compensate for the phase difference of various frequency components. It has been shown [24, 25] that

utilizing narrowband FIR filters in beamformer designs can produce robust beamformers.

Another avialable solution for the environmental noise problem is the Voice Activity Detection (VAD). Classical VAD algorithms presuppose statistical models of the speech and noise signals, and many are based on Likelihood Ratio Test (LRT). Two of the most widely used statistical models are the Gaussian and Laplacian models [26, 27], where the LRT fuses estimations of the spectral variance of the noise, together with common methods for its estimation. These methods usually assume that the statistics of noise is slowly varying with respect to speech [28,29]. This assumption is invalid for non-stationary noise and transient interferences, which are abrupt bursts of sound and vary faster than speech such as coughing, sneezing, door knocking and keyboard typing [30, 31]. Another difficulty is the presence of directional interference. Directional interference might be originated in acoustic reverberation, resulting from multiple reflections of acoustic signals, and in several signal origins, generating multiple signals from various directions. Finally, speech is often modelled in order to separate it from unwanted interference. These models are usually based on assumption that are incorrect in many cases of environmental and directional interference causing deteriorated performance in these cases. In the method recently presented in [32], the arithmetic mean of the LRT is used to weight features base mainly on the Mel-Frequency Cepstrum Coefficients (MFCC). In the presence of transients, high weights are assigned both in presence of speech and transient which are the fast varying components of the measured signal. Therefore, the features only partially separate speech from the transients, and the performance of the VAD is still limited. Voice activity detection in presence of transients remains an open problem.

The solution to the problem of speech enhancement in presence of environmental noise could be integration of the two aforementioned methods. By building a system based on two stages, the first, spatial filtering via utilization of a microphone array. By utilizing a beamformer, we enhance the speech signal impinging the array from the desired direction while suppressing all other undesired sources originating in undesired directions. This achieves a cleaner signal, comparing to the single-microphone scenario [33]. The second stage would be a VAD algorithm, cascaded to the output of the beamformer. After the incoming signal is spatially filtered, we could utilize the VAD algorithm for suppression of environmental noises that were not filtered in the beamforming stage. In particular,

non-stationary and transient noise, since beamformers do not entirely cancel these noise signals. The output of this cascaded system would yield a system much more robust to environmental noise, comparing to the performance of every method separately. The block diagram of the cascaded speech enhancement system is shown in Fig. 1.1.

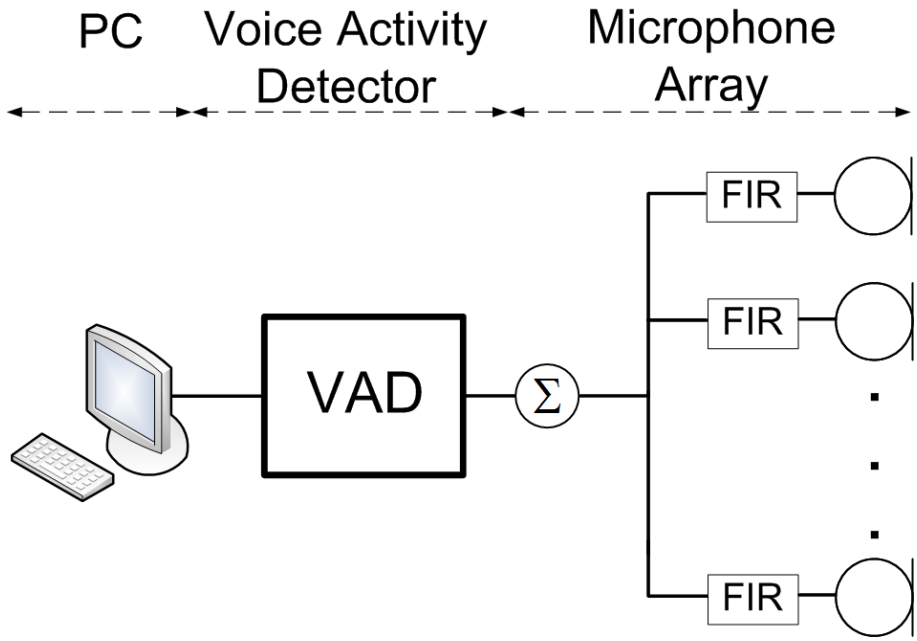

Figure 1.1: A speech enhancement system integrating between the two proposed algorithms in this thesis

Another possible application for the proposed methods would be in beamstearing. In acoustic environments, the source localization is crucial for many applications such as automatic beamformer steering for suppressing noise and reverberation. Beamformer steering is directing the beamformer's main beam to a desired direction by adding appropriate delays or phase shifts. This ability is necessary especially in applications where not only the location of the source is needed but also the ability to know when the source was active, as in teleconferencing and automatic video tracking. In the future, these two approaches could be integrated to work as a system, enabling a steerable constant beamwidth beamformer for teleconferencing or speaker tracking devices. Such a system would be able to locate the main speaker and determine when they have spoken, suppressing environmental noises and unwanted interruptions as well as enhance the energy efficiency by only working while the main speaker is talking.

In this thesis we present two speech enhancement components, the first is a microphone array design method for implementing a constant beamwidth beamformer. Custom-

tailored finite impulse response (FIR) filters are utilized for each microphone channel, manipulating the beampatterns beamwidths. The manipulated beampatterns have a constant beamwidth over a range of frequencies in a wideband. Additionally, a post summing output normalization filter is used to ensure a frequency invariant gain of the beampattern. By exploiting the physical microphone array configuration and attributes, we shape accordingly the frequency response of the FIR filters and eventually control the beamformer beamwidth. The proposed approach demonstrates improved array response results in various scenarios, compared to available methods in the field, especially in terms of sensitivity to parameters mismatch, noise robustness and side-lobe attenuation.

The second component is a supervised learning algorithm for voice activity detection transient noise suppression comprised of training and testing stages. A sample cloud is produced for every signal frame by utilizing a moving window. MFCCs are then calculated for every sample in the cloud, producing an MFCC matrix and subsequently a covariance matrix for every frame. Utilizing the covariance matrix, we calculate a similarity matrix using spectral clustering and diffusion kernels methods. Using the similarity matrix, we cluster the data and transform it to a new space where each point is labeled as speech or non-speech. We then use a Gaussian Mixture Model (GMM) in order to build a statistical model for labeling data as speech or non-speech. Simulation results demonstrate its advantages compared to a recent VAD algorithm.

1.2 Thesis Structure

The rest of this thesis is organized as follows: In Chapter 2, we review the theoretical background and present methods in the fields of array processing and voice activity detection. We start with the relevant basic theory for microphone array design. Then, we present the theory of wideband microphone array design. Specifically, we review FIR filter based array design methods. The main concept of our array processing research, which is the constant beamwidth beamformer is presented, together with two design methods in the field. We then introduce the relevant background theory and basics of VAD algorithms. We elaborate on one of the major obstacles in VAD, transient noises. We then introduce the theory behind spectral clustering, a common method for data anlysis which

is the method used for the proposed VAD algorithm. Finally, we elaborate on MFCCs, that are the representation of the sound spectrum in the proposed VAD method.

In Chapter 3, we introduce a new approach for obtaining a constant beamwidth beamformer. The proposed approach utilizes custom-tailored finite impulse response (FIR) filters for each microphone channel, manipulating the beampatterns beamwidths. The manipulated beampatterns have a constant beamwidth over a range of frequencies in a wideband. Additionally, a post summing output normalization filter is used to ensure a frequency invariant gain of the beampattern. By exploiting the physical microphone array configuration and attributes, we shape accordingly the frequency response of the FIR filters and eventually control the beamformer beamwidth. The proposed approach demonstrates improved array response results in various scenarios, compared to available methods in the field, especially in terms of sensitivity to parameters mismatch, noise robustness and side-lobe attenuation.

In Chapter 4, we introduce a voice activity detection (VAD) algorithm based on spectral clustering and diffusion kernels. The proposed algorithm is a supervised learning algorithm comprising of learning and testing stages: A sample cloud is produced for every signal frame by utilizing a moving window. Mel-frequency cepstrum coefficients (MFCCs) are then calculated for every sample in the cloud in order to produce an MFCC matrix and subsequently a covariance matrix for every frame. Utilizing the covariance matrix, we calculate a similarity matrix using spectral clustering and diffusion kernels methods. Using the similarity matrix, we cluster the data and transform it to a new space where each point is labeled as speech or non-speech. We then use a Gaussian Mixture Model (GMM) in order to build a statistical model for labeling data as speech or non-speech. Simulation results demonstrate its advantages compared to a recent VAD algorithm.

In Chapter 5, we conclude this thesis and discuss further research directions. We review the original contribution of this research thesis to the fields of beamforming and VAD and elaborate on possible future directions to this research.

Chapter 2

Related Work and Theoretical Background

In this chapter, we review contemporary beamforming and VAD algorithms, as well as providing a brief theoretical background on relevant methods and metrics in these fields. We start by reviewing the physical theory and models of propogating wave fields and plane waves in particular in Section 2.1. In Section 2.2, we introduce the concept of microphone arrays, presenting their functionality and design considerations. We then present the sampling process of the incoming wave signals by microphone arrays to form time-space signals in Section 2.3. Following the time-space signals, in Section 2.4, we elaborate on microhpone array performance measures that are utilized to evaluate microphone array capabilities. In Section 2.5, we review more advanced microphone array design methods that are suitible for wideband signals. Specifically, we review FIR filter based array design methods. In Section 2.6, we present the concept of constant beamwidth beamformers and review two design methods in the field. Achieving a constant beamwidth beamformer is the main goal of Chapter 3. Section 2.7 introduces the background and theory of VAD algorithms as well as obstacles in its implementation. In Section 2.8, we elaborate on one of the major obstacles in VAD, transient noises. Section 2.9 introduces spectral clustering, a common method for data anlysis which is the method used for the proposed VAD algorithm in Chapter 4. Finally, in Section 2.10, we elaborate on MFCCs, that are the representation of the sound spectrum in the proposed method in Chapter 4.

2.1 Propagating Wave Fields

In array signal processing, propagating waves carry signals from the source to the array. Therefore, these signals are represented in the time-space domain. The space domain is represented by either the three dimensional Cartesian coordinates (x, y, z) or the three dimensional spherical coordinates (r, ϕ, θ), where $0 \leq \phi \leq 2\pi, \;\; 0 \leq \theta \leq \pi$ are the azimuth and elevation angles, respectively. The time domain is represented by t.

Finally, let $f(t, \mathbf{r})$ denote the time-space representation of the input signal, where $\mathbf{r}$ is the radius-vector in the three-dimensional system. The relations between the Cartesian and spherical coordinates are given in Fig. 2.1.

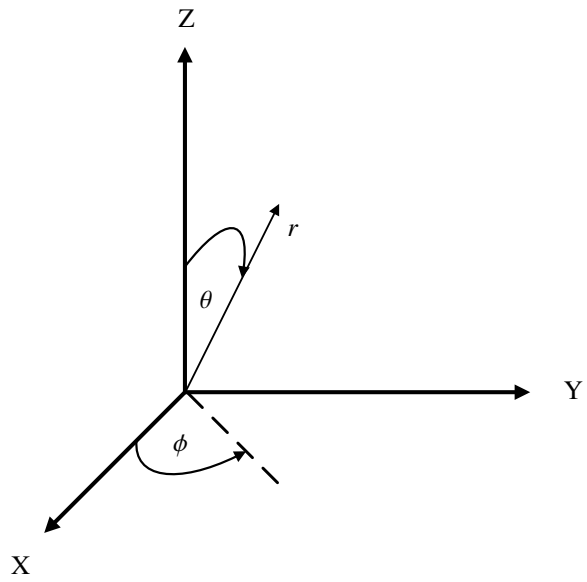

Figure 2.1: A three dimensional coordinate system with Cartesian and spherical coordinates.

$f(t, x, y, z)$ describes the signal impinging the microphone array. The physics of propagation within a homogeneous (constant speed of propagation), dispersion free (no signal degradation due to other frequencies) and lossless (no signal gain attenuation) medium is described by the wave equation:

$$\nabla^2 f\left(t, x, y, z\right) = \frac{1}{c^2} \frac{\partial^2 f\left(t, , x, y, z\right)}{\partial t^2}, \tag{2.1}$$

where ∇^2 represents the Laplacian operator and $c = 340 \frac{\mathrm{m}}{\mathrm{s}}$ represents the propagation speed of the wave.

Let $f_p(t, x, y, z)$ denote a possible solution to (2.1) of a complex exponential form:

$$f_p(t, x, y, z) = A \exp\left(j\left(\omega t - k_x x - k_y y - k_z z\right)\right), \tag{2.2}$$

where A is a complex constant, ω denotes a constant temporal frequency and k_x, k_y, k_z are real constants. Substituting (2.2) into (2.1) yields:

$$k_x^2 + k_y^2 + k_z^2 = \frac{\omega^2}{c^2} \tag{2.3}$$

This solution is called a *monochromatic plane wave*. The term *plane wave* is derived from the fact that at any given time, t_0, the value of $f(t_0, x, y, z)$ is the same at all points on a plane given by $k_x x + k_y y + k_z z = const$. Finally, writing the solution to (2.1) using vector notation we obtain:

$$f(t, \mathbf{x}) = A \exp\left(j\left(\omega t - \mathbf{k}\mathbf{x}\right)\right) \tag{2.4}$$

Let $\mathbf{k}\mathbf{x} = constant$ denote planes of constant phase. If the signal $f(t, \mathbf{x})$ is indeed propagating, planes of constant phase move by small steps of $\delta\mathbf{x}$, with small time increments of δt, i.e., $f(t + \delta t, \mathbf{x} + \delta\mathbf{x}) = f(t, \mathbf{x})$, which yields:

$$\omega\delta t - \mathbf{k}\delta\mathbf{x} = 0 \tag{2.5}$$

Assuming $\delta\mathbf{x}$ and $\mathbf{k}$ have the same direction, $\mathbf{k}\delta\mathbf{x} = |\mathbf{k}|\,|\delta\mathbf{x}|$ and $\frac{|\delta\mathbf{x}|}{\delta t} = \frac{\omega}{|\mathbf{k}|}$, where $\frac{|\delta\mathbf{x}|}{\delta t}$ can designate the propagation speed of the plane wave. Since $\mathbf{k}$ and ω are related by $|\mathbf{k}|^2 = \frac{\omega^2}{c^2}$, we have:

$$\frac{|\delta\mathbf{x}|}{\delta t} = c, \tag{2.6}$$

Assuming that $c > 0$. Thus, the speed of propagation is indeed c.

Let λ denote the distance the plane wave propagated during a single temporal period of $T = \frac{2\pi}{\omega}$. This distance is referred to as the *wavelength*. Due to its spatial traits, after one period the monochromatic plane wave appears the same as one period before, but moved forward.

Let $\mathbf{k}$ denote the *wavenumber vector*. Its magnitude $|\mathbf{k}|$ expresses the number of cycles in radians per meter of length that the plane wave has exhibited in the propagation direction. Using (2.5) with $\delta t = \frac{2\pi}{\omega}$, we obtain:

$$\lambda = \delta\mathbf{x} = \frac{2\pi}{|\mathbf{k}|} \tag{2.7}$$

Therefore, the wavenumber vector can be considered to represent spatial frequency, similarly to the manner ω represent temporal frequency.

2.2 Microphone Arrays

Microphone arrays consist of sets of microphones positioned in a way to function as a directional acoustic antenna. Microphone arrays are utilized for filtering signals in a space-time field. Filtering is enabled by exploitation of the incoming signals spatial characteristics. A desirable spatial filtering, i.e., beamforming, should result in enhancement of signals of interest, originated in a specific direction, while forcing suppression of undesired signals originated in other directions. Microphone arrays are utilized for solving many signal processing problems: dereverberation, localization of a single source, noise reduction and source separation [31, 34, 35].

Numerous factors must be taken into consideration when designing a microphone array configuration. Initially, the geometry of the microphone array plays an important role in the formulation of the processing algorithms, as it forces fundamental constraints on the array's operation. In most cases, the array geometry is the first consideration in array design due to practical and physical constraints of the design. Therefore, the degree of freedom in choosing the array geometry is limited. Nevertheless, in some other crucial problems such as noise reduction or source separation, the geometry of the array may have little importance. For instance, Uniform Linear Arrays (ULA) can only handle one source direction at a time resulting in uncertainties and possibly direction ambiguities. Therefore, ULA configurations must be ruled out when handling several signal sources. Other array geometries such as non-uniform linear arrays and circular arrays, have been studied in the field [36, 37]. This work is based on ULA and therefore we elaborate on this geometry.

A conventional beamformer [37] is composed of a ULA of microphones. That is, the microphones are positioned on an axis with a uniform spacing between the microphones. The general expression of the microphone positioning in a ULA is given by:

$$x_m = m \cdot d, \qquad m = \ 0,\ 1,\ \dots\ ,\ M-1 \tag{2.8}$$

where m denotes the microphone index; x_m denotes the position of the microphone having

index m, where $x_m = 0$ corresponds to the left-hand side of the array, i.e., the location where the microphone indexed by $m = 0$ is positioned; d denotes the spacing between microphones, and M is the array size, i.e., the number of microphones in the array, as demonstrated in Fig. 2.2.

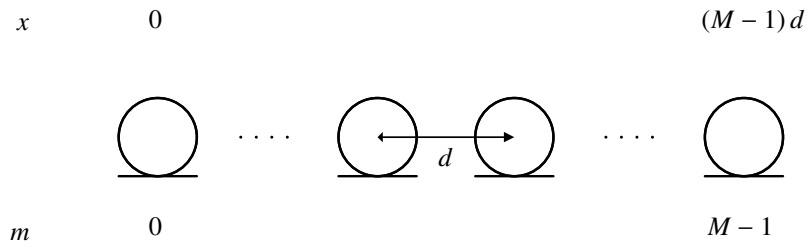

Figure 2.2: A uniform linear array of size M and spacing d.

2.3 Time-Space Signals

The incoming signals are spatially sampled by the array microphones, then the samples are processed to attenuate signals from undesired directions and extract the signal from a desired direction. A spatial response of the microphone array is obtained via a beam (main-lobe) directed to the desired signal while nulls are directed to the undesired signals. Figure 2.3. illustrates a beamformer design based on a ULA of Fig. 2.2.

Let $\mathbf{f}(t, \mathbf{x})$ denote the set of signals sampled by the microphone array at time t, expressed by

$$\mathbf{f}(t, \mathbf{x}) = [f(t, x_0), \ \dots \ , \ f(t, x_{M-1})]^T , \tag{2.9}$$

where x_m denotes the microphone position, t denotes the continuous-time variable, and ^{T} denotes the transpose operation. The beamformer output $y(t)$ is expressed by:

$$y\,(t) = \sum_{m=0}^{M-1} f(t, x_m) w_m^*, \tag{2.10}$$

where w_m is a complex weight of the microphone having index m, as shown in Fig. 2., and * denotes complex conjugation. The simplest beamformer design architecture has uniform weights, $w_m = \frac{1}{M}, \ m = 0, \cdots, M-1$.

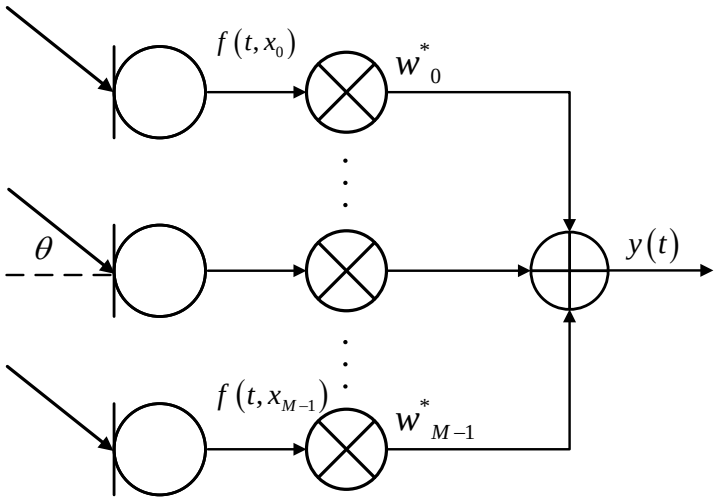

Figure 2.3: A simple beamformer design.

Let $f_\omega(t,x) = e^{j\omega t}$ denote a plane wave propagating at angular frequency ω, and let $\theta, \theta \in \left[-\frac{\pi}{2},\ \frac{\pi}{2}\right]$, denote the direction of arrival (DOA) angle measured with respect to the broadside of the linear array, as shown in Fig. 2. The wave signals spatially sampled by the microphone array inputs are given by:

$$\mathbf{f}_\omega(t,x) = \left[f_\omega(t-\tau_0),\ \dots\ ,\ f_\omega(t-\tau_{M-1})\right]^T,\ \tau_m = \frac{\sin(\theta)\cdot x_m}{c} \tag{2.11}$$

where τ_m is the propogation delay for the incoming signal and $c = 340\ \frac{\mathrm{m}}{\mathrm{s}}$ denotes the velocity of sound propagation in air. A value of $\tau_m = 0, \forall m$ implies a DOA of $\theta = 0$, i.e., a plane wave parallel to the array, propagating perpendicularly to the array. Let $\kappa = \frac{\omega}{c}\sin(\theta) = \frac{2\pi}{\lambda}\sin(\theta)$ denote the wavenumber for plane waves in a locally homogeneous medium, where λ denotes the wavelength corresponding to the angular frequency ω, and let $\mathbf{v}(\kappa)$ denote the *array manifold vector* [37], featuring all of the spatial characteristics of the microphone array. Based on (3.4), and the definition of κ above, the manifold vector can be expressed as:

$$\mathbf{v}(\kappa) = \left[e^{-j\kappa x_0}, \dots, e^{-j\kappa x_{M-1}}\right]^T \tag{2.12}$$

2.4 Microphone Array Performance Measures

Numerous performance measures are utilized for evaluating the microphone array capabilities. Each of the measures aims to quantify a significant aspect of either the response of an array to the signal environment or of the sensitivity to an array design error.

First, we review the concept of beampatterns. Beampatterns are the main tool in assessing an array performance as they express the beamformer response for various frequencies and signal angles. Let $P(\omega, \theta)$ denote the frequency and DOA dependent beamformer response. It is given by:

$$P(\omega, \theta) = \sum_{m=0}^{M-1} e^{-j\omega\tau_m} w_m^* = \mathbf{w}^H \mathbf{v}(\omega, \theta), \tag{2.13}$$

where $\mathbf{w} = [w_0, \ldots, w_{M-1}]^T$ and ^{H} denotes Hermitian transpose operation, and let $D(\omega, \theta)$ denote the beampattern of a given beamformer. It is expressed by:

$$D(\omega, \theta) = 20 \log_{10} |P(\omega, \theta)|, \tag{2.14}$$

where $|\cdot|$ denotes the absolute value. For a given angular frequency ω, the beampattern $D(\omega, \theta)$ is a function of the angle θ and the beamwidth is measured in terms of θ. In this work, the beamwidth is measured between the two lowest values at both sides of the main lobe.

A major challenge in practical beamformer applications is the potential sensitivity to mismatches between the actual array attributes and the model used to derive the desired beamformer. In practical applications, mismatches can occur either by array location perturbations, production faults or filter perturbations. The sensitivity function often used as a criterion for assessing the affect of mismatches on the array response is defined in [37] by:

$$T_{\mathrm{se}} = A_{\mathrm{w}}^{-1} = \|\mathbf{w}\|^2, \tag{2.15}$$

where A_{w}^{-1} is the inverse expression of the white noise gain given by $A_{\mathrm{w}} = \mathrm{SNR}_{\mathrm{out}}(k)$ / $\mathrm{SNR}_{\mathrm{in}}(k)$ and $\mathbf{w}$ is the weight vector corresponding to all of the FIR filter channels in the k-th frequency bin. Therefore, as the white noise gain increases, the sensitivty decreases and the array would be more robust to mismatch.

2.5 Finite Impulse Response Filter Based Filtering

Delay-and-sum beamformers, as shown in Fig. 2.3., utilize a single weight for each microphone. This makes them ineffective when dealing with wideband signals, the signals of interest in speech and audio processing, as each of the signals is composed of various frequency components. In order to design a beamformer for wideband signals, the weight values in (3.6) must be altered for different frequencies in order to obtain the desired beamformer output. That is, the weights should be frequency dependent, i.e., in the form of $\mathbf{w}(\omega) = [w_0(\omega), \ldots, w_{M-1}(\omega)]^T$. This can be acheived by introducing discrete FIR filters [19, 24].

FIR filters perform temporal filtering in order to compensate for the phase differences of the input wideband signals' various frequency components. Fig. 3. shows the realization of frequency dependent weights by FIR filters connected to the microphone array.

Let $y(t)$ denote the output of the FIR-based beamformer. It is expressed by:

$$y\left(t\right) = \sum_{m=0}^{M-1} \sum_{n=0}^{N-1} f(t - nT_{\mathrm{s}}, x_m) \cdot w_{m,n}^{*}, \tag{2.16}$$

where N denotes the number of FIR filter coefficients connected to each of the M microphones, $w_{m,n}^{*}$ is the n-th coefficient of the FIR filter connected to the microphone indexed by m, and T_{s} denotes the delay between adjacent filter elements. Given a complex plane wave signal, the beamformer output is given by:

$$y\left(t\right) = e^{j\omega t} P\left(\omega, \theta\right) = e^{j\omega t} \sum_{m=0}^{M-1} \sum_{n=0}^{N-1} e^{-j\omega(\tau_m + nT_{\mathrm{s}})} \cdot w_{m,n}^{*}, \tag{2.17}$$

Let $\mathbf{v}_{\mathrm{s}}\left(\omega, \theta\right)$ denote a *stacked array manifold vector* of dimension $M \cdot N$, where each subvector of dimension M represents the array manifold vector associated with a specific FIR filter coefficient in (3.10), i.e., the first subvector, $\left[e^{-j\omega\tau_0}, \ldots, e^{-j\omega\tau_{M-1}}\right]^T$, is associated with the coefficient indexed by $n = 0$ and all of the array microphones, indexed by $m = 0, \ldots, M-1$. Thus, it is denoted by $\mathbf{v}_0\left(\omega, \theta\right)$. The second subvector, $\left[e^{-j\omega(\tau_0 + T_{\mathrm{s}})}, \ldots, e^{-j\omega(\tau_{M-1} + T_{\mathrm{s}})}\right]^T$, is associated with the coefficient indexed by $n = 1$, and all of the array microphones. Thus, it is denoted by $\mathbf{v}_1\left(\omega, \theta\right)$, and so on. This form of

expression is called vector stacking, and $\mathbf{v}_{\mathrm{s}}(\omega,\theta)$ is given by:

$$\mathbf{v}_{\mathbf{s}}(\omega,\theta) = \begin{bmatrix} \mathbf{v}_0(\omega,\theta) \\ \mathbf{v}_1(\omega,\theta) \\ \vdots \\ \mathbf{v}_{N-1}(\omega,\theta) \end{bmatrix}. \tag{2.18}$$

Given a ULA of M microphones, micophone spacing d, and M FIR filters, each composed of N coefficients, and connected to a respective microphone. Then, from (3.10) and (3.4), the beamformer response can be expressed as:

$$P(\omega,\theta) = \sum_{m=0}^{M-1} e^{-j\omega\tau_m} \sum_{n=0}^{N-1} e^{jn\omega T_{\mathrm{s}}} \cdot w_{m,n}^{*} = \mathbf{w}_{\mathrm{s}}^{H}\mathbf{v}_{\mathrm{s}}(\omega,\theta), \tag{2.19}$$

where $\mathbf{w}_{\mathrm{s}}$ denotes the composite stacked weight vector of dimension $M \cdot N$ created by vector stacking, having $\mathbf{w}_0 = [w_{0,0}, w_{1,0}, \ldots, w_{M-1,0}]^T$ as its first subvector, $\mathbf{w}_1 = [w_{0,1}, w_{1,1}, \ldots, w_{M-1,1}]^T$ as its second subvector, and so on. The design specification of the FIR filters will be addressed in Chapter 3. Figure 3. illustrates an FIR beamformer architecture.

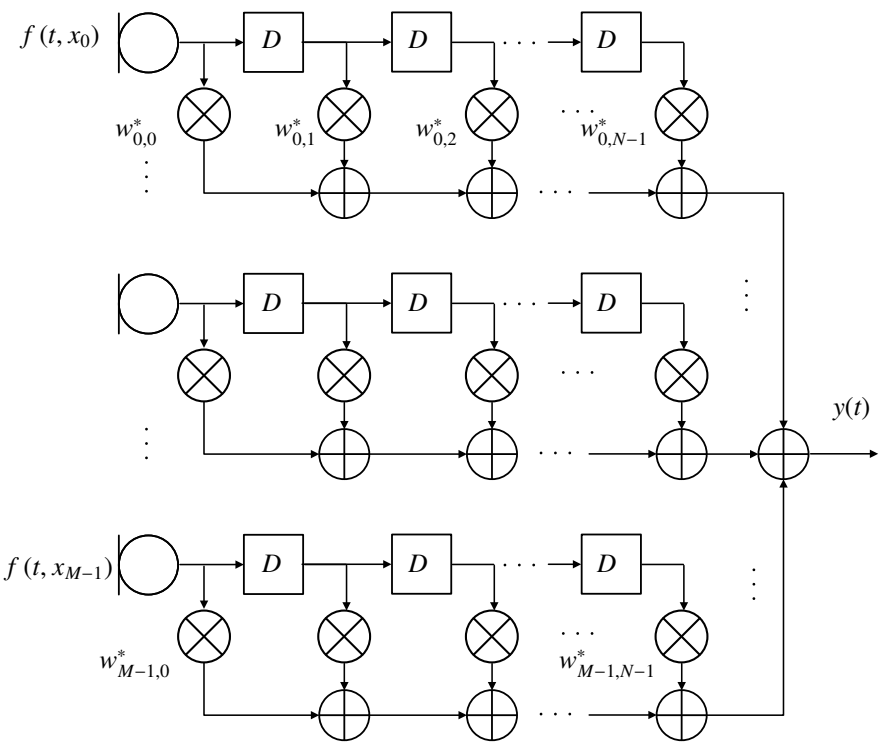

Figure 2.4: FIR beamformer architecture, where D denotes a delay element.

The second summation in (3.12) can be expressed in terms of the Discrete-time Fourier transform (DTFT) of the m-th channel filter coefficients as follows:

$$\sum_{n=0}^{N-1} e^{jn\omega T_s} w_{m,n}^* = W_m^* \left(e^{j\omega T_s}\right), \tag{2.20}$$

where $W_m \left(e^{j\omega T_s}\right)$ denotes the DTFT of $w_{m,n}$ with the summation variable n. Hence, the expression for $P(\omega, \theta)$ in (3.12) can be written as:

$$P(\omega, \theta) = \sum_{m=0}^{M-1} e^{-j\omega\tau_m} \cdot W_m^* \left(e^{j\omega T_s}\right). \tag{2.21}$$

Since the channel filters have each a finite number of coefficients (N), their frequency responses can be represented by the Discrete Fourier transform (DFT) of size N of each filter coefficients. This corresponds to sampling ω at $\frac{2\pi}{NT_s}k, \;\; k = 0, \ldots, N-1$. Examining the beamformer response for frequencies corresponding to the bin centers defined by the DFT, we obtain:

$$P(k, \theta) = \sum_{m=0}^{M-1} e^{-j\frac{2\pi\tau_m}{NT_s}k} \cdot W_m^* \left(e^{j\frac{2\pi}{N}k}\right), \quad k = 0, \ldots, N-1, \tag{2.22}$$

where k denotes the bin index of the DFT. This expression will be the basis for controlling the beamformer frequency response by specifying the frequency response of the FIR channel filters.

2.6 Constant Beamwidth Beamformers

Constant beamwidth beamformers are beamformers that have a constant beamwidth over a range of frequencies in a wideband. The beamwidth of a ULA decreases as frequency increases. Thus, in narrowband applications, the inverse proportionality of the beamwidth with respect to frequency is generally insignificant. A constant beamwidth is desirable in wideband applications such as speech processing with microphone arrays and multiple user conferencing. Traditional beamformer design approaches did not provide sufficient performance in terms of beamwidth constancy and other performance criteria. Therefore, numerous contemporary approaches to robust beamformer designs were proposed. The minimum variance distortionless response (MVDR) [14,15], linearly constrained minimum

variance (LCMV) [16] and least-squares [17, 18] are several widely used beamforming design techniques developed for improving the traditional methods.

One of the popular beamformer design approaches is the FIR based beamformer [19–23]. FIR beamformers perform temporal filtering that results in a frequency dependent response. The filtering is performed in order to compensate for the phase difference of various frequency components. It has been shown [24, 25] that utilizing narrowband FIR filters in beamformer designs can produce robust beamformers.

2.6.1 Multi Beamforming with FIR Filtering Approach

A beamformer can be modeled as a tapped delay line, where the delays determine the beam steering angle. Arrays intended for wideband uses are typically capable of beam steering, i.e., the main-lobe can be rotated from the broadside for different delay values. In conventional delay lines, the delays are constant as a function of frequency, resulting in a frequency independent steering angle. Modeling the beamformer as a tapped all-pass filter line, results in frequency dependent delays. These delays are equivalent to the phase delays of the constituent all-pass filters. If these all-pass filters have linear phase with zero phase at DC, the delays are constant, implying that the fixed delay line is a specific case of this revised beamformer model.

In multi-beamforming, a broadside beam and several steered beams are simultaneously formed, where the steered beams are formed symmetrically with respect to broadside at fixed steering angles. The inter-null beamwidth of the resultant multi-beam is approximately given by the angular distance between the outermost nulls of the outermost beams. This is only an approximation due to the effects of interfering side-lobes from the constituent beams. Since the outermost beams narrow as frequency increases, the beamwidth of the multibeam decreases as well, by roughly the same amount as that of a single beam. Thus, this technique does not yield beamwidth constancy.

A constant beamwidth can be obtained by introducing low-pass filters to the microphone array. The cutoff frequency of these filters depend on the position of their corresponding element with respect to the array center, i.e., the farther the element is from the center, the lower the cutoff of its filter. At low frequencies, all of the elements are used and for increasing frequency, the array shortens in length since the signals corresponding

to the outer elements are progressively attenuated. The design of the elemental low-pass filters has been neglected in the literature due to the apparent computational difficulty.

In the constant beamwidth beamformer design method presented in [38], it is shown that constant beamwidth beamforming can be obtained by incorporating the capability of frequency-dependent beam steering into the multi-beamforming approach. The multi-beambeamwidth decreases as frequency increases due to the narrowing of the outermost beams. If the steering angles are made frequency-dependent, the narrowing can be prevented by steering the outermost beams to larger angles as frequency increases. In this way the angular position of the outermost nulls can be kept constant, resulting in a constant beamwidth.

In the revised beamformer, a constant beamwidth can be achieved over an extended frequency range. At the low end of the frequency band, $2r + 1$ beams are formed simultaneously at broadside. As frequency increases, the outermost beams are steered to keep the outermost nulls stationary. The inner beams are steered proportionally to maintain the integrity of the beam shape.

For a uniformly excited array, the approximate null-to-null beamwidth of the multi-beam is twice the angle at which the outermost null is located. The beamwidth is given by:

$$\theta_{BW} = 2\sin^{-1}\left(\frac{2\pi}{M\omega\tau_0} + \frac{\tau(\omega)}{\tau_0}\right), \tag{2.23}$$

where $\tau(\omega)$ denotes the delay of the all-pass filters. Let ϕ_r denote the frequency-dependent steering angle of the outermost beam expressed by:

$$\phi_r = 2\sin^{-1}\left(\frac{2\pi}{M\omega\tau_0} + \frac{\tau(\omega)}{\tau_0}\right) \tag{2.24}$$

$\tau(\omega)$ is chosen to keep the arcsine argument in (2.24) constant as a function of frequency. Choosing such a $\tau(\omega)$ results in a constant beamwidth beamformer.

Let $\Phi(\omega)$ denote the phase function corresponding to $\tau(\omega)$ expressed by:

$$\Phi(\omega) = \frac{2\pi}{M}\left(1 - \frac{\omega}{\omega_0}\right), \tag{2.25}$$

where ω_0 denotes the lower frequency limit, i.e., the frequency at which all of the constituent beams are formed at broadside. This phase function is affine, i.e., linear in ω but have a DC offset.

Since $2r+1$ beams are being formed simultaneously, the far field response of the multi-beamformer is given by:

$$A_m(\omega,\theta) = \sum_{i=-r}^{r}\sum_{n=-N}^{N} a_n \exp\left(-jn\omega\tau_0 \sin(\theta)\right) \exp\left(jn\Phi(\omega)\frac{i}{r}\right) \tag{2.26}$$

where $\Phi(\omega)$ denotes the proper phase function to achieve constant beamwidth given the taps a_n. Interchanging the summation order and invoking the symmetry of the multi-beam yields:

$$\begin{aligned} A_m(\omega,\theta) &= \sum_{n=-N}^{N} B_n(\omega) \exp\left(-jn\omega\tau_0 \sin(\theta)\right) \\ B_n(\omega,\theta) &= a_n \left[1 + \sum_{i=-r}^{r} 2\cos\left(n\Phi(\omega)\tfrac{i}{r}\right)\right] \end{aligned} \tag{2.27}$$

The zero-phase lowpass filters $B_n(\omega)$ are the appropriate elemental lowpass filters discussed in Section 3.2. If $B_n(\omega)$ are used as frequency dependent shading weights for an ULA, a nearly constant inter-null beamwidth results.

The use of the elemental lowpass filters results in a low-pass broadside response, which is undesirable since it reduces the fidelity of signals corresponding to the main beam. This nonuniformity can be removed by a compensation filter given by:

$$G(\omega) = \frac{1}{\sum_{n=-N}^{N} B_n(\omega)} \tag{2.28}$$

2.6.2 Least Squares Approach

The least squares (LS) approach is a prominent design method for both the FIR filters and broadband beamformers [18]. It can provide a closed-form solution to the problem and is more computationally efficient compared with the convex optimization method. Nevertheless, most contemporary LS methods are utilized for the design of general broadband beamformers and not necessarily for designing constant beamwidth beamformers.

In the work presented in [18], a spatial variation (SV) formulation is introduced into the cost function as a frequency invariance controlling element. As a result, the unity response used as the desired response over the whole signal bandwidth is replaced by constraining the response at a single reference frequency. Then, a linearly constrained least squares formulation is derived and it can be solved either by the Lagrange multipliers method, which is a direct solution to the LS problem with linear constraints, or by transforming

the constrained optimization problem into an unconstrained problem by decomposing the coefficient vector into two orthogonal components.

Let J_{LS} denote a LS cost function given by:

$$J_{LS} = \int_{\Omega_i} \int_{\Theta} F(\Omega, \theta) \left| \mathbf{w}^T \mathbf{s}(\Omega, \theta) - D(\Omega, \theta) \right|^2 d\Omega d\theta \tag{2.29}$$

where Ω_i and Θ represent the frequency and angle range of interest, respectively, $F(\Omega, \theta)$ denotes a positive real-valued weighting function and $D(\Omega, \theta)$ denotes a desired response function.

Let (Ω_n, θ_k) denote the grid uniformly chosen from the continuous frequency and angle ranges so (2.29) can now be expressed by:

$$J_{LS_D} = \sum_{\Omega_n \in \Omega_i} \sum_{\theta_k \in \Theta_m} \left| \mathbf{w}^T \mathbf{s}(\Omega_n, \theta_k) - 1 \right|^2 + \alpha \sum_{\Omega_n \in \Omega_i} \sum_{\theta_k \in \Theta_s} \left| \mathbf{w}^T \mathbf{s}(\Omega_n, \theta_k) \right|^2 \tag{2.30}$$

where Θ_s denotes the side-lobe region and Θ_m d denotes the main-lone region. (2.30) can be expressed as a quadratic function:

$$J_{LS_D} = \mathbf{w}^T \mathbf{Q}_{LS} \mathbf{w} - 2\mathbf{w}^T \mathbf{a} + d_{LS}, \tag{2.31}$$

with

$$\begin{aligned} \mathbf{Q}_{LS} &= \sum_{\Omega_n \in \Omega_i} \sum_{\theta_k \in \Theta_m} \mathbf{S}_R(\Omega_n, \theta_k) + \alpha \sum_{\Omega_n \in \Omega_i} \sum_{\theta_k \in \Theta_s} \mathbf{S}_R(\Omega_n, \theta_k), \\ \mathbf{S}_R(\Omega_n, \theta_k) &= \mathrm{Re}\left\{ \mathbf{S}_R(\Omega_n, \theta_k) = \mathbf{s}(\Omega_n, \theta_k) \mathbf{s}(\Omega_n, \theta_k)^H \right\} \end{aligned} \tag{2.32}$$

$$\begin{aligned} \mathbf{a} &= \sum_{\Omega_n \in \Omega_i} \sum_{\theta_k \in \Theta_m} \mathbf{s}_R(\Omega_n, \theta_k), \\ \mathbf{s}_R(\Omega_n, \theta_k) &= \mathrm{Re}\{\mathbf{s}(\Omega_n, \theta_k)\} \end{aligned} \tag{2.33}$$

$$d_{LS} = \sum_{\Omega_n \in \Omega_i} \sum_{\theta_k \in \Theta_m} 1 \tag{2.34}$$

Finally, the minimization solution of (2.30) is given by:

$$\mathbf{w}_{LS} = \mathbf{Q}_{LS}^{-1} \mathbf{a} \tag{2.35}$$

Here, there is no constraint that guarantees a beamwidth constancy. Thus, the introduction of a frequency invariance controlling element into the design is necessary and it is denoted as SV and defined as:

$$SV = \sum_{\Omega_n \in \Omega_i} \sum_{\theta_k \in \Theta_{FI}} \left| \mathbf{w}^T \mathbf{s}(\Omega_n, \theta_k) - \mathbf{w}^T \mathbf{s}(\Omega_r, \theta_k) \right|^2 \tag{2.36}$$

where Θ_{FI} denotes the direction range in which beamwidth constancy is considered and r is a fixed reference frequency. The parameter SV is a measurement of the Euclidean distance between the response at the fixed reference frequency r and that at all the other operating frequencies over a range of directions in which beamwidth constancy is considered. When the beamformer has a constant beamwidth, the value of SV will be zero.

Since the beamwidth constancy property is expected to be held also in the side-lobe region, there is only a need to minimize the spectrum energy of the beamformer at the reference frequency r over the side-lobe region, which is given by:

$$J_1 = \sum_{\theta_k \in \Theta_s} \left| \mathbf{w}^T \mathbf{s}\left(\Omega_r, \theta_k\right) \right|^2 \tag{2.37}$$

Moreover, the unity response over the whole frequency band of interest in the look direction in the original formulation can be replaced by constraining the response of the beamformer at the reference frequency in the look direction θ_r to be unity, which is given by:

$$\mathbf{w}^T \mathbf{s}\left(\Omega_r, \theta_k\right) = 1 \tag{2.38}$$

Then, a constrained LS formulation of the constant beamwidth beamformer design problem is obtained by combining (2.36),(2.37) and (2.38):

$$\begin{aligned} J_{CLS} &= \sum_{n=0}^{N-1} \sum_{k=0}^{K-1} \left| \mathbf{w}^T \mathbf{s}\left(\Omega_n, \theta_k\right) - \mathbf{w}^T \mathbf{s}\left(\Omega_r, \theta_k\right) \right|^2 + \beta \sum_{\theta_k \in \Theta_s} \left| \mathbf{w}^T \mathbf{s}\left(\Omega_r, \theta_k\right) \right|^2 \\ s.t \quad & \mathbf{w}^T \mathbf{s}\left(\Omega_r, \theta_r = 1\right) \end{aligned} \tag{2.39}$$

where N and K denote the number of samples chosen uniformly over the frequency and the angle ranges considered for beamwidth constancy, respectively, and β is a trade off parameter between the beamwidth constancy property and the sidelobe attenuation. (2.39) can be written as:

$$\begin{aligned} J_{CLS} &= \mathbf{w}^T \mathbf{Q}_{CLS} \mathbf{w} \\ s.t \quad & \mathbf{s}\left(\Omega_r, \theta_r = 1\right)^H \mathbf{w} = 1 \end{aligned} \tag{2.40}$$

where,

$$\mathbf{Q}_{CLS} = \sum_{n=0}^{N-1} \sum_{k=0}^{K-1} \mathrm{Re}\left\{ \left(\mathbf{s}\left(\Omega_n, \theta_k\right) - \mathbf{s}\left(\Omega_r, \theta_k\right)\right) \left(\mathbf{s}\left(\Omega_n, \theta_k\right) - \mathbf{s}\left(\Omega_r, \theta_k\right)\right)^H \right\} + \beta \sum_{\theta_k \in \Theta_s} \mathbf{S}\left(\Omega_r, \theta_k\right)_R \tag{2.41}$$

Since $\mathbf{s}(\Omega_r, \theta_r)$ is complex valued, the single complex constraint can be changed into two real constraints:

$$\begin{aligned} &\mathbf{C}^T\mathbf{w} = \mathbf{f} \\ &\mathbf{C} = \left[\mathbf{s}(\Omega_r, \theta_r)_R, \mathbf{s}(\Omega_r, \theta_r)_I\right], \quad \mathbf{f} = [1, 0]^T \end{aligned} \tag{2.42}$$

And (2.40) can be rewritten as:

$$\begin{aligned} &J_{CLS} = \mathbf{w}^T\mathbf{Q}_{CLS}\mathbf{w} \\ &s.t \quad \mathbf{C}^T\mathbf{w} = \mathbf{f} \end{aligned} \tag{2.43}$$

which can be solved by the Lagrange multipliers method:

$$\mathbf{w} = \mathbf{Q}_{CLS}^{-1}\mathbf{C}\left(\mathbf{C}^T\mathbf{Q}_{CLS}\mathbf{C}\right)^{-1}\mathbf{f} \tag{2.44}$$

Additionally, the constrained optimization problem in (2.43) can be transformed into an unconstrained problem by decomposing the coefficient vector $\mathbf{w}$ into two orthogonal components, $\mathbf{w}_q$ and $-\mathbf{v}$ as:

$$\mathbf{w} = \mathbf{w}_q - \mathbf{v}, \tag{2.45}$$

where $\mathbf{w}_q$ lies in the range of matrix $\mathbf{C}$ and $\mathbf{v}$ is in the null space of $\mathbf{C}$, i.e. the space of all $\mathbf{v}$ fulfilling $\mathbf{C}^T\mathbf{v} = 0$. The range and null space of a matrix span the entire space. Thus, this decomposition can be used to represent any $\mathbf{w}$. $\mathbf{C}^T\mathbf{w}_q = \mathbf{f}$ is a condition that must be met in order to meet the constraint equation (2.42) and have:

$$\mathbf{w}_q = \left(\mathbf{C}^T\right)^\dagger\mathbf{f} = \mathbf{C}\left(\mathbf{C}^T\mathbf{C}\right)^{-1}\mathbf{f}, \tag{2.46}$$

where $\dagger$ denotes the pseudo-inverse operator.

$\mathbf{v}$ can be expressed as a linear combination of the basis vectors of the null space of $\mathbf{C}$:

$$\mathbf{v} = \mathbf{B}\mathbf{w}_a \tag{2.47}$$

where $\mathbf{B}$ satisfying $\mathbf{C}^T\mathbf{B} = 0$ can be obtained from $\mathbf{C}$ using orthogonalization methods, such as the singular value decomposition, and $\mathbf{w}_a$ is given by:

$$\mathbf{w}_a = \left(\mathbf{B}^T\mathbf{Q}_{CLS}\mathbf{B}\right)^{-1}\mathbf{B}^T\mathbf{Q}_{CLS}\mathbf{w}_q \tag{2.48}$$

Finally, the solution for $\mathbf{w}$ can be obtained with $\mathbf{w}_a$, $\mathbf{w}_q$ and $\mathbf{B}$.

2.7 Voice Activity Detection

Time Assignment Speech Interpolation (TASI) [39] was the first method to use voice activity detection for enhancing trans-Atlantic telecommunication capacity by switching users onto idle channels. Today, the most widely used cases of VAD are the Global System for Mobile Communication (GSM) [7] for mobile communication and the G.729 [8], used mainly in Voice over IP. GSM includes two VAD operations: First, computation of the Signal-to-Noise Ratio (SNR) in nine bands and applying a threshold to these values. Second, calculation of various parameters such as noise and channel power and voice metrics. The algorithm then thresholds the voice metrics using a varying threshold which varies according to the estimated SNR. G.729 utilizes basic features such as the energy of the signal and zero-crossing rate. These standards demonstrate fairly good performance, especially for clean signals and are therefore widely used in communication. Nevertheless, their performances degrade in presence of environmental noise, even for relatively high SNR values.

To overcome this shortcoming, several statistical model based VAD algorithms have been proposed in the last two decades [26, 27, 40, 41]. Although much progress has been made in improving VAD algorithms performance in the presence of environmental noise, overcoming transient noise still remains a big obstacle.

Let $x_sp(n)$ denote a speech signal and $x_n(n)$ denote an additive interfering background noise signal. The microphone input signal, denoted by $y(n)$ is thus given by a signal contaminated with additive background noise, given by:

$$y(n) = x_{sp}(n) + x_n(n) \tag{2.49}$$

The signal is processed using consecutive frames in the STFT domain, such that (2.49) is given in by:

$$Y(t,k) = Y_s(t,k) + Y_n(t,k), \quad k = (1,2,...K_m), \quad t = (1,2,...,N) \tag{2.50}$$

where $Y(t,k)$, $Y_s(t,k)$ and $Y_n(t,k)$ denote the STFT coefficients of $y(n)$, $x_{sp}(n)$ and $x_n(n)$, respectively, k denotes the frequency bin index, and t the time frame index. Let $\mathcal{H}_0$ and $\mathcal{H}_1$ denote speech absence and presence hypotheses, respectively, and let $f(\cdot;\mathcal{H}_0)$ and

$f(\cdot;\mathcal{H}_1)$ be PDF of the input signal in the STFT domain conditioned on the hypotheses, defining a log of the likelihood ratio:

$$\Lambda_t(k) = \log\left(\frac{f\left(Y(t,k);\mathcal{H}_1\right)}{f\left(Y(t,k);\mathcal{H}_0\right)}\right). \tag{2.51}$$

In the method presented in [26], both signal noise are assumed to be complex Gaussian uncorrelated processes in the STFT domain expressing the PDF functions by:

$$f\left(Y(t,k);\mathcal{H}_0\right) = \frac{1}{\pi\lambda_n(t,k)}\exp\left(-\frac{|Y(t,k)|^2}{\lambda_n(t,k)}\right), \tag{2.52}$$

for the speech absence hypotheses, and:

$$f\left(Y(t,k);\mathcal{H}_1\right) = \frac{1}{\pi\left[\lambda_s(t,k)+\lambda_n(t,k)\right]}\exp\left\{-\frac{|Y(t,k)|^2}{\lambda_s(t,k)+\lambda_n(t,k)}\right\}, \tag{2.53}$$

for the speech presence hypotheses, where $\lambda_s(t,k)$ and $\lambda_n(t,k)$ denote the spectral variance of speech and noise, respectively. For the Gaussian model, $\Lambda_t(k)$ is given in [26] by :

$$\Lambda_t(k) = \left(\frac{\gamma(t,k)\cdot\xi(t,k)}{1+\xi(t,k)} - \log\left(1+\xi(t,k)\right)\right), \tag{2.54}$$

where $\xi(t,k) \equiv \frac{\lambda_s(t,k)}{\lambda_n(t,k)}$ and $\gamma(t,k) \equiv \frac{|\lambda_s(t,k)|^2}{\lambda_n(t,k)}$ are the *a-priori* and *a-posteriori* SNR, respectively.

Let $\lambda_n(t,k)$ denote the estimated spectral variance, and let $Y_s(t,k)$ denote the Minimum mean square error (MMSE) estimator of the speech signal, the estimated a-priori SNR is given by:

$$\xi(t,k) = \alpha\frac{|Y_s(t-1,k)|^2}{\lambda_n(t-1,k)} + (1-\alpha)P[\gamma(t,k)-1], \tag{2.55}$$

where $\alpha \in (0,1)$ is a system smoothing parameter, $\tilde{\gamma}(t,k)-1$ is the maximum likelihood estimator of $\xi(t,k)$, and $P(x)$ is utilized for keeping non-negative values of the estimator [42].

The estimated log of the likelihood ratio in (2.54) is then averaged over the frequency bins, and the arithmetic mean of the log of the likelihood ratio is given by:

$$\Lambda_t = \frac{1}{K^f}\sum_{k=1}^{K^f}\Lambda_t(k), \tag{2.56}$$

where Λ_t is a feature indicating voice activity in a frame indexed by t. In [26], voice activity is detected by comparing Λ_t to a threshold such that speech is present in the frame if Λ_t is greater than a certain threshold. The decision is then smoothed using a Hang-Over scheme which assumes a strong correlation in the occurrences of consecutive speech frames [26].

2.8 Transient Noises

Transient noise signals are high energy, non-stationary signals, such as coughing, door knocking and typing. These signals are characterized by short outbreaks of sound that vary faster than speech [32]. Traditional methods reviewed in the previous section, assume that noise signals vary slowly with respect to speech signals. Thus, transients are often detected as speech signals by these algorithms. Traditional algorithms utilize spectral variance estimation of the noise, $\lambda_n(t,k)$, and their performance confide in the accuracy of noise statistics estimations. Moreover, for low SNR values with non-stationary noise, speech components may have substantial noise in both speech segments, in the form of distorted speech and noise segments, in the form of non-existent speech features. These degrade the traditional VAD algorithm performance and require the use VAD algorithms to distinguish speech absence from speech presence.

One of the prominent methods for the estimation of the spectral variance of the noise is the Minima Controlled Recursive Averaging (MCRA) method [28,29], where the spectral variance is recursively smoothed in speech absence intervals. Although MCRA has been successful in estimation of the spectral variance of various quasi-stationary noises, it ineffective for the estimation of spectral variance of transients.

Spectral variance estimation of the noise is given by smoothing the energy of the noisy signal over time in speech absent intervals , while keeping previous values of the estimate in speech intervals:

$$\hat{\lambda}_n(t+1,k) = \left\{ \begin{array}{ccc} \alpha_n \hat{\lambda}_n(t,k) + (1-\alpha_n)|Y(t,k)|^2 & ; & \mathcal{H}_0' \\ \hat{\lambda}_n(t,k) & ; & \mathcal{H}_1' \end{array} \right\}, \tag{2.57}$$

where $\alpha_n \in (0,1)$ is a smoothing parameter, $\mathcal{H}_0'$ and $\mathcal{H}_1'$ are speech absence and speech presence hypotheses for noise spectrum estimation, respectively. Here, a decision that speech is absent in a frame is taken with a lower confidence, i.e., $f(\mathcal{H}_0'|Y(t,k)) \leq f(\mathcal{H}_0|Y(t,k))$. Both $\mathcal{H}_0'$ and $\mathcal{H}_1'$ are utilized for avoiding the smoothing of $\hat{\lambda}_n$ over speech components due to wrong speech detections. Since $\mathcal{H}_0'$ and $\mathcal{H}_1'$ are unknown, from (2.57) we obtain:

$$\hat{\lambda}_n(t+1,k) = \hat{\lambda}_n(j,k)p'(t,k) + \left[\alpha_n \hat{\lambda}_n(t,k) + (1-\alpha_n)|Y(t,k)|^2\right](1-p'(t,k)), \tag{2.58}$$

where $p'(t,k)$ denotes the probability of speech presence conditioned on the noisy signal, i.e., $p'(j,k) = f(\mathcal{H}_1'|Y(t,k)$.

$p'(t,k)$ is estimated by the noisy signal energy, smoothed in time and frequency.

Let $S_f(t,k)$ be a local energy of the signal smoothed in the frequency domain using a window of length $2\tilde{w}+1$:

$$S_f(t,k) = \sum_{i=-\tilde{w}}^{\tilde{w}} b(i)|Y(t,k-i)|^2, \tag{2.59}$$

where $b(i)$ denotes a window function. Let $S(t,k)$ denote the energy of the noisy signal, which is smoothed in time and frequency, and is expressed by:

$$S(t,k) = \alpha_s S(t-1,k) + (1-\alpha_S)S_f(t,k), \tag{2.60}$$

where $\alpha_s \in (0,1)$ is a smoothing parameter. Here, the presence of speech is assumed when the smoothed signal energy is greater than the energy of the noise.

Let $I(t,k)$ denote an indicator of speech given by:

$$I(t,k) = \left\{ \begin{array}{ccc} 1 & ; & S(t,k) > \delta S_{\min}(t,k) \\ 0 & ; & \text{otherwise} \end{array} \right\}, \tag{2.61}$$

where δdenotes some constant parameter and $S_{\min}(t,k)$ denotes the minimum of the noisy signal's smoothed energy.

We remark that the main assumption in the estimation of the spectral variance of the noise lies in equation (2.61), where speech is associated with abrupt changes of the smoothed energy of the signal. Namely, the noise is assumed to slowly vary with respect to speech. This assumption does not hold for transient interferences which are characterized by abrupt bursts of sound and vary faster than speech [30, 43]. Therefore, transients are wrongly estimated as speech by the indicator of speech presence, $I(j,k)$, leading to false low levels of the spectral variance of the noise and to high levels of the log of the likelihood ratio. As a result, the performance of VADs which are based on the LRT significantly deteriorates in the presence of transients. In the method presented in [32], the arithmetic mean of the log likelihood ratio, Λ_j, is used to weight the features. In the presence of transients, high weights are assigned both in presence of speech and transient which are the fast varying components of the measured signal. Therefore, the features only partially

separate speech from the transients, and the performance of the VAD is still limited. Voice activity detection in presence of transients remains an open problem.

2.9 Spectral Clustering

Spectral clustering is a common method for data analysis. It utilizes the spectrum, i.e., eigenvalues of the similarity matrix of the data to perform dimensionality reduction prior to clustering the data in less dimensions. The similarity matrix is provided as an input and composed of a quantitative assessment of the relative similarity of each pair of points in the dataset.

Similarity graphs are a common data representation method in signal processing. Let $G = (V, E)$ denote a weighted graph , where V and E represent the set of vertices and edges of the graph, respectively. Each vertex v_i represents a data point $\boldsymbol{Y}(:, i)$ and each edge e_{ij} between two vertices v_i and v_j has a non-negative weight $\boldsymbol{W}(i, j) \geq 0$. These weights are a measure of similarity between points. We assume that the graph G is undirected, i.e., $\boldsymbol{W}(i, j) = \boldsymbol{W}(j, i)$.

Let $\boldsymbol{W}$ denote a similarity matrix whose (i, j)-th element equals to $\boldsymbol{W}(i, j)$. In [44], a spectral clustering algorithm using the eigenvectors of the matrix $\boldsymbol{D}^{-1/2}\boldsymbol{W}\boldsymbol{D}^{-1/2}$ was proposed. $\boldsymbol{D}$ denotes a diagonal matrix whose i-th diagonal element is $\sum_{j=1}^{N} \boldsymbol{W}(i, j)$.

Let K denote the number of desired clusters and $\boldsymbol{U}$ denote a matrix consisting of the first K eigenvectors of $\boldsymbol{D}^{-1/2}\boldsymbol{W}\boldsymbol{D}^{-1/2}$. These K eigenvectors represent the K largest eigenvalues of $\boldsymbol{D}^{-1/2}\boldsymbol{W}\boldsymbol{D}^{-1/2}$. The clustering is implemented by applying a k-means algorithm on either $\boldsymbol{U}$, where each point is represented by a row of $\boldsymbol{U}$, or on $\boldsymbol{V} = \boldsymbol{D}^{1/2}\boldsymbol{U}\left(\boldsymbol{U}^T\boldsymbol{D}\boldsymbol{U}\right)^{-1}$, where each point is represented by a row of $\boldsymbol{V}$.

The main part of spectral clustering algorithms is the aforementioned similarity matrix expressed by a Gaussian kernel:

$$\boldsymbol{W}(i, j) = \exp\left(-\frac{\|\boldsymbol{Y}(:, i) - \boldsymbol{Y}(:, j)\|_2^2}{\sigma}\right), \tag{2.62}$$

where $\boldsymbol{Y}(:, i)$ is the i-th data point and σ is commonly done manually. Other algorithms [44] introduced a method for estimating the parameters of the kernel based on minimization of a cost function that characterizes how close the eigenstructure of the similarity matrix .

2.10 Mel Frequency Cepstrum Coefficients

Mel Frequency Cepstrum Coefficients (MFCCs) are coefficients that form a representation of the short-term power spectrum of a sound. MFCC is based on a linear cosine transformation of a log power spectrum on a non-linear Mel scale frequency, thus convenient for human auditory applications.

Let $y_i(n)$ denote a sampled speech signal, divide into M short frames, $1 < i < M$, and N samples each, and let $Y_i(K)$ denote the complex DFT of $y_i(n)$ expressed by:

$$Y_i\left(k\right) = \sum_{n=1}^{N} y_i\left(n\right) w\left(n\right) e^{-\frac{j2\pi kn}{N}}, \quad 1 \leq k \leq K, \tag{2.63}$$

where $w(n)$ is an analysis window of size N, and K denotes the length of DFT.

Let $P_i(k)$ denote the power spectrum of the i-th frame given by:

$$P_i\left(k\right) = \frac{1}{N}\left|Y_i\left(k\right)\right|^2 \tag{2.64}$$

Next, the Mel-spaced filterbank is calculated. This filterbank is of size $m \times K$, where m denotes the number of MFCCs and K is the length of the DFT. The filterbank is composed of a set of m triangular filters applied to the power spectral estimate in (2.64). To calculate the filterbank energies, each filterbank is multiplied with the power spectrum and then added up to the coefficients. This yields a vector of length m, indicating the amount of energy in each filterbank. The log operator is then applied on each of the size m vector values and finally, a DCT is applied, resulting in the desired MFCCs.

Chapter 3

FIR-Based Symmetrical Acoustic Beamformer With a Constant Beamwidth

In this chapter, we present a method for the design of a constant beamwidth beamformer utilizing FIR filters. We start with a relevant mathematical background and formulate the problem in Section 3.1. In Section 3.2, we review our proposed method for an FIR filter based beamformer and elaborate on the design steps. We review the experimental results of the proposed method in Section 3.3 and present the various scenarios we had simulated, as well as compare the proposed method to other available methods in the field. Finally, we conclude the FIR based constant beamwdith beamformer research chapter and discuss future research directions in Section 3.4.

3.1 Background and Problem Formulation

In this section, we provide background material on filter-based beamformer design and formulate the constant beamwidth problem. Microphone arrays are utilized for filtering signals in a space-time field. Filtering is enabled by exploitation of the incoming signals spatial characteristics and may be expressed in terms of angle and wave number dependency. A desirable spatial filtering, i.e., beamforming, should result in enhancement of signals of interest, originated in a specific direction, while forcing suppression of undesired

signals originated in other directions. Many factors must be taken into consideration when designing a beamformer. First of all, the array geometry forces fundamental constraints on the beamformer's operation. In most cases, the array geometry is the first consideration in array design due to practical and physical constraints. Therefore, the degree of freedom in choosing the array geometry is limited. Secondly, the weights applied to array microphones determine the spatial filtering characteristics of the beamformer as well as the array performance in terms of measures like sensitivity and directivity.

3.1.1 Microphone Array Configuration

A conventional beamformer [37] is composed of a Uniform Linear Array (ULA) of microphones. That is, the microphones are positioned on an axis with a uniform spacing between the microphones. The general expression of the microphone positioning in a ULA is given by

$$x_m = m \cdot d, \qquad m = \ 0,\ 1,\ \dots\ ,\ M-1 \tag{3.1}$$

where m denotes the microphone index; x_m denotes the position of the microphone having index m, where $x_m = 0$ corresponds to the left-hand side of the array, i.e., the location where the microphone indexed by $m = 0$ is positioned; d denotes the spacing between microphones, and M is the array size, i.e., the number of microphones in the array, as demonstrated in Fig. 3.1(a) for the case of an even number of microphones and (b) for the case of an odd number of microphones. The center of the microphone array, i.e., the symmetry point, is set to be at $x = \left(\frac{M-1}{2}\right) d$.

The array microphones sample the incoming signals, collecting spatial samples that are then processed to attenuate signals from undesired directions and extract the signal from a desired direction. A spatial response of the microphone array is obtained via a beam (main-lobe) directed to the desired signal while nulls are directed to the undesired signals. As in Section 2.3, Figure 2.3 illustrates a beamformer design based on a linear array shown in Fig. 3.1.

Let $\mathbf{f}(t, \mathbf{x})$ denote the set of signals sampled by the microphone array at time t, ex-

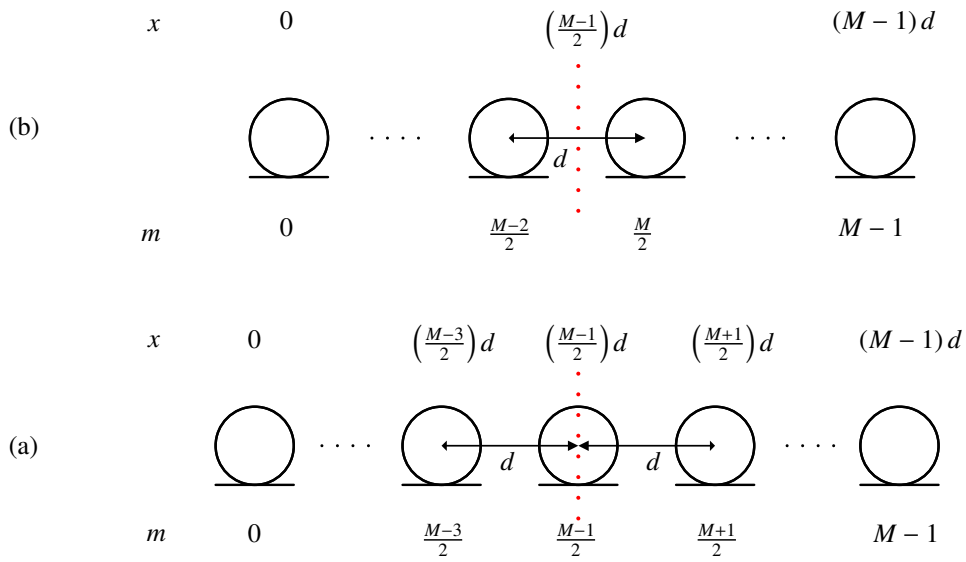

Figure 3.1: A uniform linear array of size M: (a) M even and (b) M odd, with spacing d. The red dotted line denotes the symmetry point of the array located at $x = \left(\frac{M-1}{2}\right) d$.

pressed by

$$\mathbf{f}(t, \mathbf{x}) = \left[f(t, x_0),\ \dots\ ,\ f(t, x_{M-1})\right]^T, \tag{3.2}$$

where x_m denotes the microphone position, t denotes the continuous-time variable, and ^{T} denotes the transpose operation. The beamformer output $y(t)$ is expressed by:

$$y\,(t) = \sum_{m=0}^{M-1} f(t, x_m) w_m^*, \tag{3.3}$$

where w_m is a complex weight of the microphone having index m, as shown in Fig. 2.3, and * denotes complex conjugation. The simplest beamformer design architecture has uniform weights, $w_m = \frac{1}{M},\ m = 0, \cdots, M-1$.

Let $f_\omega(t, x) = e^{j\omega t}$ denote a plane wave propagating at angular frequency ω, and let $\theta, \theta \in \left[-\frac{\pi}{2},\ \frac{\pi}{2}\right]$, denote the direction of arrival (DOA) angle measured with respect to the broadside of the linear array, as shown in Fig. 2.3. The wave signals spatially sampled by the microphone array inputs are given by:

$$\mathbf{f}_\omega(t, x) = \left[f_\omega(t - \tau_0),\ \dots\ ,\ f_\omega(t - \tau_{M-1})\right]^T,\ \tau_m = \frac{\sin(\theta) \cdot x_m}{c} \tag{3.4}$$

where τ_m is the propogation delay for the incoming signal and $c = 340\ \frac{\mathrm{m}}{\mathrm{s}}$ denotes the velocity of sound propagation in air. A value of $\tau_m = 0, \forall m$ implies a DOA of $\theta = 0$,

i.e., a plane wave parallel to the array, propagating perpendicularly to the array. Let $\kappa = \frac{\omega}{c}\sin(\theta) = \frac{2\pi}{\lambda}\sin(\theta)$ denote the wavenumber for plane waves in a locally homogeneous medium, where λ denotes the wavelength corresponding to the angular frequency ω, and let $\mathbf{v}(\kappa)$ denote the *array manifold vector* [37], featuring all of the spatial characteristics of the microphone array. Based on (3.4), and the definition of κ above, the manifold vector can be expressed as:

$$\mathbf{v}(\kappa) = \left[e^{-j\kappa x_0}, \ldots, e^{-j\kappa x_{M-1}}\right]^T \tag{3.5}$$

Let $P(\omega, \theta)$ denote the frequency and DOA dependent beamformer response. It is given by:

$$P(\omega, \theta) = \sum_{m=0}^{M-1} e^{-j\omega\tau_m} w_m^* = \mathbf{w}^H \mathbf{v}(\omega, \theta), \tag{3.6}$$

where $\mathbf{w} = [w_0, \ldots, w_{M-1}]^T$ and ^{H} denotes Hermitian transpose operation.

Beampatterns are the main tool in assessing an array performance as they express the beamformer response for various frequencies and signal angles. Let $D(\omega, \theta)$ denote the beampattern of a given beamformer. It is expressed by:

$$D(\omega, \theta) = 20\log_{10}|P(\omega, \theta)|, \tag{3.7}$$

where $|\cdot|$ denotes the absolute value. For a given angular frequency ω, the beampattern $D(\omega, \theta)$ is a function of the angle θ and the beamwidth is measured in terms of θ. In this work, the beamwidth is measured between the two lowest values at both sides of the main lobe. So, when attainable, it is the *beamwidth null to null*, i.e., the width between zeroes of the main lobe [37], given by $2\sin^{-1}\left(\frac{2\pi c}{M\,d\,\omega}\right)$.

The relation between the temporal frequency, $f = \frac{\omega}{2\pi}$, the number of microphones and the beamwidth, θ_{BW} can be obtained from the following expression:

$$\sin\left(\frac{\theta_{\mathrm{BW}}}{2}\right) = \frac{2\pi c}{M\,d\,\omega} = \frac{c}{M\,d\,f} \tag{3.8}$$

Thus, as the temporal frequency f increases, the beamwidth decreases.

3.1.2 Temporal Filtering by an FIR Filter Array

Simple beamformers, as shown in Fig. 2.3, utilize a single weight for each microphone. This makes them ineffective when dealing with wideband signals, the signals of interest

in speech and audio processing, as each of the signals is composed of various frequency components. In order to design a beamformer for wideband signals, the weight values in (3.6) must be altered for different frequencies in order to obtain the desired beamformer output. That is, the weights should be frequency dependent, i.e., in the form of $\mathbf{w}(\omega) = [w_0(\omega), \ldots, w_{M-1}(\omega)]^T$. This can be acheived by introducing discrete FIR filters [19, 24].

FIR filters perform temporal filtering in order to compensate for the phase differences of the input wideband signals' various frequency components. Fig. 2.4 shows the realization of frequency dependent weights by FIR filters connected to the microphone array.

Let $y(t)$ denote the output of the FIR-based beamformer. It is expressed by:

$$y\left(t\right) = \sum_{m=0}^{M-1} \sum_{n=0}^{N-1} f(t - nT_{\mathrm{s}}, x_m) \cdot w_{m,n}^{*}, \tag{3.9}$$

where N denotes the number of FIR filter coefficients connected to each of the M microphones, $w_{m,n}^{*}$ is the n-th coefficient of the FIR filter connected to the microphone indexed by m, and T_{s} denotes the delay between adjacent filter elements. Given a complex plane wave signal, the beamformer output is given by:

$$y\left(t\right) = e^{j\omega t} P\left(\omega, \theta\right) = e^{j\omega t} \sum_{m=0}^{M-1} \sum_{n=0}^{N-1} e^{-j\omega(\tau_m + nT_{\mathrm{s}})} \cdot w_{m,n}^{*}, \tag{3.10}$$

Let $\mathbf{v}_{\mathrm{s}}\left(\omega, \theta\right)$ denote a *stacked array manifold vector* of dimension $M \cdot N$, where each subvector of dimension M represents the array manifold vector associated with a specific FIR filter coefficient in (3.10), i.e., the first subvector, $[e^{-j\omega\tau_0}, \ldots, e^{-j\omega\tau_{M-1}}]^T$, is associated with the coefficient indexed by $n = 0$ and all of the array microphones, indexed by $m = 0, \ldots, M-1$. Thus, it is denoted by $\mathbf{v}_0\left(\omega, \theta\right)$. The second subvector, $\left[e^{-j\omega(\tau_0 + T_{\mathrm{s}})}, \ldots, e^{-j\omega(\tau_{M-1} + T_{\mathrm{s}})}\right]^T$, is associated with the coefficient indexed by $n = 1$, and all of the array microphones. Thus, it is denoted by $\mathbf{v}_1\left(\omega, \theta\right)$, and so on. This form of expression is called vector stacking, and $\mathbf{v}_{\mathrm{s}}\left(\omega, \theta\right)$ is given by:

$$\mathbf{v}_{\mathbf{s}}\left(\omega, \theta\right) = \begin{bmatrix} \mathbf{v}_0\left(\omega, \theta\right) \\ \mathbf{v}_1\left(\omega, \theta\right) \\ \vdots \\ \mathbf{v}_{N-1}\left(\omega, \theta\right) \end{bmatrix}. \tag{3.11}$$

Given a ULA of M microphones, micophone spacing d, and M FIR filters, each composed of N coefficients, and connected to a respective microphone. Then, from (3.10) and (3.4), the beamformer response can be expressed as:

$$P(\omega,\theta) = \sum_{m=0}^{M-1} e^{-j\omega\tau_m} \sum_{n=0}^{N-1} e^{jn\omega T_s} \cdot w_{m,n}^* = \mathbf{w}_s^H \mathbf{v}_s(\omega,\theta), \tag{3.12}$$

where $\mathbf{w}_s$ denotes the composite stacked weight vector of dimension $M \cdot N$ created by vector stacking, having $\mathbf{w}_0 = [w_{0,0}, w_{1,0}, \ldots, w_{M-1,0}]^T$ as its first subvector, $\mathbf{w}_1 = [w_{0,1}, w_{1,1}, \ldots, w_{M-1,1}]^T$ as its second subvector, and so on. The design specification of the FIR filters will be addressed in Section 3.3. Figure 2.4. illustrates an FIR beamformer architecture.

The second summation in (3.12) can be expressed in terms of the Discrete-time Fourier transform (DTFT) of the m-th channel filter coefficients as follows:

$$\sum_{n=0}^{N-1} e^{jn\omega T_s} w_{m,n}^* = W_m^*\left(e^{j\omega T_s}\right), \tag{3.13}$$

where $W_m\left(e^{j\omega T_s}\right)$ denotes the DTFT of $w_{m,n}$ with the summation variable n. Hence, the expression for $P(\omega,\theta)$ in (3.12) can be written as:

$$P(\omega,\theta) = \sum_{m=0}^{M-1} e^{-j\omega\tau_m} \cdot W_m^*\left(e^{j\omega T_s}\right). \tag{3.14}$$

Since the channel filters have each a finite number of coefficients (N), their frequency responses can be represented by the Discrete Fourier transform (DFT) of size N of each filter coefficients. This corresponds to sampling ω at $\frac{2\pi}{NT_s}k, \;\; k = 0, \ldots, N-1$. Examining the beamformer response for frequencies corresponding to the bin centers defined by the DFT, we obtain:

$$P(k,\theta) = \sum_{m=0}^{M-1} e^{-j\frac{2\pi\tau_m}{NT_s}k} \cdot W_m^*\left(e^{j\frac{2\pi}{N}k}\right), \quad k = 0, \ldots, N-1, \tag{3.15}$$

where k denotes the bin index of the DFT. This expression will be the basis for controlling the beamformer frequency response by specifying the frequency response of the FIR channel filters.

Many methods have been proposed for determining the FIR filter coefficients. The main goal of these methods is obtaining a desirable beamformer output while dealing

with trade-offs between conflicting array performance measures. Tradtionally, the performance measures of interest are the main lobe response, side-lobe levels, sensitivity to parameters mismatch, robustness to noise, directivity and aliasing. Frequency dilation based FIR beamformers [25] derive the FIR filter coefficients from a single reference frequency response, thus deriving all of the filter coefficients, which are microphone location dependent, from a single set of coefficients. This results in a constant beamwidth approximation in a wideband on one hand, but also in high side-lobe levels and low robustness on the other hand. Optimization-based beamformer designs such as the MVDR and LCMV beamformers [18], [20] force specific constraints on the beamformer weights and output. Therefore, these methods are chosen when a specific beamformer performance measure is needed to be optimized. The following section elaborates on the proposed method for determining the FIR filter coefficients that result in an approximate constant beamwidth beamformer for a wide range of input frequencies. Although the proposed method yields inferior beamwidth constancy in the lower frequency range than some methods, it offers improved array performance in terms of side-lobe attenuation, sensitivity and robustness, as well as a simple design method which is closed form.

3.2 Proposed FIR Design Algorithm

In this section, we present the proposed FIR design method that aims to obtain a constant beamwidth beamformer while maintaining lower levels of side-lobes compared to traditional methods [25]. The main feature of the proposed method is the determination of the FIR filter coefficients that provide a good approximation to a desired beamformer response. We consider real FIR coefficients since the signals of interest, i.e., acoustic signals, are real. For this purpose, we need first to determine the *minimal frequency*, i.e., the lowest frequency for which the desired beampattern beamwidth is feasible, given the array configuration. Then, the frequency response of each of the FIR filters is specified. To maintain a fixed delay by all the filters, they are designed to have a linear phase and use each the same number of coefficients. Finally, a post-summing FIR normalization filter is introduced at the output of the array to maintain a uniform gain of the beam at all the frequencies for which it is designed to have a constant beamwidth.

3.2.1 Frequency Range Determination for Constant Beamwidth Realization

The beamwidth of a given array is generally frequency dependent and gets smaller as the frequency increases. Thus, for a given desired beamwidth θ_{BW}, and a given array of size M, there exists a *minimal frequency*, denoted f_0, for which θ_{BW} is realized. It is given from (3.8) by:

$$f_0 = \frac{c}{M\, d\, \sin\left(\frac{\theta_{\mathrm{BW}}}{2}\right)}, \tag{3.16}$$

where the desired beamwidth, i.e., the main lobe, extends from $-\frac{\theta_{\mathrm{BW}}}{2}$ to $\frac{\theta_{\mathrm{BW}}}{2}$. Hence, for input frequencies below f_0 the given array will produce a wider beamwidth than desired. Moreover, at higher frequencies than f_0, a lower beamwidth will be realized if no FIR filters are added.

To keep a constant beamwidth of θ_{BW}, as the frequency of the impinging wave increases, we need to keep the product $M \cdot f$ constant. Since only a single frequency satisfies a constant $M \cdot f$ for a given M, M must be changed to satisfy this relation for various f values. We designate the microphones that satisfy a constant $M \cdot f$ as *effective microphones*. That is, as the wave frequency increases, the effective number of participating microphones in the array, denoted by M_p, is reduced by means of signal attenuation by the appropriate FIR filters. Since M_p must be an integer, the product constancy will be satisfied exactly only for a set of frequencies, while between those frequencies it is approximately satisfied.

For a given array size, M, M_p is limited to the range: $M_{\min} \leq M_p \leq M$, $M_p = M - 2p, p = 1, 2, ..., \frac{\mathrm{M}-\mathrm{M}_{\min}}{2}$. Theoretically, $M_{\min} = 1$, but this value is not feasible since a single microphone is necessarily omni-directional and therefore cannot produce the deisred beamwidth, assuming $\theta_{\mathrm{BW}} < 2\pi$. Thus, the minimal value of M_p is $M_{\min} = 3$, for an odd number of microphones (M odd), and $M_{\min} = 2$ for an even number of microphones (M even), maintaining symmetry around $x = \left(\frac{M-1}{2}\right) d$. Substituting the value of $M_{\min}$ in (3.16) we obtain the maximal frequency, denoted $f_{\max}$, for which we can still maintain the fixed beamwidth. For frequencies beyond $f_{\max}$ the beam will be narrower than desired. Thus, the proposed approach can provide an approximate constant beamwidth in the range $[f_0, f_{\max}]$.

Different applications may desire a narrower range of frequencies for which the beamwidth is constant, say $[f_{\mathrm{L}}, f_{\mathrm{H}}]$, $f_0 \leq f_{\mathrm{L}} < f_{\mathrm{H}} \leq f_{\max}$, allowing a reduced complexity array, as will be discussed in Sections 3.3.2 and 3.3.4.

We continue here with the maximal range, i.e., $f_{\mathrm{L}} = f_0$ and $f_{\mathrm{H}} = f_{\max}$. As the frequency increases within that range, the number of effective microphones needs to be reduced. This can be done only in decrement steps of 2, i.e., $M_1 = M - 2$, $M_2 = M - 4$, and so on, maintaining symmetry by effectively removing at each step one microphone from each end of the array and calculating a corresponding minimal frequency f_p, $f_{\mathrm{L}} < f_p \leq f_{\mathrm{H}}$, by replacing M by M_p in (3.16). Note that because M_p varies in decrements of 2 and not continuously, the beamwidth will fluctuate for frequencies between adjacent f_p values. This issue will be demonstrated and alleviated in the sequel.

3.2.2 FIR Filter Design

Consider a symmetric ULA and let $P(f, \theta)$, denote its beamforming response. The proposed algorithm plugs in an FIR filter at each microphone input line, as in Fig. 2.4. Each FIR filter is of length N and can be represented by its frequency response, calculated by applying a length N DFT to the filters coefficients. This results in N frequency coefficients, one per each of the N frequency bins in $[0, \frac{1}{T_{\mathrm{s}}})$, where T_{s} is the sampling interval of the input signal, i.e., the temporal sampling period of the system. The rationale behind the selection of T_{s} is discussed in this section. The design algorithm specifies custom frequency response coefficients of each filter needed to obtain a constant beamwidth beamformer.

Basic Design

The proposed approach for maintaining an approximate fixed beamwidth in the specified frequency range is to reduce the number of effective microphones by attenuating the signal from specific microphones as the frequency increases. This is achieved by letting the real FIR filters to be lowpass filters with cutoff frequencies set according to the values of $f_p, p = 1, 2, ..., \frac{M - M_{\min}}{2}$, as shown in Fig. 3.2, for M odd.

The expression in (3.15) gives the beamformer frequency response at N discrete fre-

quencies in terms of the DFT of the FIR filters coefficients. Let $\mathbf{W}$ denote an $N \times M$ matrix denoted the *filter array matrix* based on this expression. The matrix is composed of m columns, $m = 0, 1, 2, ..., M-1$, where each column elements are given by $W_m^* \left(e^{j\frac{2\pi}{N}k}\right)$, corresponding to the DFT of the m-th channel filter coefficients. For the sake of simplified notation, and because the magnitude response of a causal linear-phase filter is the same as that of a zero-phase filter, we continue here with a zero phase filter. Since the magnitude responses of the considered filters have mirror-image symmetry with respect to half the sampling frequency, we partition $\mathbf{W}$ into two blocks:

$$W = \begin{bmatrix} \mathbf{W}_{\mathrm{L}} \\ \mathbf{W}_{\mathrm{H}} \end{bmatrix}, \tag{3.17}$$

where both $\mathbf{W}_{\mathrm{L}}$ and $\mathbf{W}_{\mathrm{H}}$ are of size $L \times M$, and L is the number of frequency bins in the lower band, i.e., up to half the sampling frequency, such that the columns of $\mathbf{W}_{\mathrm{L}}$ represent the magnitude response of the filters in the lower band, i.e., up to half the sampling frequency, and the columns of $\mathbf{W}_{\mathrm{H}}$ represent those of the upper band, up to the sampling frequency. Hence, we refer only to $\mathbf{W}_{\mathrm{L}}$ in the following design process.

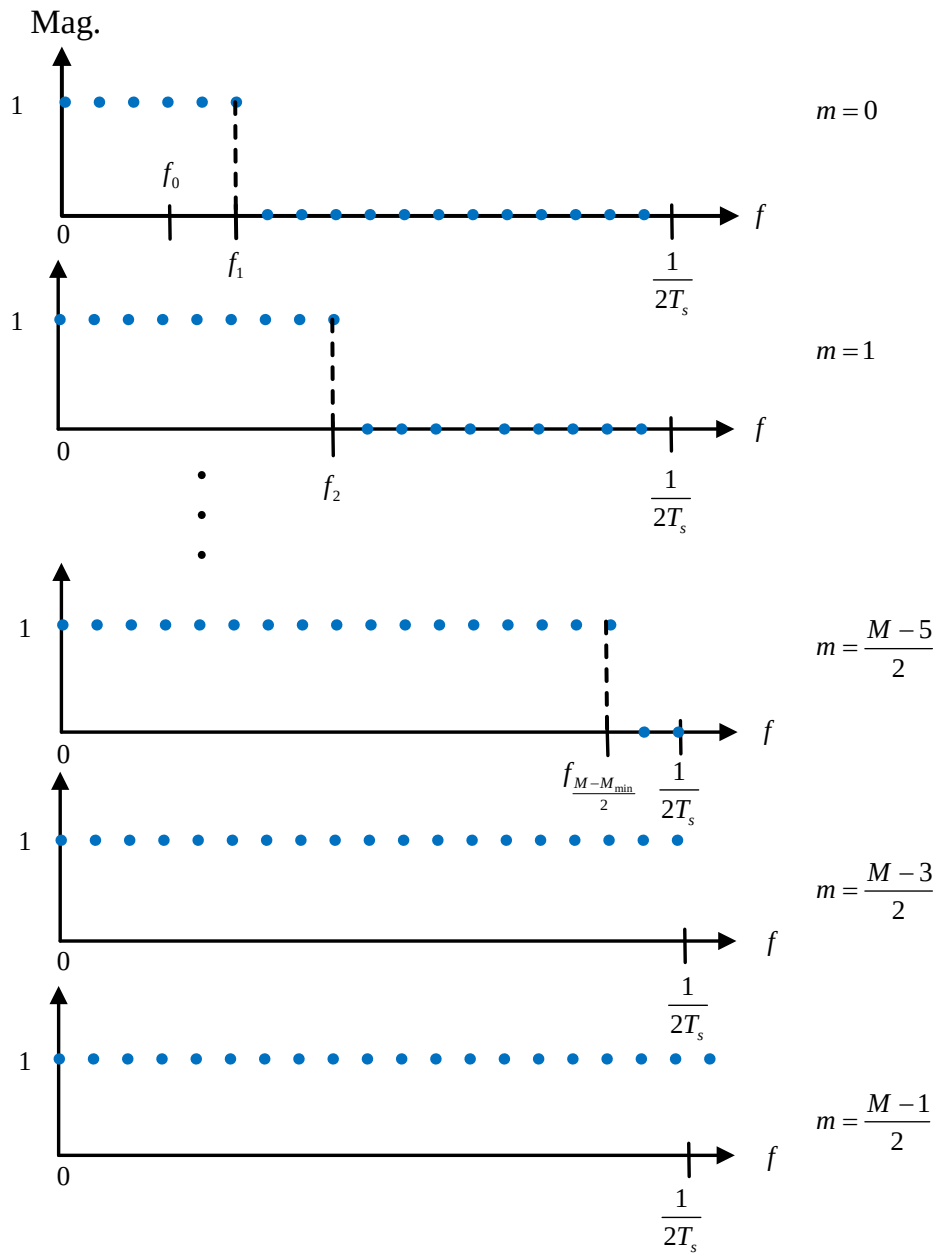

Figure 3.2: The desired frequency responses of the FIR filters for the lower half of the frequency range, indexed by microphone index $m = 0, \ldots, \frac{M-1}{2}$, M odd. Due to the microphone array symmetry, the magnitude response specification for the filters connected to the second half of the array, i.e., for $m = \frac{M+1}{2}, \ldots, M-1$, is a mirror image of first half of the array. Each dot in the specified response is the value of the filter magnitude at a corresponding frequency bin. Since M is odd and due to symmetry, the two bottom rows of Fig. 3.2 represent all-pass FIR filters since $M_{\min} = 3$. This means that three microphones are effective at all frequencies. For M even, only two microhpones would be effective at all frequencies since $M_{\min} = 2$ and therefore only the FIR filter connected to the microphone indexed by $m = \frac{M-1}{2}$, i.e., the last row, would be an all-pass filter.

For an odd number of microphones (M odd), $\mathbf{W}_{\mathrm{L}}$ is specified as:

$$\mathbf{W}_{\mathrm{L}} = \begin{array}{c} \begin{array}{ccccccccccccc} m=0 & & & & & m=\frac{M-1}{2} & & & & & & m=M-1 & \end{array} \\ \left(\begin{array}{ccccccccccccc} 1 & 1 & 1 & 1 & \dots & 1 & 1 & 1 & \dots & 1 & 1 & 1 & 1 \\ \vdots & & & & & \vdots & \vdots & \vdots & & & & & \vdots \\ 1 & 1 & 1 & 1 & \dots & 1 & 1 & 1 & \dots & 1 & 1 & 1 & 1 \\ 1 & 1 & 1 & 1 & \dots & 1 & 1 & 1 & \dots & 1 & 1 & 1 & 1 \\ \vdots & & & & & \vdots & \vdots & \vdots & & & & & \vdots \\ 1 & 1 & 1 & 1 & \dots & 1 & 1 & 1 & \dots & 1 & 1 & 1 & 1 \\ 0 & 1 & 1 & 1 & \dots & 1 & 1 & 1 & \dots & 1 & 1 & 1 & 0 \\ \vdots & & & & & \vdots & \vdots & \vdots & & & & & \vdots \\ 0 & 1 & 1 & 1 & \dots & 1 & 1 & 1 & \dots & 1 & 1 & 1 & 0 \\ 0 & 0 & 1 & 1 & \dots & 1 & 1 & 1 & \dots & 1 & 1 & 0 & 0 \\ \vdots & & & & & \vdots & \vdots & \vdots & & & & & \vdots \\ 0 & \dots & \dots & \dots & 0 & 1 & 1 & 1 & 0 & \dots & \dots & \dots & 0 \end{array}\right) \end{array} \begin{array}{l} \\ f=0 \\ \\ \\ f=f_0 \\ \\ \\ f=f_1 \\ \\ \\ f=f_2 \\ \\ \\ \end{array}, \tag{3.18}$$

The columns of $\mathbf{W}_{\mathrm{L}}$ are the magnitude specifications of the FIR channel filters, as shown in Fig. 3.2. The row indices of $\mathbf{W}_{\mathrm{L}}$ correspond to the bin frequencies in the lower band. That is, the first row of $\mathbf{W}_{\mathrm{L}}$ in (3.18), corresponds to the frequency bin centered at $f = 0$, and the last row corresponds to half the sampling frequency. Since M is odd in (3.18), the 3 central columns of $\mathbf{W}_{\mathrm{L}}$, corresponding to $M_{\min} = 3$, are specified as all 1's, i.e., allpass filters. For an even number of microphones M, the matrix in (3.18) would contain 2 central columns with all 1's, corresponding to $M_{\min} = 2$.

The first column of $\mathbf{W}_{\mathrm{L}}$ is the magnitude response of the FIR filter indexed by $m = 0$. The row corresponding to frequency f_1, indicates the cutoff frequency of that filter. For frequencies from f_1 up to f_2 , $M_1 = M - 2$ microphones are effective. For the range $[0, f_1)$ all the M microphones are effective. The second column of $\mathbf{W}_{\mathrm{L}}$ is the magnitude response of the FIR filter indexed by $m = 1$. Similarly, the frequency f_2 indicates the cutoff frequency of the filter associated with the second column. For frquencies from f_2 up to f_3 (not shown in (3.18)), $M_2 = M - 4$ microphones are effective, and so on. The number of effective microphones may reach $M_{\min} = 3$ at a lower frequency than half the

sampling frequency, unless $f_{\max} = \frac{1}{2T_s}$. If $f_H < f_{\max}$, the number of effective microphones need not reach $M_{\min}$ but would be higher (matching f_H), so more columns in $\mathbf{W}_L$ should be set all 1's. i.e., all-pass filters. A similar situation will occur if the sampling frequency is set so that $\frac{1}{2T_s} < f_{\max}$, since f_H must then be set to half the sampling frequency, i.e., $\frac{1}{2T_s}$.

In reality, a causal filter is eventually implemented by shifting the filter coefficients, resulting in a linear-phase causal filter with the same magnitude response. The basic design above improves the beamformer response, compared to the conventional one, in terms of beamwidth constancy, as demonstrated in Fig. 3.3(a) and Fig. 3.3(b). Yet, because M_p varies in steps of 2, the beamwidth does vary at frequencies that are between adjacent cutoff frequencies, causing fluctuations in the beamwidth, as clearly seen in Fig. 3.3(b). To reduce these fluctuations in beamwidth a modified design is proposed next.

Note also that for frequencies in between adjacent bins, the frequency response of the FIR filters also diverts from the desired ideal low-pass response because of the finite number of filter coefficients (N). By increasing N, the latter effect is reduced but at the expense of increased computational complexity.

Modified Design

The beamwidth fluctuations noted above can be alleviated by modifying the specifications of some of the FIR filters in the array to include intermediate magnitude values, denoted as *smoothing magnitude coefficients*, in the transition band between the cutoff frequency of those filters to the cutoff frequency of the next filter in the array, as shown in Fig. 3.4. The corresponding form of the modified FIR magnitude response matrix $\mathbf{W}_L$ is shown in (3.19). As in the basic design, we initially design a zero-phase FIR filter and eventually implement a causal filter by shifting the filter coefficients, resulting in a linear-phase causal filter with the same magnitude response. Let k denote the index corresponding to the k-th bin frequency. A row of $\mathbf{W}_L$ consists of the responses of all the array filters at a given bin frequency, e.g., the row of $\mathbf{W}_L$ corresponding to the frequency of f_0, is given the frequency bin index k_0. Due to the microphone array symmetry attributes, we define pairs of smoothing magnitude coefficients where every pair of coefficients is placed

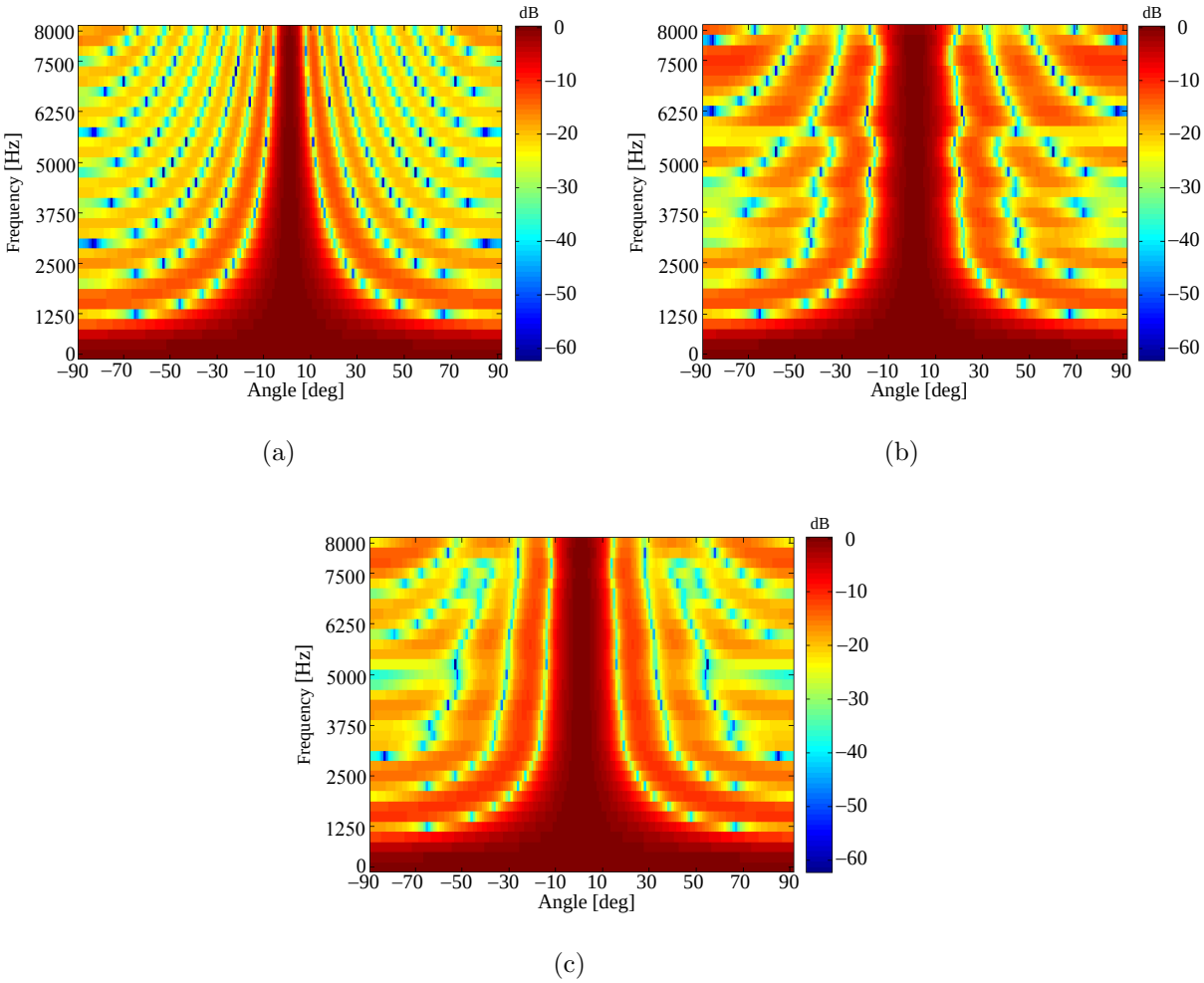

Figure 3.3: Array beampattern of (a) a conventional array without FIR filters. (b) an FIR array with magnitude response $\mathbf{W}_{\mathrm{L}}$, as given in (3.18). And (c) the modified design presented in the next section. The frequency range of $[0, \frac{1}{2T_{\mathrm{s}}}] = [0, 8]$ kHz is represented by the Y axis and is quantized into $N = 32$ frequency bins. The DOA range of $\theta = [-90, 90]$ ° is represented by the X axis. For display purposes, the frequency response at a higher resolution is computed from the FIR filter coefficents. The deisred beampattern beamwidth is $\theta_{\mathrm{BW}} = 30°$ and the minimal frequency is $f_0 = 3412$ Hz.

at symmetrical microphone indices, i.e., at $m = 0,\ M-1$, for frequency bins indexed by $k_0 > k \geq k_2$; $m = 1,\ M-2$, for frequency bins indexed by $k_2 > k \geq k_3$, and so on. Although M effective microphones should be used in the transition band $k_0 > k \geq k_1$ and $M-2$ effective microphones should be used in the transition band $k_1 > k \geq k_2$, we use $M-2$ effective microphones for all bins in $k_0 > k \geq k_2$ to achieve the desired beamwidth. Utilizing M effective microphones in $k_0 > k \geq k_1$ would prevent controlling the beamwidth since there is no degree of freedom to widen the narrowing beamwidth in that range. We show below that these coefficients help in reducing the beamwidth fluctuations by adding a degree of freedom in controlling the beamwidth at those frequency bins that are between adjacent cuttoff frequencies. Let $W_{k,m}$ denote the smoothing magnitude coefficients that are shwon in Fig. 3.4.

As depicted in Fig. 3.4, $\mathbf{W}_{\mathrm{L}}$ takes the form shown in (3.19).

$$\mathbf{W}_{\mathrm{L}} = \begin{pmatrix} 1 & 1 & \cdots & 1 & 1 & 1 & \cdots & 1 & 1 \\ \vdots & & & \vdots & \vdots & \vdots & & & \vdots \\ 1 & 1 & \cdots & 1 & 1 & 1 & \cdots & 1 & 1 \\ W_{k_0+1,0} & 1 & \cdots & 1 & 1 & 1 & \cdots & 1 & W_{k_0+1,M-1} \\ W_{k_0+2,0} & 1 & \cdots & 1 & 1 & 1 & \cdots & 1 & W_{k_0+2,M-1} \\ \vdots & & & & \vdots & & & & \vdots \\ W_{k_2-1,0} & 1 & \cdots & 1 & 1 & 1 & \cdots & 1 & W_{k_2-1,M-1} \\ 0 & W_{k_2,1} & 1\cdots & 1 & 1 & 1 & \cdots 1 & W_{k_2,M-2} & 0 \\ \vdots & & & & \vdots & & & & \vdots \\ 0 & \cdots 0 & W_{\lfloor \frac{N}{2} \rfloor, \frac{m}{2}} & 1 & 1 & 1 & W_{\lfloor \frac{N}{2} \rfloor, \frac{(M-m)}{2}-1} & 0\cdots & 0 \end{pmatrix} \begin{matrix} \\ \\ k = k_0 \\ \\ \\ \\ \\ k = k_2 \\ \\ \\ \end{matrix} \tag{3.19}$$

Because the array is symmetric, the pair of smoothing coefficients in the relevant rows, i.e., rows corresponding to $k > k_0$, are set to have equal values. Furthermore, to allow a closed form solution for these coefficients, at most one pair of such coefficients appear in each row. The smoothing coefficients values are then derived as follows:

Let f_k denote the k-th frequency bin, where $k = 0, \ldots, L-1$. The beamformer response

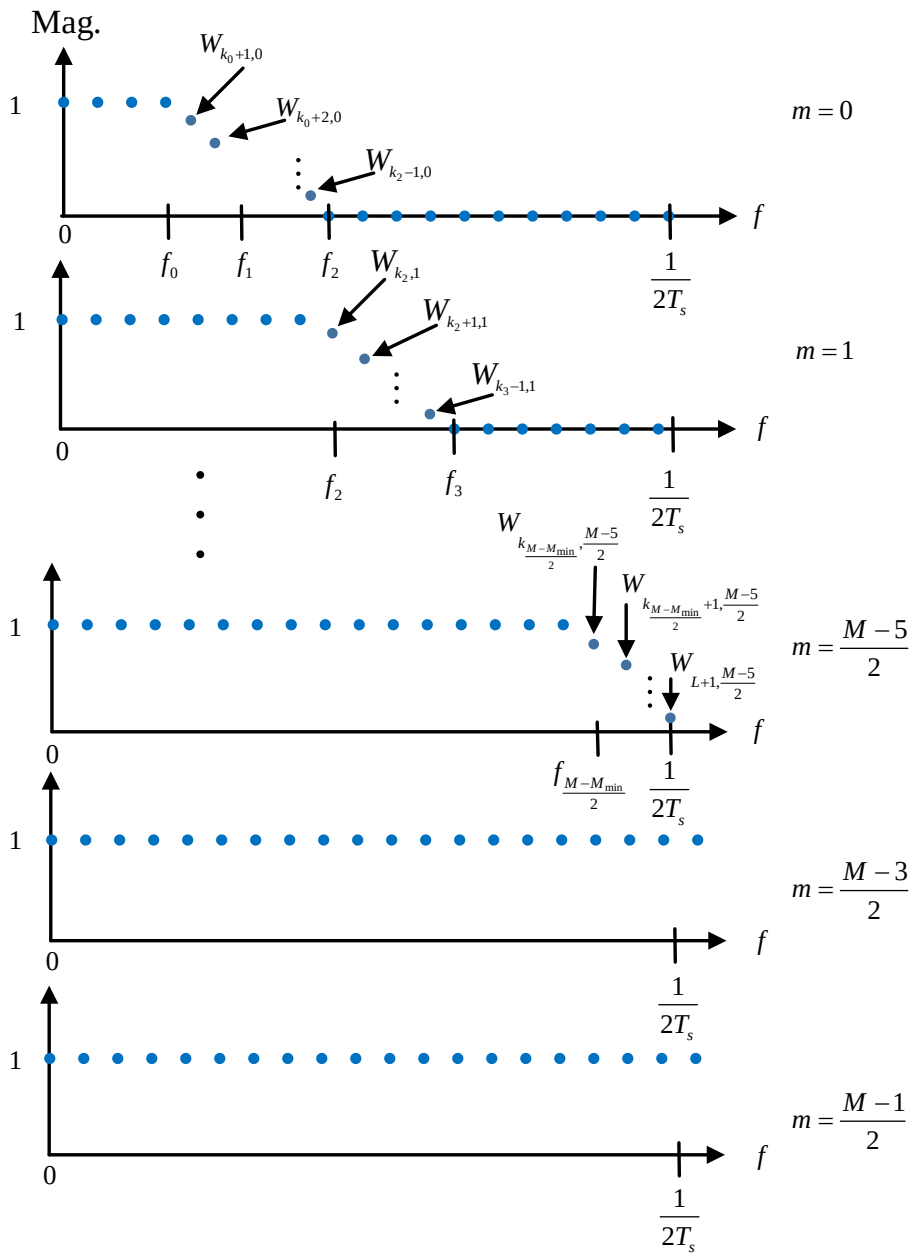

Figure 3.4: Modified FIR magnitude responses for M odd, where $W_{k,m}$ denotes the FIR filter magnitude response at the frequency bin indexed by k and the microphone indexed by m.

at f_k, with the modified FIR filter array, is given, from (3.15) by:

$$P\left(f_k,\theta\right)=\frac{1}{M_p+2W_{k,\left\lfloor\frac{M-M_p}{2}\right\rfloor-1}}\cdot\left(\sum_{m=\left\lfloor\frac{M-M_p}{2}\right\rfloor}^{M-\left\lfloor\frac{M-M_p}{2}\right\rfloor-1}\left(e^{-j\frac{2\pi f_k}{c}m\,d\,\sin(\theta)}\right)+\right.$$

$$\left.+W_{k,\left\lfloor\frac{M-M_p}{2}\right\rfloor-1}\cdot e^{j\frac{2\pi f_k}{c}\left(\left\lfloor\frac{M-M_p}{2}\right\rfloor-1\right)d\,\sin(\theta)}+W_{k,M-\left\lfloor\frac{M-M_p}{2}\right\rfloor}\cdot e^{-j\frac{2\pi f_k}{c}\left(M-\left\lfloor\frac{M-M_p}{2}\right\rfloor\right)d\,\sin(\theta)}\right),\tag{3.20}$$

where $W_{k,\left\lfloor \frac{M-M_p}{2} \right\rfloor -1}$ and $W_{k,M-\left\lfloor \frac{M-M_p}{2} \right\rfloor}$ denote the real smoothing magnitude coefficients at the k-th frequency bin of the filter , k_p denotes the k-th frequency bin corresponding to f_p, and $\frac{\sin(\theta)\cdot m\cdot d}{c}$ is substituted for τ_m in (3.15).

As stated above, the two unknown coefficients in (3.20) are set to have the same value, so that the unknown coefficient value can be found by forcing the beampattern to have a null at $\theta_{\text{null}} = \pm\frac{\theta_{\text{BW}}}{2}$. Thus, we can find the smoothing magnitude coefficient $W_{k,\left\lfloor \frac{M-M_p}{2} \right\rfloor -1}$ by setting $P\left(f_k, \theta_{\text{null}}\right) = 0$.

Since $\frac{1}{M_p+2W_{k,\left\lfloor \frac{M-M_p}{2} \right\rfloor -1}} \neq 0$, we get:

$$\sum_{m=\left\lfloor \frac{M-M_p}{2} \right\rfloor}^{M-\left\lfloor \frac{M-M_p}{2} \right\rfloor -1} e^{j\,\frac{2\pi f_k}{c}\,m\,d\,\sin(\theta_{\text{null}})} =$$

$$= -W_{k,\left\lfloor \frac{M-M_p}{2} \right\rfloor -1}\left(e^{-j\,\frac{2\pi f_k}{c}\left(\left\lfloor \frac{M-M_p}{2} \right\rfloor -1\right)d\,\sin(\theta_{\text{null}})} + e^{j\,\frac{2\pi f_k}{c}\left(\left\lfloor \frac{M-M_p}{2} \right\rfloor -1\right)d\,\sin(\theta_{\text{null}})}\right)$$

Using Euler and other trigonometric identities, we get:

$$\sum_{m=0}^{\left\lfloor \frac{M_p-1}{2} \right\rfloor} 2\cos\left(\frac{2\pi f_k}{c}\,m\,d\,\sin\left(\theta_{\text{null}}\right)\right) =$$

$$= -W_{k,\left\lfloor \frac{M-M_p}{2} \right\rfloor -1}\cdot\left(2\cos\left(\frac{2\pi f_k}{c}\left(\left\lfloor \frac{M-M_p}{2} \right\rfloor - 1\right)d\,\sin\left(\theta_{\text{null}}\right)\right)\right)$$

The final expression of the smoothing magnitude coefficient $W_{k,\left\lfloor \frac{M-M_p}{2} \right\rfloor -1}$ is finally given by:

$$W_{k,\left\lfloor \frac{M-M_p}{2} \right\rfloor -1} = -\frac{\sum_{m=0}^{\left\lfloor \frac{M_p-1}{2} \right\rfloor}\cos\left(\frac{2\pi f_k}{c}\,m\,d\,\sin\left(\theta_{\text{null}}\right)\right)}{\cos\left(\frac{2\pi f_k}{c}\left(\left\lfloor \frac{M-M_p}{2} \right\rfloor - 1\right)d\,\sin\left(\theta_{\text{null}}\right)\right)}, \tag{3.21}$$

Following the construction of $\mathbf{W}_{\text{L}}$ in (3.19) and the placement of the new magnitude response coefficients calculated by (3.21), the discrete-time filter coefficients of each FIR filter are calculated by applying the IDFT to the corresponding column of $\mathbf{W}$. The construction of $\mathbf{W}$ requires the construction of $\mathbf{W}_{\text{H}}$ from $\mathbf{W}_{\text{L}}$ based on the mirror image symmetry of the magnitude response of $\mathbf{W}_{\text{L}}$. Fig. 3.3(c) demonstrates the effect of the modification introduced in this section. It is clearly seen that the proposed modification

results in a better approximation of a constant beamwidth beamformer, compared to the results shown in Fig. 3.3(a) and Fig. 3.3(b).

3.2.3 Post Summing FIR Filter Design

Following the input FIR filter array, an additional normalization FIR filter is added. It is needed to achieve a uniform gain at all the frequencies in the range $[f_{\mathrm{L}}, f_{\mathrm{H}}]$, as the frequency responses of the different FIR filters are not all the same. It is inserted at the beamformer output.

Let $\tilde{w}_k, k = 0, \ldots, N-1$, denote the samples of the normalization filter frequency response at N discrete frequencies, i.e., the DFT coefficients of the post summing normalization FIR filter. The k-th DFT coefficient is set to:

$$\tilde{w}_k = \frac{1}{\sum\limits_{m=0}^{M-1} |W_{k,m}|}, \tag{3.22}$$

where $W_{k,m}$ denotes the coefficient of $\mathbf{W}_{\mathrm{L}}$ in (3.19) at the k-th row (frequency bin) and at the column indexed by m (the microphone index). For every frequency bin, the normalization filter sums the absolute values of the frequency response coefficients for the microphone filters from $m = 0$ to $m = M-1$. To achieve a uniform gain also at frequencies that are in between the N bin frequencies, more than N coefficients for the normalization filter are needed. The additional coefficients values can be computed by first obtaining a higher resolution frequency response of the FIR filters by zeros padding, as mentioned earlier, and then applying normalization as in (3.22) for the additional frequencies. The normalization filter coefficients are then obtained by applying the IDFT to the frequncy response coefficients. Fig. 3.5 illustrates the proposed complete FIR filter based beamformer structure.

3.2.4 Comments

If it is desired that the microphone array should not pass signal frequencies below f_0, because the beamwidth at those frequencies is wider than desired, one can use FIR filters of the bandpass type, having their lower cutoff frequency at f_0. However, bandpass filters are generally more complex to implement, therefore, the lowpass type would be

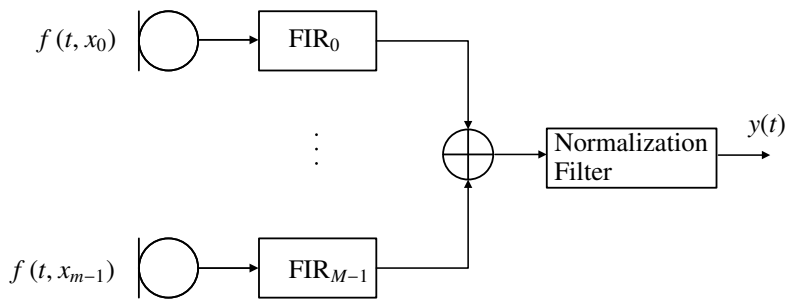

Figure 3.5: Proposed FIR-based beamformer structure.

usually preferred. Note that the bandpass filters could be designed to attenuate also signal frequencies above $f_{\max}$, if it is below $\frac{1}{2T_s}$.

In the design presented above we assumed that $[f_L, f_H] = [f_0, f_{\max}]$. However, if $f_L > f_0$, one can use less microphones in the array so as to match f_0 to the desired f_L.

The proposed algorithm's main stages of array configuration and FIR filter design are summarized in Table 3.1.

3.3 Experimental Results

In this section, we demonstrate the performance and advantages of the proposed algorithm via several experiments. We compare the aqcuired results to three different beamforming algorithms: (i) Parra's algorithm [20], where a least-squares optimal basis transform is calculated, decoupling the frequency response from the spatial response. (ii) The algorithm by Tourbabin et al. [63], where a real-valued solution to the maximum directivity optimization problem is presented. (iii) Doblinger's algorithm [16], where second-order cone programming based optimization is used together with sensor calibration. All of the simulated microphone arrays are configured with $M = 11$ omnidirectional microphones. Moreover, each input channel is connected to a $N = 32$ coefficient long FIR filter and the sampling frequency of the system is $f_s = 16$ kHz, where $f_s = \frac{1}{T_s}$. In Section 3.4.1 we run simulations for a uniform linear array with $d = 3.5$ cm spacing. Section 3.4.2 provides simulation results when microphone gain imperfection are induced by a random signal amplitude difference of up to 15% between the microphones. In Section 3.4.3 we provide simulation results for microphone array spacings perturbations induced by a random

Table 3.1: Proposed FIR based constant beamwidth beamformer algorithm

Array Configurations:

1. Calculate the minimal and maximal frequency values f_0 and $f_{\max}$ given the array specifications (number of array microphones M, desired beamwidth θ_{null} and spacing d) using (3.16).
2. Calculate f_p, $f_{\text{L}} < f_p \leq f_{\text{H}}$, by replacing M by M_p in (3.16);
   $M_{\min} \leq M_p \leq M - 2, \quad p = 1, 2, ..., (M - M_{\min})/2.$

Input FIR Filters:

3. Construct the matrix $\mathbf{W}_{\text{L}}$ as in (3.19).
4. Construct the matrix $\mathbf{W}_{\text{H}}$ on the basis of the mirror image property of $\mathbf{W}$.
5. Construct the matrix $\mathbf{W}$ by concatenating $\mathbf{W}_{\text{L}}$ and $\mathbf{W}_{\text{H}}$.
6. Calculate the smoothing magnitude coefficients $W_{k,\left\lfloor \frac{M-M_p}{2} \right\rfloor - 1}$ using (3.21);
   $k = 0, \ldots, L - 1.$

Post Summing FIR Filter:

7. Calculate the post summing FIR filter coefficients using (3.22).

microphone positioning error of up to 10% from the nominal microphone positionings.

3.3.1 ULA Experiments

In this section, the spacing between each of the $M = 11$ microphones is $d = 3.5$ cm , the desired beamwidth is $30°$, the frequency range is $[f_{\mathrm{L}}, f_{\mathrm{H}}] = [f_0, \frac{1}{2T_{\mathrm{s}}}] = [3400, 8000]$ Hz. The simulation results are shown in Fig. 3.6 where the null-to-null beamwidth is bounded by the two black arrows in Fig. 3.6(a), the side-lobes are marked by the two white arrows in Fig. 3.6(b) and the aliasing phenomena is marked by the two gray arrows in Fig. 3.6(c).

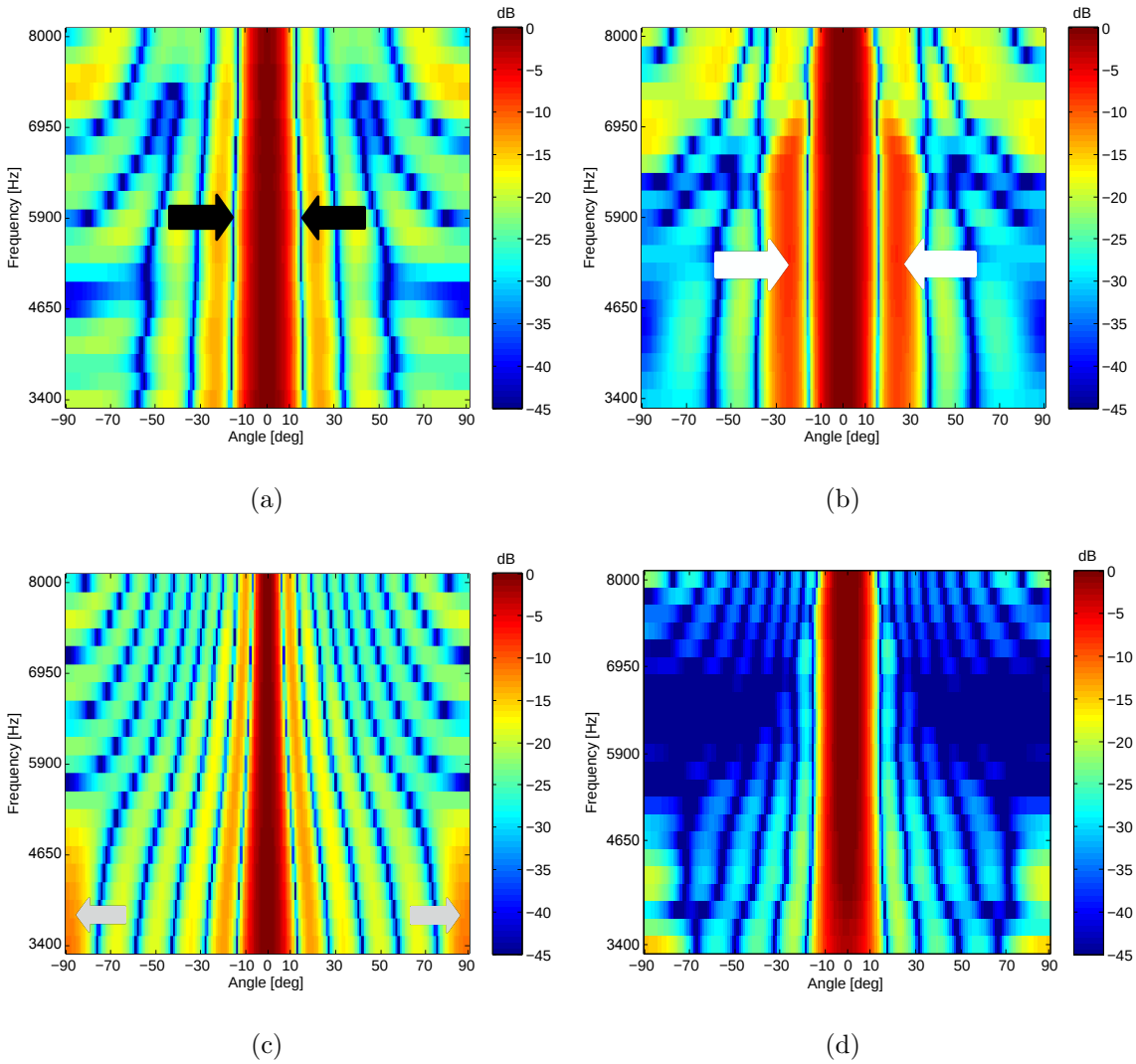

Figure 3.6: Simulation results for ULA frequency response of (a) the proposed algorithm. (b) Parra's algorithm. (c) Tourbabin's algorithm. (d) Doblinger's algorithm.

In the following sections, we elaborate on the performance of the various methods

in beampattern beamwidth constancy, side-lobe attenuation, aliasing effects attenuation, sensitivity, microphone gain imperfections and array spacings perturbations.

Beampattern Beamwidth

In Fig. 3.7 the effective beampattern beamwidths of the various mathods are compared. The beamwidths are compared by their error relatively to the desired beamwidth $\theta_{\mathrm{BW}} = 2\theta_{\mathrm{null}}$, i.e., the difference between the null-to-null beamwidth of each algorithm and the desired beamwidth in the wideband.

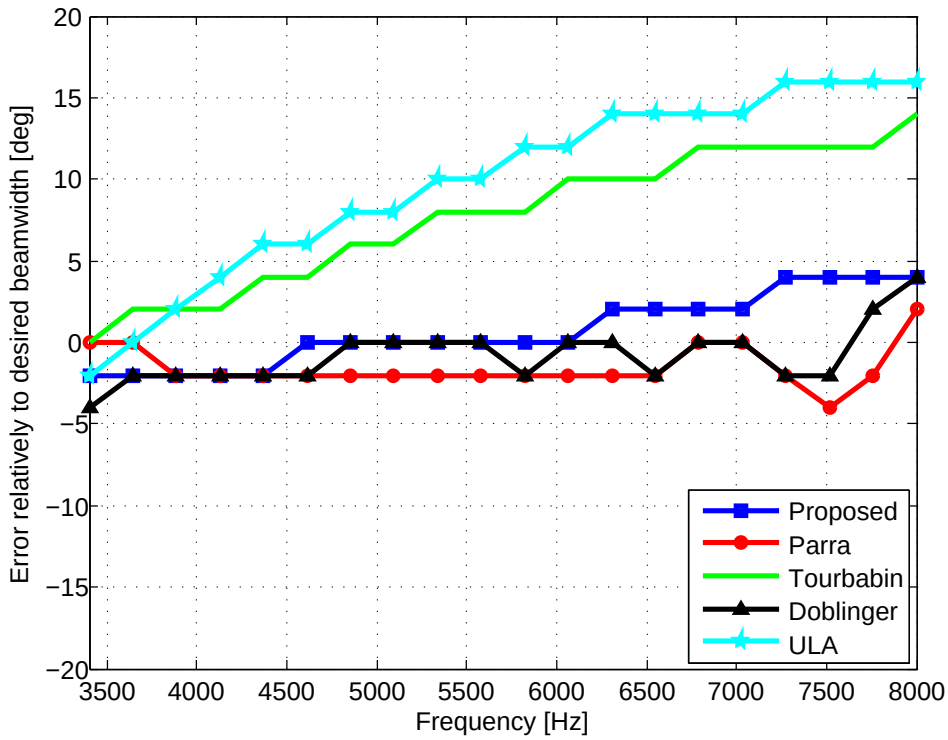

Figure 3.7: Beampattern beamwidth error of the proposed algorithm (blue square). Parra's algorithm (red circle). Tourbabin's algorithm (green solid). Doblinger's algorithm (black triangle). conventional ULA (cyan star).

The beamwidth constancy can be measured by the mean absolute error (MAE) between the beamwidth received by the various methods and the desired beamwidth in the examined frequency range. The received MAE values were 1.7°, 1.7°, 7.7°, 1.4° and 10° for the proposed, Parra's, Tourbabin's, Doblinger's and ULA delay and sum methods, respectively. The reason for the somewhat inferior results of the proposed method, in comparison to two of the examined methods, is that these methods use optimization. However, the other methods do not offer direct control over the desired beamwidth as in

the proposed method and have a more complex design algorithm because of optimization. The proposed method also offers better side-lobe attenuation and aliasing attenuation, as well as more robust perofrmance when microphone gain imperfections and array spacings perturbations are introduced, as shown in the next sections.

Side-lobe Attenuation and Output Gain

To compare the side-lobe attenuation performance, Fig. 3.8 presents the beampatterns obtained for the different methods. The curves shown in Fig. 3.8 represent the beampatterns at different frequencies in the frequency range of $[3400, 8000]$ Hz with increments of 230 Hz. The proposed algorithm demontrates better side-lobe attenuation without compromising main-lobe beamwidth and output gain. The side-lobe levels are marked by the red dashed lines. A side-lobe attenuation of 13.42 dB is obtained for the proposed algorithm in Fig. 3.8(a), while side-lobe attenuations of 7.71 dB, 10.78 dB, and 14.72 dB are obtained for the other algorithms, as seen in Fig. 3.8(b)-(d), respectively. The primary reason for the better side-lobe attenuation performance in the proposed algorithm is the explicit calculation of the beampattern beamwidth for every frequency bin, shown in $(3.18) - (3.21)$, together with the attenuation caused by the decreasing number of effective microphones, causing most of the power to stay within the main-lobe and not leak to the side-lobes. The algorithm proposed by Doblinger [16] minimizes the side-lobe levels at the expense of the main-lobe level, which is lower than 0 dB some frequencies, as shown in Fig. 3.8(d). The other methods do not take side-lobe levels attenuation performance into consideration. In Tourbabin's algorithm [63], lowering the side-lobe levels by using different cost functions decreases the performance of the algorithm's main objective.

In Fig. 3.8(a) and Fig. 3.8(c) the beampatterns have a uniform gain due to normalization factors. The proposed algorithm utilizes an output FIR post-summing normalization filter and Tourbabin's algorithm utilizes normalization constants for obtaining a uniform gain beampattern. Parra's and Doblinger's algorithms in Fig. 3.8(b) and Fig. 3.8(d) do not use normalizations factors and therefore yield non-uniform gain beampatterns. In Parra's algorithm, the phenomena is more prevalent at low frequencies, while in Doblinger's algorithm it is more noticeable at higher frequencies. Output FIR normalization filters have been utilized as part of the FIR filter design in several beamforming design meth-

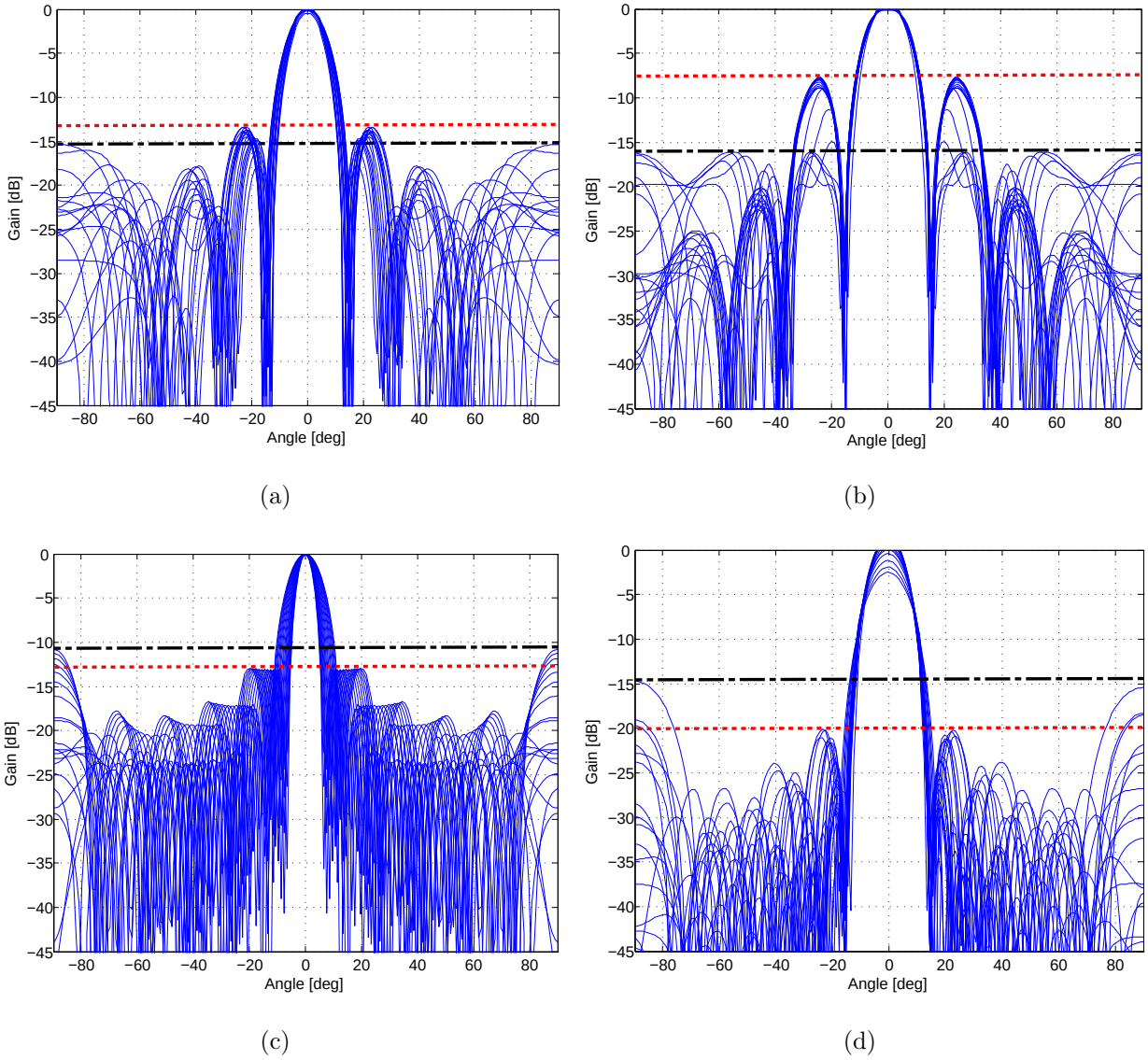

Figure 3.8: Simulation results for ULA beampatterns at different frequencies of (a) the proposed algorithm. (b) Parra's algorithm. (c) Tourbabin's algorithm. (d) Doblinger's algorithm. The side-lobe levels near the main-lobe are marked by the red dashed lines and the side-lobe levels at the edges, due to aliasing, are marked by the black dash-dot lines.

ods [50], [25].

Aliasing Attenuation

Spatial aliasing occurs when the array microphones sample the impinging signals from different locations not densely enough, i.e., the microphone spacing d is too large. This causes sources at different locations to have the same manifold vector (3.5). As a result, these sources locations cannot be uniquely determined based on the received array signals.

Avoiding aliasing requires to satisfy the condition $d < \frac{\lambda}{2}$, where λ denotes the wavelength corresponding to the angular frequency ω. On the other hand, larger d values are often used for spatial resolution improvement. Although spatial resolution can be improved by increasing the number of array microphones, hardware costs and array size constraints are the leading consideration in most real world applications. Aliasing is a phenomenon whose effect is stronger at higher frequencies, inducing high side-lobe levels at $\pm 90°$. The proposed algorithm provides better attenuation of the high side-lobe levels at $\pm 90°$, caused by aliasing, than most of the other examined methods, as seen in Fig. 3.8. Parra's algorithm offers slightly better aliasing attenuation because most of the energy outside of the main-lobe goes to side-lobes adjacent to the main-lobe.

Sensitivity

A major challenge in practical beamformer applications is the potential sensitivity to mismatches between the actual array attributes and the model used to derive the desired beamformer. In practical applications, mismatches can occur either by array spacings perturbations, production faults or filter perturbations. The sensitivity function often used as a criterion for assessing the affect of mismatches on the array response is defined in [37] by:

$$T_{\mathrm{se}} = A_{\mathrm{w}}^{-1} = \|\mathbf{w}\|^2 \,, \tag{3.23}$$

where A_{w}^{-1} is the inverse expression of the white noise gain given by $A_{\mathrm{w}} = \mathrm{SNR}_{\mathrm{out}}(k)$ / $\mathrm{SNR}_{\mathrm{in}}(k)$ and $\mathbf{w}$ is the weight vector corresponding to all of the FIR filter channels in the k-th frequency bin. Therefore, as the white noise gain increases, the sensitivity decreases and the array would be more robust to mismatch. In Fig. 3.9 the sensitivity as a function of frequency of the various algorithms is compared. The proposed algorithm yields better results for a small part of the frequency spectrum, $(3400 - 4400)$ Hz, thanks to the decreasing number of effective microphones with frequency and the normalization FIR filter calculated in (23). At the higher part of the spectrum $(4400 - 8000)$ Hz, the proposed algorithm produces inferior results only to the method proposed by Tourbabin since the latter minimizes the sensitivity for higher frequencies [63].

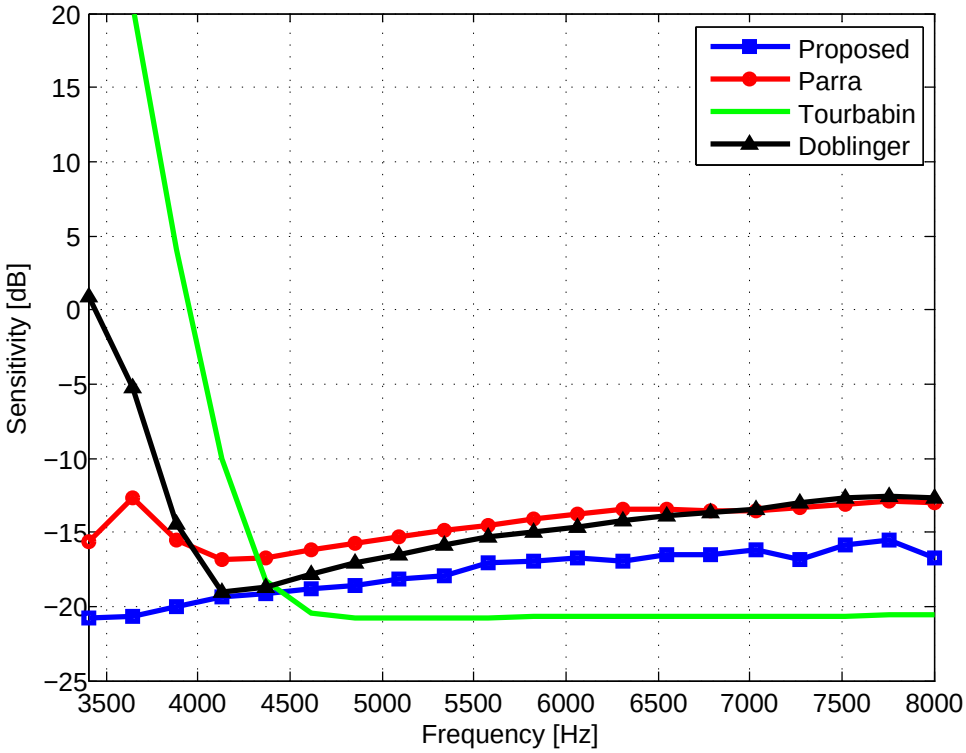

Figure 3.9: Sensitivity performance of proposed algorithm (blue square). Parra's algorithm (red circle). Tourbabin's algorithm (green solid). Doblinger's algorithm (black triangle).

3.3.2 Micophone Gain Imperfections

For simulating microphone gain imperfections of a parctical microphone array, we ran 10 simulations with a random micophone gain deviation of up to $\pm 15\%$ of the original gain and averaged the results. Figure 3.10 compares the effective beampattern beamwidths of the various algorithms before and after the gain imperfection introduction. This is done by subtracting the beamwidth of the gain mismatched array from the beamwidth of the original array shown in Fig. 3.9, for every method.

Table 3.2 shows the side-lobe attenuation and the MAE from the desired beamwidth of the various methods before and after the microphone array gain perturbation. The proposed method yields the best results for side-lobe attenuation and aliasing effects attenuation when array gain perturbations are introduced. Moreover, the array perturbations have the smallest effect on the beamwidth of the proposed method since the mean absolute error has the smallest deviation before and after the gain perturbations.

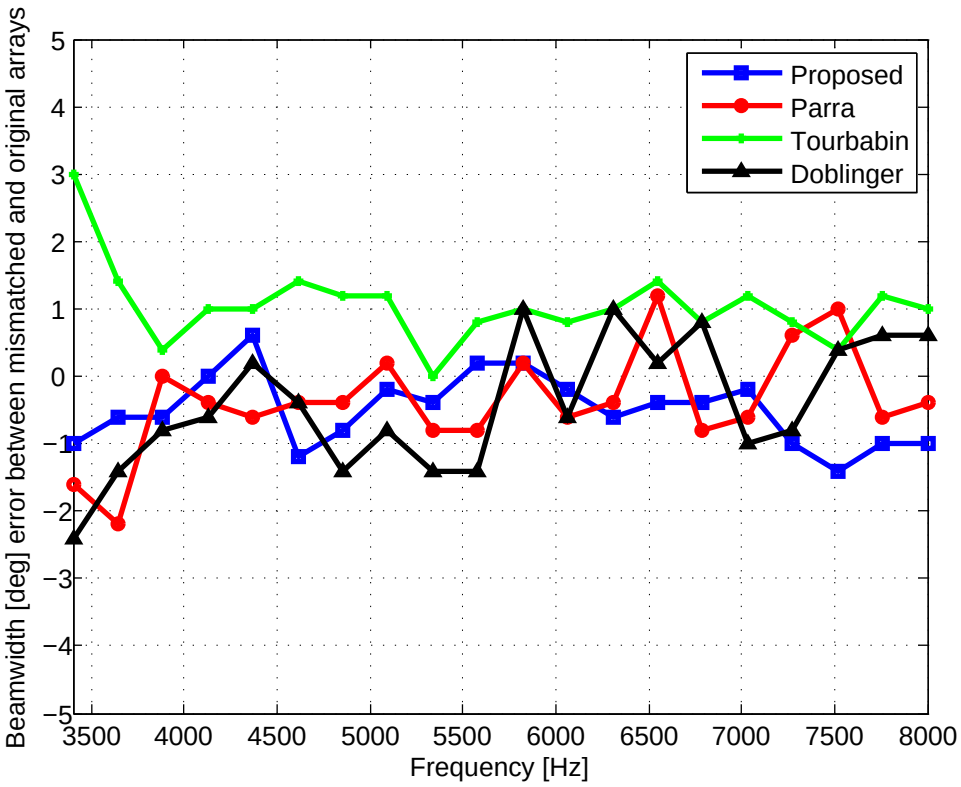

Figure 3.10: Beamwidth error between the microphone gain mismatched array and original array of the proposed algorithm (blue square), Parra's algorithm (red circle), Tourbabin's algorithm (green solid) and Doblinger's algorithm (black triangle).

Table 3.2: Side-lobe attenuation of the various methods before and after the microphone array gain perturbation. The percent of degredation for every method is given in brackets.

Method	Side-lobe Atten. Before/After [dB]	Side-lobe Atten. at 90° Before/After [dB]	MAE Before/After [°]
Proposed	13.42/12.84 (**4.32%**)	15.36/14.54 (**5.34%**)	1.7/1.64 (**3.53%**)
Parra's	7.71/4.95 (35.8%)	16.42/13.96 (15%)	1.7/2.03 (19.4%)
Tourbabin's	12.92/11.09 (14.2%)	10.78/8.43 (21%)	7.7/8.76 (13.8%)
Doblinger's	20.14/16.48 (18.1%)	14.72/15.86 (7.7%)	1.4/2.11 (50%)

3.3.3 Array Spacings Perturbations

Similarly to the previous section, we simulate a practical microphone array considering array spacings perturbations due to inaccuracies in microphone positioning. We ran 10 simulations with random spacing deviations of up to ±10% in inter-micophones spacing. We computed the beampattern as a function of frequency using (3.15), and then averaged the results. Figure 3.11 compares the change in the effective beamwidths of the various algorithms, before and after introducing the array spacings perturbations. This is done

by subtracting the beamwidth of the spacing mismatched array from the beamwidth of the original array shown in Fig. 3.7, for every method. It is seen that the array spacings

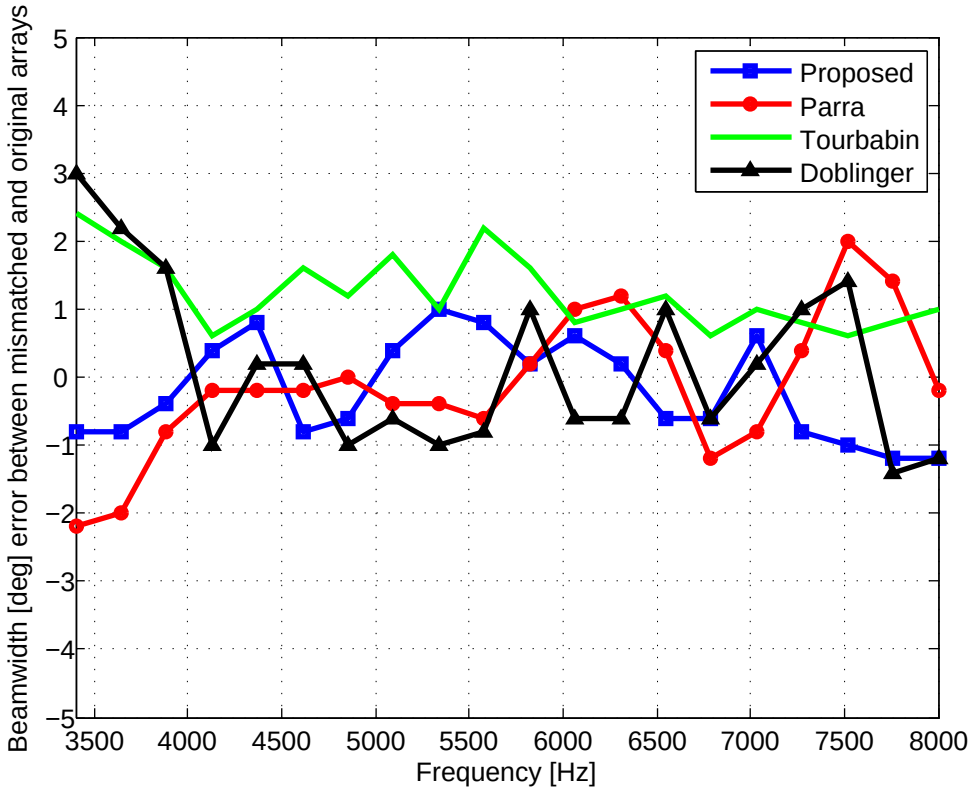

Figure 3.11: Beamwidth error between the microphone spacing mismatched array and original array of the proposed algorithm (blue square), Parra's algorithm (red circle), Tourbabin's algorithm (green solid) and Doblinger's algorithm (black triangle).

perturbations have very little effect on the effective beamwidth of the proposed method, compared to the other examined methods, as also seen by the MAE values in the left column of Table 3.3.

The scenarios of array spacings perturbations and microphone gain imperfection were examined in [64]. Altough an optimal solution has been succefully obtained via a minimax criterion, the solution runtime is relatively long and suitable mainly for small arrays.

Table 3.3 also shows that the side-lobe levels of the various methods before and after the microphone array spacings perturbations. The proposed method is seen to yield the best results for side-lobe and aliasing attenuation, when array spacings perturbations are introduced.

Table 3.3: Side-lobe attenuation of the various methods before and after the microphone array spacings perturbation. The percent of degredation for every method is given in brackets.

Method	Side-lobe Atten. Before/After [dB]	Side-lobe Atten. at 90° Before/After[dB]	MAE Before/After [°]
Proposed	13.42/12.19 (**9.17%**)	15.36/13.1 (**14.7%**)	1.7/1.73 (**1.76%**)
Parra's	7.71/5.85 (24.12%)	16.42/13.54 (17.54%)	1.7/1.81 (6.47%)
Tourbabin's	12.92/9.84 (23.84%)	10.78/8.05 (25.32%)	7.7/8.94 (16.1%)
Doblinger's	20.14/11.21 (44.34%)	14.72/6.21 (57.81%)	1.4/1.03 (26.43%)

3.3.4 Experimental Results Conclusions

Although the proposed method achieved inferior results to some methods in terms of the MAE in beamwidth, in some part of the frequency band, Fig. 3.8 shows that the proposed method yields better side-lobe and aliasing attenuation. The proposed method provides also a better performance, in terms of the sensitivity criterion, than the other examined algorithms in the lower part of the spectrum, as shown in Fig. 3.9. Finally, according to Fig. 3.10, Fig. 3.11, Table 3.2, and Table 3.3 , when micorphone gain and positioning imperfections were introduced, the proposed method provided the most robust results in beamwidth error, having the smallest change from the nominal performance.

3.4 Conclusions

A new method for the design of an FIR-based constant beamwidth beamformer has been proposed. First, an input FIR filter array is desgined to obtain a fixed main-lobe width in a wide frequency range. Then, an output FIR normalizing filter is desgined to keep a fixed gain over that band. The proposed design method achieves a good approximation to a constant beamwidth output response, with better side-lobe and aliasing attenuation, as well as robustness to array mismatches, as compared to the other examined methods. When inducing random microphone gain and array spacings perturbations, the proposed

algorithm produces steady beampatterns throughout the specified frequency band. The new method is based on designing the FIR filter array such that its frequency response reduces the number, of what we call, "effective microphones", when signal frequency increases, affecting an approximate fixed beamwidth in a wide range of frequencies. Simulations of the proposed beamformer also demonstrate low computational complexity due to its simple closed form FIR filter design procedure. A possible future research direction could be the application of the proposed design method to other array geometries besides ULAs.

Chapter 4

Voice Activity Detection in Presence of Transient Noise Using Spectral Clustering and Diffusion Kernels

In this chapter, we present a voice activity detection algorithm based on spectral clustering and diffusion maps and evaluate its performance. This chapter begins with the problem formulation in Section 4.1, where we also elaborate the discussion on the theory of the proposed method. Section 4.2 presents the performance and advantages of the simulation results of the proposed VAD method. Finally, Section 4.3 concludes the proposed VAD research and reviews possible future research directions.

4.1 Problem Formulation

In this section, we elaborate the discussion on the theory of the proposed algorithm. The proposed VAD system utilizes spectral clustering [32] and diffusion kernel [71] methods in order to find a novel way of calculating a similarity matrix.

Let $x_{\mathrm{sp}}(n)$ denote a speech signal and let $x_{\mathrm{tr}}(n)$ and $x_{\mathrm{st}}(n)$ denote additive interfering transient and stationary noise signals, respectively. The microphone input signal is given by

$$y(n) = x_{\mathrm{sp}}(n) + x_{\mathrm{tr}}(n) + x_{\mathrm{st}}(n). \tag{4.1}$$

The proposed VAD algorithm generates a cloud of samples for each short frame (approximately 20 ms long) of the input signal, calculates MFCCs for each sample in order to from an MFCC matrix. Then, the algorithm calculates a covariance matrix for each frame. The covariance matrix adds additional factor of similarity between frames, which is utilized for the calculation of a similarity matrix.

4.1.1 Sample Cloud

Given an audio input signal, the algorithm divides it into N frames, approximately 20 ms long. A moving window of size M is then utilized in order to generate i new samples of the frame. Every sample of the frame is regarded as an iteration of the generation process for the sample cloud given by

$$\hat{y}_j(n-k) = y(n) \cdot w_M(n-k-M \cdot (j-1) + \frac{i}{2}),\ k = 1, ..., i \tag{4.2}$$

where $\hat{y}_j(n-k)$ is the generated sample cloud of the j-th frame (out of N), $y(n)$ is the original signal, w_M is the moving window of size M, i is the desired number of samples per frame and k is the current iteration index. For every iteration k of the sample cloud, the algorithm calculates m MFCCs. MFCCs are coefficients that form a representation of the short-term power spectrum of a sound. MFCC is based on a linear cosine transformation of a log power spectrum on a non-linear Mel scale frequency, thus convenient for human auditory applications. An $m \times i$ matrix of MFCCs is created in this fashion for each frame of the N frames. Finally, for each of the MFCC matrices the algorithm calculates a $m \times m$ covariance matrix.

Let $\boldsymbol{X}_m^j$ be the $m \times i$ matrix of MFCCs of the j-th frame. The covariance matrix for the j-th frame is given by

$$\boldsymbol{\Sigma} = \mathbb{E}\left(\left(\boldsymbol{X}_m^j - \mathbb{E}\left(\boldsymbol{X}_m^j\right)\right)\left(\boldsymbol{X}_m^j - \mathbb{E}\left(\boldsymbol{X}_m^j\right)\right)^T\right) \tag{4.3}$$

Where $\mathbb{E}$ denotes the expected value of a matrix. With the covariance matrix $\boldsymbol{\Sigma}$, we find the correlation between samples in the sample cloud.

4.1.2 Similarity Matrix

The most important part of the proposed VAD algorithm is the similarity matrix. The similarity matirx is utilized in order to effectively cluster the data and label it as speech or non-speech. Given an audio input signal composed of a combination of speech, stationary noise and transient noise components (i.e., $x_{\mathrm{sp}}(n)$, $x_{\mathrm{st}}(n)$ and $x_{\mathrm{tr}}(n)$, respectively), we choose absolute value of MFCCs and the arithmetic mean of the log-likelihood ratios for the individual frequency bins as the feature space, as in [32].

Let $\boldsymbol{Y}_m(t,k)$ $(t = 1,...,N; k = 1,...,K_m)$ and $\boldsymbol{Y}_s(t,k)$ $(t = 1,...,N; k = 1,...,K_s)$ be the absolute value of the MFCC and the STFT coefficients in a given time frame, respectively. Both MFCC and STFT coefficients are computed in K_m and K_s frequency bins, respectively. Then, each frame is represented by a column vector of dimension $(K_m + 1)$ defined as follows

$$\boldsymbol{Y}(:,t) = \begin{bmatrix} \boldsymbol{Y}_{\mathrm{m}}(:,t) \\ \Lambda_{\mathrm{t}} \end{bmatrix} \tag{4.4}$$

where $\boldsymbol{Y}_{\mathrm{m}}(:,t)$ denotes the absolute value of MFCCs in a specific time frame t. Λ_{t} denotes the arithmetic mean of the log-likelihood ratios for frame t. The expression combines various statistical calculations on the noise in the training stage as well as STFT coefficients of the input audio signal. Λ_{t} is given by

$$\Lambda_t = \frac{1}{K_s} \sum_{k=1}^{K_s} \left(\frac{\gamma_k(t)\,\xi_k(t)}{1+\xi_k(t)} - \log\left(1+\xi_k(t)\right) \right) \tag{4.5}$$

where $\xi_k(t) = \lambda_s(t,k)/\lambda_N(t,k)$ and $\gamma_k(t) = |\boldsymbol{Y}_s(t,k)|^2/\lambda_N(t,k)$ denote the a-priori and a-posteriori SNR [42], respectively. $\lambda_s(t,k)$ denotes the variance of speech signal in the k-th frequency bin of the t-th frame and $\lambda_N(t,k)$ denotes the variance of stationary noise in t-th time frame and k-th frequency bin.

Combining (4.3)-(4.5), we can now define the expression for the similarity matrix

$$\boldsymbol{W}_\theta^\ell(i,j) = \exp\left(\sum_{p=-P}^{P} -\alpha_{\mathrm{p}} \boldsymbol{Q}(i+p, j+p) \right) \tag{4.6}$$

$$\begin{aligned}
&\boldsymbol{Q}\left(i,j\right) = \\
&\left[\boldsymbol{Y}_{\mathrm{m}}^{\ell}(:,i)\left(1-\exp\left(-\Lambda_{\mathrm{i}}^{\ell}/\varepsilon\right)\right)-\boldsymbol{Y}_{\mathrm{m}}^{\ell}(:,j)\left(1-\exp\left(-\Lambda_{\mathrm{j}}^{\ell}/\varepsilon\right)\right)\right] \\
&\cdot\left(\boldsymbol{\Sigma}_{i}^{\ell}+\boldsymbol{\Sigma}_{j}^{\ell}\right)^{\dagger} \\
&\cdot\left[\boldsymbol{Y}_{\mathrm{m}}^{\ell}(:,i)\left(1-\exp\left(-\Lambda_{\mathrm{i}}^{\ell}/\varepsilon\right)\right)-\boldsymbol{Y}_{\mathrm{m}}^{\ell}(:,j)\left(1-\exp\left(-\Lambda_{\mathrm{j}}^{\ell}/\varepsilon\right)\right)\right]^{T}
\end{aligned} \tag{4.7}$$

where $\boldsymbol{\theta} = [\epsilon, \alpha_{-P}, \alpha_{-P+1}, \cdots, \alpha_{P-1}, \alpha_P] \in \mathrm{R}^{2P+2}$ is a vector of system parameters, $\boldsymbol{Y}_{\mathrm{m}}^{\ell}(:,i)$, $\Lambda_{\mathrm{i}}^{\ell}$ and $\boldsymbol{\Sigma}_{\mathrm{i}}^{\ell}$ are the absolute value of the MFCC, the arithmetic mean of the log-likelihood ratio and the covariance matrix of the i-th frame in the ℓ-th sequence, respectively, ϵ is the kernel width obtained during the training stage and † denotes the pseudo-inverse of a matrix. The main motivation behind the proposed similarity matrix calculation in (4.7) is finding a model for the signal generating system, i.e. the speech system of the speaker. With the new representation, we gain a smaller degree of freedom for the system model. We tag the system as a "black box" and try to find a model for the system by viewing its' outputs. In fact, a second order approximation is applied on the parameters in order to receive random Gaussian perturbations. A covariance matrix is then calculated and used in order to express a Jacobian matrix. Finally, the Jacobian is used in order to find a similarity matrix. In order to calculate the pseudo-inverse of the expression $\boldsymbol{\Sigma}_{\mathrm{i}}^{\ell}+\boldsymbol{\Sigma}_{\mathrm{j}}^{\ell}$ in (4.7), we use the first three largest eigenvectors received in singular vector decomposition (SVD).

Let $\boldsymbol{\Sigma}$ be a covarince matrix as in (4.3), applying SVD yields

$$\boldsymbol{\Sigma}^{\dagger} = \boldsymbol{V}\boldsymbol{S}^{\dagger}\boldsymbol{\Delta}^{T} \tag{4.8}$$

Where $\boldsymbol{\Delta}$ is an orthogonal matrix of size $3 \times N$, the columns of $\boldsymbol{\Delta}$ are the eigenvectors of $\boldsymbol{\Sigma}\boldsymbol{\Sigma}^{T}$. $\boldsymbol{S}$ is a diagonal matrix at the same size of $\boldsymbol{\Sigma}$, its' values are the square roots of the non-zero eigenvalues of both $\boldsymbol{\Sigma}\boldsymbol{\Sigma}^{T}$ and $\boldsymbol{\Sigma}^{T}\boldsymbol{\Sigma}$. $\boldsymbol{V}$ is an orthogonal matrix, the same size of $\boldsymbol{\Delta}$. The columns of $\boldsymbol{V}$ are the eigenvectors of $\boldsymbol{\Sigma}^{T}\boldsymbol{\Sigma}$.

4.1.3 Training Stage

The training algorithm in our research is based on [32]. Given databases of clean speech, transient noise and stationary noise signals, We choose L different signals from each database. Without loss of generality, we take the ℓ-th speech signal, transient noise and

stationary noise and combine them as in Fig. 4.1. We assume that all of these signal are of the same length of N_ℓ. With the new database and by utilizing (4.4) and (4.5), we

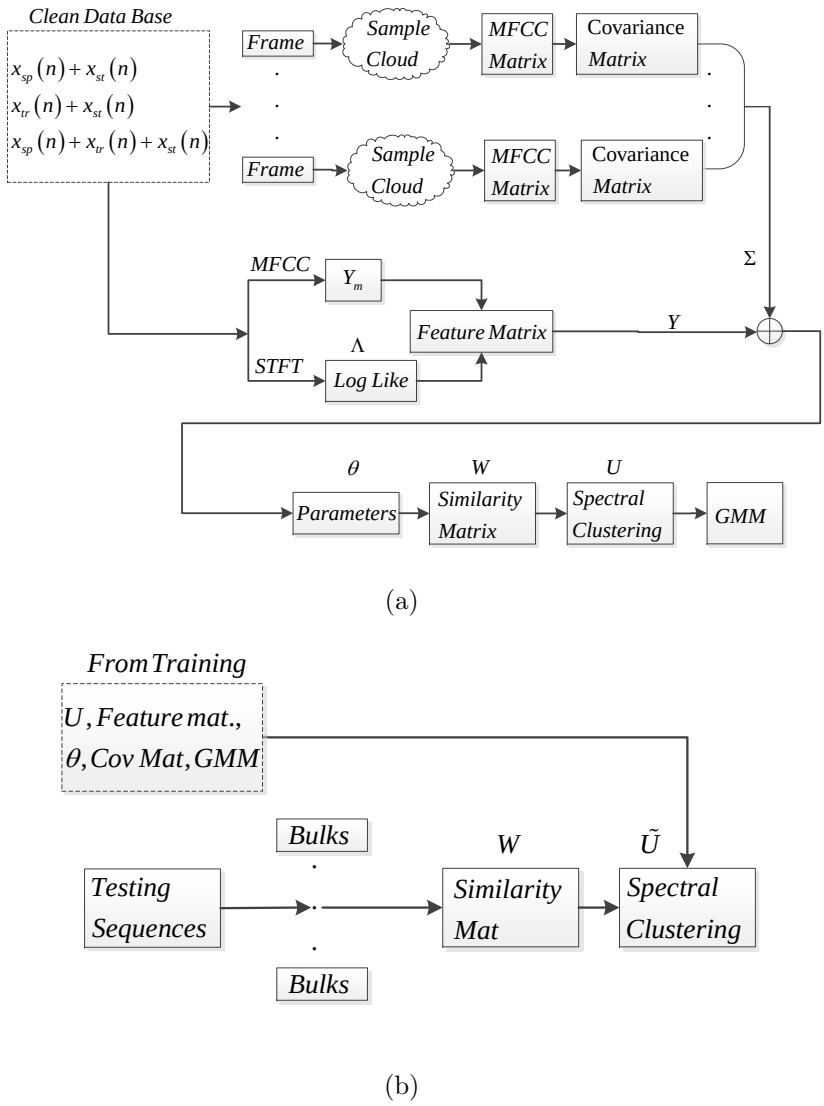

Figure 4.1: A block scheme of the proposed (a) training, and (b) testing stages.

extract the feature matrix $\boldsymbol{Y}_1^\ell$, $\boldsymbol{Y}_2^\ell$, $\boldsymbol{Y}_3^\ell$. By concatenating the feature matrix, we build the ℓ-th training sequence, $\boldsymbol{Y}^\ell$, as shown in Fig. 4.1. For each frame t, in the training sequence ℓ we compute an indicator matrix $\boldsymbol{C}_{\mathrm{t}}^\ell$ in order to indicate a speech containing frame. For further discussion, see [32].

Next, we define a kernel which preserves the similarity between points, as the similarity matrix in (4.6) and (4.7). This metric guarantees small similarity between two frames

of different classes, i.e., speech and transient noise, even if they are very similar to each other (in the Euclidean sense). This is enabled due the large distance between neighboring frames. Upon defining the parametric weight function, the parameters can be obtained by solving the following optimization problem [44]:

$$\boldsymbol{\theta}^{opt} = \arg\min_{\theta} \frac{1}{L} \sum_{\ell=1}^{L} F(\boldsymbol{W}_{\boldsymbol{\theta}}^{\ell}, \boldsymbol{C}^{\ell}) \tag{4.9}$$

$$F(\boldsymbol{W}, \boldsymbol{C}) = \frac{1}{2} \left\| \boldsymbol{\Upsilon}\boldsymbol{\Upsilon}^T - \boldsymbol{D}^{1/2}\boldsymbol{C}(\boldsymbol{C}^T\boldsymbol{D}\boldsymbol{C})^{-1}\boldsymbol{C}^T\boldsymbol{D}^{1/2} \right\|_F^2 \tag{4.10}$$

where $\boldsymbol{\Upsilon}$ is an approximate orthonormal basis of the projections on the second principal subspace of $\boldsymbol{D}^{-1/2}\boldsymbol{W}\boldsymbol{D}^{-1/2}$.

Let $\boldsymbol{W}_{\boldsymbol{\theta}^{opt}}^{\ell}$ be the similarity matrix of the ℓ-th training sequence and $\boldsymbol{U}_{\ell}$ be a matrix consisting of the two eigenvectors of $\boldsymbol{D}^{\ell^{-1/2}}\boldsymbol{W}^{\boldsymbol{\ell}}\boldsymbol{D}^{\ell^{-1/2}}$ corresponding to the first two largest eigenvalues, where $\boldsymbol{D}$ is a diagonal matrix whose i-th diagonal element equals to $\sum_{j=1}^{N} \boldsymbol{W}(i,j)$. We then define $\boldsymbol{U}$ as the column concatenation of $\boldsymbol{U}_1$ through $\boldsymbol{U}_L$. $\boldsymbol{U}$ is a new representation of the training data such that each row of U corresponding to a specific training frame. For further information, see [32].

We use Gaussian mixture modeling to model each cluster, i.e., label as speech presence or absence, with a different Gaussian Mixture Model (GMM). This means that we model the low dimensional representation of the original data using two different GMMs, one for each cluster. Let $f(\cdot;\mathcal{H}_0)$ and $f(\cdot;\mathcal{H}_1)$ be the probability density function corresponding to speech absence and presence frames, respectively. The likelihood ratio for each labeled frame t is then obtained by

$$\Gamma_{\mathrm{t}}^{\mathrm{train}} = \frac{f(\boldsymbol{U}(t,:);\mathcal{H}_1)}{f(\boldsymbol{U}(t,:);\mathcal{H}_0)} \tag{4.11}$$

where $\boldsymbol{U}(t,:)$ is the t-th row of the matrix $\boldsymbol{U}$, and $\mathcal{H}_1$ and $\mathcal{H}_0$ are the speech presence and absence hypotheses, respectively.

4.1.4 Testing Stage

The main goal of the testing stage is to to cluster the unlabeled data and decide whether a given unlabled frame contains speech or not. In order to compute the likelihood ratio for a new unlabled frame, [32] utilizes GMM to model the eigenvectors of normalized

Laplacian matrix.

$$\Gamma_{\mathrm{t}}^{\mathrm{test}} = \frac{f(\tilde{\boldsymbol{U}}(t,:);\mathcal{H}_1)}{f(\tilde{\boldsymbol{U}}(t,:);\mathcal{H}_0)} \tag{4.12}$$

where $\tilde{\boldsymbol{U}}(t,:)$ is the t-th row of the new representation of the unlabeled data in terms of eigenvectors of the normalized Laplacian of the similarity matrix. In [40] it was shown that using the information supplied by neighboring frames can improve the performance of VAD algorithms. The improvement is enabled due to the fact that frames containing speech signal are usually followed by a frame that contains speech signal as well. In the contrary, transient signals usually last for a single time frame. Using this fact, the decision rule for an unlabeled time frame is obtained by:

$$\mathrm{VA}_t = \sum_{j=-J}^{J} \Gamma_{t+j} \underset{\boldsymbol{\mathcal{H}}_0}{\overset{\boldsymbol{\mathcal{H}}_1}{\gtrless}} T_h \qquad t = 1, 2, \cdots, T \tag{4.13}$$

where T_h is a threshold which controls the tradeoff between probability of detection and false alarm. Increasing (decreasing) this parameter leads to a decrease (increase) of both the probability of false alarm and the probability of detection. Both the training and testing stages are summarized in Table 4.1. The block schemes of both learning and testing stage are depicted in Fig. 4.1.

4.2 Simulations Results

In this section we demonstrate the performance and advantages of the proposed VAD algorithm via several simulations. We compare the results acquired to the results of the VAD algorithm proposed in [32]. We run the simulations for various SNR values, stationary noises and transient noises. We confiugre the number of sequences to 4 training sequences and 20 testing sequences. Speech signals are taken from the TIMIT database [72], and transient noise signals are taken from [73]. The sampling frequency is set to 16kHz. Furthermore, we pick a window of size 512 for STFT calculations, $m = 14$ mel-frequency bands, $M = 257$ as the size of the moving window to utilize in order to create the sample cloud and $i = 45$ as the number of samples for each frame. The graphs of probability of detection, P_d, vs. probability of false alarm, P_{Fa}, are depicted in Fig 4.2.

We use identical experiment conditions with both the proposed algorithm and [32] in every simulation. In Fig 4.3, we provide the clustering results, i.e. the U space representation where speech labeled data is marked with blue rings and non-speech data is marked with red crosses. The proposed VAD algorithm has superior performance in the entire SNR range, especially for low SNR values. Moreover, the proposed algorithm performs better in cases of very small training sets.

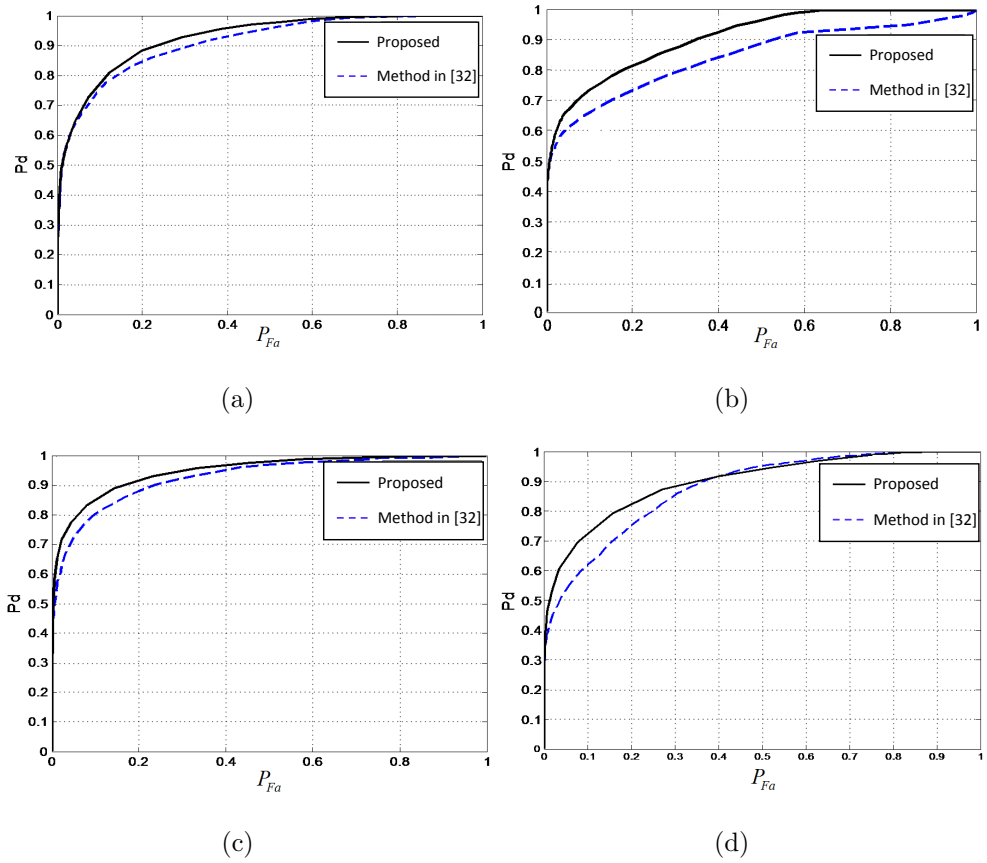

Figure 4.2: Probability of detection (P_{d}) versus probability of false alarm (P_{fa}), for various noise environments. (a) Babble noise with SNR of 5dB, and transient noise of door knocks. (b) White noise with SNR of 5dB, and transient noise of door knocks. (c) White noise with SNR of 10dB, and transient noise of typing. (d) Babble noise with SNR of 5dB, and transient noise of typing.

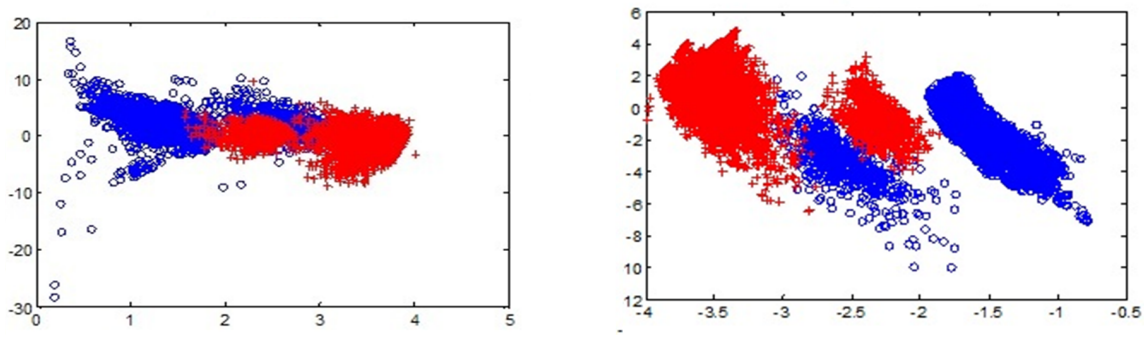

(a) (b)

Figure 4.3: Clustering results of training stage for babble noise with SNR of 5dB, and transient noise of typing of (a) the proposed algorithm, and (b) the algorithm proposed in [44].

4.3 Conclusions

We have presented a VAD algorithm based on spectral clustering and diffusion kernel methods. The main challenge was providing good results in presence of environmental noise and transient noise in particular. The key features of the proposed algorithm are the covariance matrix calculations via sample clouds and the novel similarity matrix computations. We demonstrated better results compared to a work that has already been proven to be superior to conventional methods of dealing transient noises, especially in cases of low SNR and small data bases. The goal in the near future would be trying to improve the algorithm's results using enhanced features. Another possible research direction would be choosing better parameters for the GMM.

Table 4.1: Proposed Voice Activity Detection Algorithm Based on Spectral Clustering Method.

Learning algorithm:

1. Construct a training data set consisting of L training signals $\{\boldsymbol{Y}^{\ell} \in \mathrm{R}^{K_m+1\times 3N^{\ell}}; \ell = 1, ..., L\}$ and L indicator vectors $\{\boldsymbol{C}^{\ell} \in \mathrm{R}^{3N^{\ell}\times 4}; \ell = 1, ..., L\}$.
2. Solve the optimization problem given in (4.9), to find the optimum value of the parameters (i.e. $\boldsymbol{\theta}^{opt}$).
3. Construct $\boldsymbol{U}$ by concatenation of U^1 through U^L K largest eigenvectors of $\boldsymbol{D}^{-1/2}\boldsymbol{W}\boldsymbol{D}^{-1/2}$.
4. Fit a GMM model to the rows of $\boldsymbol{U}$ for each cluster (see ([32])).

Output:

$\boldsymbol{U}$, $f(\cdot;\boldsymbol{\mathcal{H}}_1)$ and $f(\cdot;\boldsymbol{\mathcal{H}}_0)$

Testing Procedure:

Let $z_t(n)$ be the test sequence and $\boldsymbol{Z}_t$ the feature matrix of t-th unlabeled frame obtained by (4.5).

for $t = 0 : T : N^z - T$ $(T \ll N^z)$

1. $\boldsymbol{Z} = \boldsymbol{Z}_t(:, t+1 : t+P)$.
2. Compute $\boldsymbol{B}$ by
   $\boldsymbol{B}^{\ell}_{\boldsymbol{\theta}^{opt}}(i,j) = \exp\left(\sum_{p=-P}^{P} -\alpha_p^{opt}\boldsymbol{Q}^{\ell}(i+p, j+p)\right)$
   $\boldsymbol{B} = \left[(\boldsymbol{B}^1_{\boldsymbol{\theta}^{opt}})^T, (\boldsymbol{B}^2_{\boldsymbol{\theta}^{opt}})^T, \cdots, (\boldsymbol{B}^L_{\boldsymbol{\theta}^{opt}})^T\right]^T$
3. Compute the new representation of the unlabeled data (4.12)
   $\tilde{\boldsymbol{U}} = \mathrm{diag}\left((\boldsymbol{1}\boldsymbol{B}_{k_{nn}})^{-1}\right)\boldsymbol{B}^T_{k_{nn}}\boldsymbol{U}$.
4. Compute the likelihood ratio for a new unlabeled frame
   $\Gamma_t = \frac{f(\tilde{U}(t,:);\boldsymbol{\mathcal{H}}_1)}{f(\tilde{U}(t,:);\boldsymbol{\mathcal{H}}_0)}$.
5. The decision rule for an unlabeled time frame is given
   $$\mathrm{VA}_t = \sum_{j=-J}^{J}\Gamma_{t+j} \underset{\boldsymbol{\mathcal{H}}_0}{\overset{\boldsymbol{\mathcal{H}}_1}{\gtrless}} T_h \quad .$$
6. Use VA_t to obtain the final VAD decision.

end

Chapter 5

Conclusion

5.1 Summary

In this thesis, we have addressed the problem of speech enhancement systems in presence of environmental noise, and presented two methods for overcoming this problem. The first, a supervised learning algorithm for voice activity detection based on representation of speech signals by spectral clustering, i.e., labeling, separating speech and non speech frames. This algorithm is composed of learning and testing stages: A sample cloud is produced for every signal frame by utilizing a moving window. MFCCs are then calculated for every sample in the cloud in order to produce an MFCC matrix and subsequently a covariance matrix for every frame. Utilizing the covariance matrix, we calculate a similarity matrix using spectral clustering and diffusion kernels methods. Using the similarity matrix, we cluster the data and transform it to a new space where each point is labeled as speech or nonspeech. We then use a GMM in order to build a statistical model for labeling data as speech or nonspeech. The main challenge was providing good results in presence of environmental noise and transient noise in particular. The key features of the proposed algorithm are the covariance matrix calculations via sample clouds and the novel similarity matrix computations. We demonstrated better results compared to a work that has already been proven to be superior to conventional methods of dealing transient noises, especially in cases of low SNR and Simulation results demonstrate its advantages compared to a recent VAD algorithm [32].

The second method is a constant beamwidth beamfromer. The proposed approach

utilizes custom-tailored FIR filters for each microphone channel, manipulating the beampatterns beamwidths. The manipulated beampatterns have a constant beamwidth over a range of frequencies in a wideband. Additionally, a post summing output normalization filter is used to ensure a frequency invariant gain of the beampattern. By exploiting the physical microphone array configuration and attributes, we shape accordingly the frequency response of the FIR filters and eventually control the beamformer beamwidth. The proposed approach demonstrates improved array response results in various scenarios, compared to available methods in the field [16,20,63], especially in terms of sensitivity to parameters mismatch, noise robustness and side-lobe attenuation.

First, an input FIR filter array is designed to obtain a fixed main-lobe width, in a wide frequency band. Then, an output FIR normalizing filter is designed to keep a fixed gain over that band. The proposed design method achieves an approximation to a constant beamwidth output response, with better side-lobe attenuation performance and robustness to array mismatches, as compared to other methods examined. The new method is based on designing the FIR filter array such that its frequency response reduces the number, of what we call, "effective microphones", when signal frequency increases, affecting an approximate fixed beamwidth in a wide band of frequencies. Simulations of the proposed beamformer also demonstrate better side-lobe attenuation and sensitivity performance, especially at the lower frequency spectrum. Moreover, the proposed algorithm offers a small deviation from the desired beamwidth in a wide band as well as low computational complexity due to its simple closed form FIR filter design procedure. Additionally, we have shown that when inducing random microphone gain and location inaccuracies, the proposed algorithm produces steady beampatterns throughout the frequency spectrum.

5.2 Future Research

This thesis unveils numerous possible research directions that can be studied:

1. The two speech enhancement methods proposed in this research thesis, i.e., the VAD system and constant beamwidth beamformer were individually researched. Integrating these two systems, as shown in Fig. 1.1, could yield a speech enhancement system robust to environmental noises. The beamformer degree would filter signals from undesired directions, effectively attenuating interference, noise and signals other than the desired signal. The VAD degree would further enhance the input signal since it would determine a desired speech signal from an undesired environmental noise, even if they originate from the same direction. In addition, this method would enable better power efficiency thanks to the fact that it would operate only when a desired signal from a desired direction is present.

2. A source localization system could also be implemented by integrating these two methods. Source localization is necessary for applications as automatic beamformer steering for suppressing noise and reverberation. Directing the main-lobe to a desired direction could be done by adding appropriate delays or phase shifts. This ability is necessary especially in applications where not only the location of the source is needed but also the ability to know when the source was active, as in teleconferencing and automatic video tracking. The straight-forward design of the beamformer allows us to easily introduce the delays or phase shifts that are required for the beam steering.

3. Research of an algorithm that would find the optimal placing of microphones in space so that the beamformer preformance specifications can be met. Most microphone array design algorithm dictate the placing of the array microphones and force a specific geometry, e.g., ULA and circular arrays. In many cases, this drags substential handicaps on the beamformer capabilities and performance. For instance, ULAs can only handle one source direction at a time resulting in uncertainties and possibly direction ambiguities. Therefore, ULA configurations must be ruled out when handling several signal sources. A novel beamformer design method that is

based on optimization can be researched. This method would take into consideration only the desired beamformer specification, e.g., the desired beamwidth or frequency range of interest, and would derive the placing of the microphones to achieve these desired specifications. Optimization of the microphone placings in space is a nonlinear, non-convex optimization problem. Thus, simple optimization methods would not give the best results. Genetic algorithms have been researched to find solutions in nonlinear, non-convex scenarios where conventional methods do not provide sufficient results [74]. Genetic algorithm research in the field of beamforming and microphone placing in particular was recently done [75]. Yet, it is a small niche in the world of array processing and much additional contribution can be made.

Bibliography

[1] J. Ming, T. J. Hazen, J. R. Glass, D. Reynolds *et al.*, "Robust speaker recognition in noisy conditions," *IEEE Transactions on Audio, Speech, and Language Processing*, vol. 15, no. 5, pp. 1711–1723, 2007.

[2] I. Cohen, "Noise spectrum estimation in adverse environments: Improved minima controlled recursive averaging," *IEEE Transactions on Speech and Audio Processing*, vol. 11, no. 5, pp. 466–475, 2003.

[3] T. Van den Bogaert, S. Doclo, J. Wouters, and M. Moonen, "Speech enhancement with multichannel wiener filter techniques in multimicrophone binaural hearing aids," *The Journal of the Acoustical Society of America*, vol. 125, no. 1, pp. 360–371, 2009.

[4] R. Martin, *Statistical methods for the enhancement of noisy speech.* Springer, 2005.

[5] Y. Ephraim and I. Cohen, "15.2 recent advancements in speech enhancement," *Circuits, Signals, and Speech and Image Processing*, 2006.

[6] Y. Ephraim and H. L. Van Trees, "A signal subspace approach for speech enhancement," *IEEE Transactions on Speech and Audio Processing*, vol. 3, no. 4, pp. 251–266, 1995.

[7] M. Mouly, M.-B. Pautet, and T. Foreword By-Haug, *The GSM system for mobile communications.* Telecom publishing, 1992.

[8] A. Benyassine, E. Shlomot, H. Y. Su, D. Massaloux, C. Lamblin, and J.-P. Petit, "Itu-t recommendation g. 729 annex b: a silence compression scheme for use with g. 729 optimized for v. 70 digital simultaneous voice and data applications," *IEEE Communications Magazine*, vol. 35, no. 9, pp. 64–73, 1997.

[9] C. Zhang, D. Florêncio, D. E. Ba, and Z. Zhang, "Maximum likelihood sound source localization and beamforming for directional microphone arrays in distributed meetings," *IEEE Transactions on Multimedia*, vol. 10, no. 3, pp. 538–548, 2008.

[10] M. Valente and K. M. Mispagel, "Unaided and aided performance with a directional open-fit hearing aid," *International Journal of Audiology*, vol. 47, no. 6, pp. 329–336, 2008.

[11] S. Markovich, S. Gannot, and I. Cohen, "Multichannel eigenspace beamforming in a reverberant noisy environment with multiple interfering speech signals," *IEEE Transactions on Audio, Speech, and Language Processing*, vol. 17, no. 6, pp. 1071–1086, 2009.

[12] E. Habets, J. Benesty, I. Cohen, S. Gannot, and J. Dmochowski, "New insights into the mvdr beamformer in room acoustics," *IEEE Transactions on Audio, Speech, and Language Processing*, vol. 18, no. 1, pp. 158–170, 2010.

[13] D. Van Compernolle, "Switching adaptive filters for enhancing noisy and reverberant speech from microphone array recordings," pp. 833–836, 1990.

[14] R. G. Lorenz and S. P. Boyd, "Robust minimum variance beamforming," *IEEE Transactions on Signal Processing*, vol. 53, no. 5, pp. 1684–1696, 2005.

[15] Y. Bucris, I. Cohen, and M. Doron, "Bayesian focusing for coherent wideband beamforming," *IEEE Transactions on Audio, Speech, and Language Processing*, vol. 20, no. 4, pp. 1282–1296, 2012.

[16] G. Doblinger, "Optimization of wideband fixed beamformers with adaptive sensor calibration," *18th European Signal Processing Conference*, pp. 2062–2066, 2010.

[17] T. Yardibi, J. Li, P. Stoica, M. Xue, and A. B. Baggeroer, "Source localization and sensing: A nonparametric iterative adaptive approach based on weighted least squares," *IEEE Transactions on Aerospace and Electronic Systems*, vol. 46, no. 1, pp. 425–443, 2010.

[18] Y. Zhao, W. Liu, and R. Langley, "A least squares approach to the design of frequency invariant beamformers," *Proceedings of European Signal Processing Conference, Glasgow, Scotland*, pp. 844–848, 2009.

[19] S. Yan and Y. Ma, "Design of fir beamformer with frequency invariant patterns via jointly optimizing spatial and frequency responses," *IEEE International Conference on Acoustics, Speech, and Signal Processing 2005 (ICASSP'05)*, vol. 4, pp. 789–792, 2005.

[20] L. C. Parra, "Steerable frequency-invariant beamforming for arbitrary arrays," *The Journal of the Acoustical Society of America*, vol. 119, p. 3839, 2006.

[21] S. Yan, "Optimal design of fir beamformer with frequency invariant patterns," *Applied Acoustics*, vol. 67, no. 6, pp. 511–528, 2006.

[22] S. Yan, H. Sun, X. Ma, U. Svensson, and C. Hou, "Time-domain implementation of broadband beamformer in spherical harmonics domain," *IEEE Transactions on Audio, Speech, and Language Processing*, vol. 19, no. 5, pp. 1221–1230, 2011.

[23] S. Doclo and M. Moonen, "Design of far-field and near-field broadband beamformers using eigenfilters," *Signal Processing*, vol. 83, no. 12, pp. 2641–2673, 2003.

[24] W. Liu and S. Weiss, *Wideband beamforming: concepts and techniques.* John Wiley & Sons, 2010, vol. 17.

[25] D. B. Ward, R. A. Kennedy, and R. C. Williamson, "Fir filter design for frequency invariant beamformers," *IEEE Signal Processing Letters*, vol. 3, no. 3, pp. 69–71, 1996.

[26] J. Sohn, N. S. Kim, and W. Sung, "A statistical model-based voice activity detection," *IEEE Signal Processing Letters*, vol. 6, no. 1, pp. 1–3, 1999.

[27] J.-H. Chang and N. S. Kim, "Voice activity detection based on complex laplacian model," *IET Electronics Letters*, vol. 39, no. 7, pp. 632–634, 2003.

[28] I. Cohen, B. Berdugo, "Noise estimation by minima controlled recursive averaging for robust speech enhancement," *IEEE Signal Processing Letters*, vol. 9, no. 1, pp. 12–15, 2002.

[29] I. Cohen and B. Berdugo, "Speech enhancement for non-stationary noise environments," *Signal processing*, vol. 81, no. 11, pp. 2403–2418, 2001.

[30] R. Talmon, I. Cohen, and S. Gannot, "Single-channel transient interference suppression with diffusion maps," *IEEE Transactions on Audio, Speech, and Language Processing*, vol. 21, no. 1, pp. 132–144, 2013.

[31] I. Cohen, "Multichannel post-filtering in nonstationary noise environments," *IEEE Transactions on Signal Processing*, vol. 52, no. 5, pp. 1149–1160, 2004.

[32] S. Mousazadeh and I. Cohen, "Voice activity detection in presence of transient noise using spectral clustering," *IEEE Transactions on Audio, Speech, and Language Processing*, vol. 21, no. 6, pp. 1261–1271, 2013.

[33] J. Benesty, J. Chen, and Y. Huang, *Microphone array signal processing.* Springer Science & Business Media, 2008, vol. 1.

[34] E. A. Habets, S. Gannot, and I. Cohen, "Dual-microphone speech dereverberation in a noisy environment," pp. 651–655, 2006.

[35] D. Pavlidi, A. Griffin, M. Puigt, and A. Mouchtaris, "Real-time multiple sound source localization and counting using a circular microphone array," *IEEE Transactions on Audio, Speech, and Language Processing*, vol. 21, no. 10, pp. 2193–2206, 2013.

[36] W. Liu and S. Weiss, "Design of frequency invariant beamformers for broadband arrays," *IEEE Transactions on Signal Processing*, vol. 56, no. 2, pp. 855–860, 2008.

[37] H. L. Van Trees, *Detection, Estimation, and Modulation Theory, Optimum Array Processing.* John Wiley & Sons, 2004.

[38] M. M. Goodwin and G. W. Elko, "Constant beamwidth beamforming," vol. 1, pp. 169–172, 1993.

[39] C. Clinch, "Time assignment speech interpolation (tasi)," *The Post Office Electrical Engineers Journal*, vol. 53, no. 3, pp. 197–200, 1960.

[40] J. Ramírez, J. C. Segura, C. Benítez, L. García, and A. Rubio, "Statistical voice activity detection using a multiple observation likelihood ratio test," *IEEE Signal Processing Letters*, vol. 12, no. 10, pp. 689–692, 2005.

[41] S. Mousazadeh and I. Cohen, "Ar-garch in presence of noise: parameter estimation and its application to voice activity detection," *IEEE Transactions on Audio, Speech, and Language Processing*, vol. 19, no. 4, pp. 916–926, 2011.

[42] Y. Ephraim and D. Malah, "Speech enhancement using a minimum-mean square error short-time spectral amplitude estimator," *IEEE Transactions on Acoustics, Speech and Signal Processing*, vol. 32, no. 6, pp. 1109–1121, 1984.

[43] R. Talmon, I. Cohen, and S. Gannot, "Clustering and suppression of transient noise in speech signals using diffusion maps," *IEEE International Conference on Acoustics, Speech and Signal Processing 2011 (ICASSP'11.)*, pp. 5084–5087, 2011.

[44] F. R. Bach and M. I. Jordan, "Multichannel post-filtering in nonstationary noise environments," *Journal of Machine Learning Research*, vol. 7, pp. 1963–2001, 2006.

[45] J. Capon, "High-resolution frequency-wavenumber spectrum analysis," *Proceedings of the IEEE*, vol. 57, no. 8, pp. 1408–1418, 1969.

[46] D. Johnson and S. DeGraaf, "Improving the resolution of bearing in passive sonar arrays by eigenvalue analysis," *IEEE Transactions on Acoustics, Speech and Signal Processing*, vol. 30, no. 4, pp. 638–647, 1982.

[47] G. C. McLaskey, S. D. Glaser, and C. U. Grosse, "Beamforming array techniques for acoustic emission monitoring of large concrete structures," *Journal of Sound and Vibration*, vol. 329, no. 12, pp. 2384–2394, 2010.

[48] S. Fischer and K. U. Simmer, "Beamforming microphone arrays for speech acquisition in noisy environments," *Speech communication*, vol. 20, no. 3, pp. 215–227, 1996.

[49] R. C. de Lamare, L. Wang, and R. Fa, "Adaptive reduced-rank lcmv beamforming algorithms based on joint iterative optimization of filters: Design and analysis," *Signal processing*, vol. 90, no. 2, pp. 640–652, 2010.

[50] D. B. Ward, Z. Ding, and R. A. Kennedy, "Broadband doa estimation using frequency invariant beamforming," *IEEE Transactions on Signal Processing*, vol. 46, no. 5, pp. 1463–1469, 1998.

[51] W. Liu, S. Weiss, J. G. McWhirter, and I. K. Proudler, "Frequency invariant beamforming for two-dimensional and three-dimensional arrays," *Signal Processing*, vol. 87, no. 11, pp. 2535–2543, 2007.

[52] A. Khabbazibasmenj, S. Vorobyov, and A. Hassanien, "Robust adaptive beamforming based on steering vector estimation with as little as possible prior information," *IEEE Transactions on Signal Processing*, vol. 60, no. 6, pp. 2974–2987, 2012.

[53] M. Crocco and A. Trucco, "Design of robust superdirective arrays with a tunable tradeoff between directivity and frequency-invariance," *IEEE Transactions on Signal Processing*, vol. 59, no. 5, pp. 2169–2181, 2011.

[54] W. Liu, "Adaptive wideband beamforming with sensor delay-lines," *Signal Processing*, vol. 89, no. 5, pp. 876–882, 2009.

[55] Y. I. Wu, K. T. Wong, X. Yuan, S.-k. Lau, and S.-k. Tang, "A directionally tunable but frequency-invariant beamformer on an acoustic velocity-sensor triad to enhance speech perception," *The Journal of the Acoustical Society of America*, vol. 131, p. 3891, 2012.

[56] W. Liu and S. Weiss, "New class of broadband arrays with frequency invariant beam patterns," *IEEE International Conference on Acoustics, Speech, and Signal Processing 2004 (ICASSP'04)*, vol. 2, pp. 185–188, 2004.

[57] W. Zhu and W. Wu, "Design of wide-band array with frequency invariant beam pattern by using adaptive synthesis method," *IEEE International Conference on Image Analysis and Signal Processing (IASP) 2011*, pp. 688–693, 2011.

[58] Y. Zhao, W. Liu, and R. J. Langley, "Efficient design of frequency invariant beamformers with sensor delay-lines," pp. 335–339, 2008.

[59] J. Li, P. Stoica, and Z. Wang, "On robust capon beamforming and diagonal loading," *IEEE Transactions on Signal Processing*, vol. 51, no. 7, pp. 1702–1715, 2003.

[60] D. Feldman and L. Griffiths, "A projection approach for robust adaptive beamforming," *IEEE Transactions on Signal Processing*, vol. 42, no. 4, pp. 867–876, 1994.

[61] O. Hoshuyama, A. Sugiyama, and A. Hirano, "A robust adaptive beamformer for microphone arrays with a blocking matrix using constrained adaptive filters," *IEEE Transactions on Signal Processing*, vol. 47, no. 10, pp. 2677–2684, 1999.

[62] K. Slavakis and I. Yamada, "Robust wideband beamforming by the hybrid steepest descent method," *IEEE Transactions on Signal Processing*, vol. 55, no. 9, pp. 4511–4522, 2007.

[63] V. Tourbabin, M. Agmon, B. Rafaely, and J. Tabrikian, "Optimal real-weighted beamforming with application to linear and spherical arrays," *IEEE Transactions on Audio, Speech, and Language Processing*, vol. 20, no. 9, pp. 2575–2585, 2012.

[64] S. Doclo and M. Moonen, "Design of broadband beamformers robust against gain and phase errors in the microphone array characteristics," *IEEE Transactions on Signal Processing*, vol. 51, no. 10, pp. 2511–2526, 2003.

[65] A. Kondoz and B. Evans, "A high quality voice coder with integrated echo canceller and voice activity detector for vsat systems," pp. 196–200, 1993.

[66] J. Ramírez, J. C. Segura, C. Benítez, A. De la Torre, and A. Rubio, "An effective subband osf-based vad with noise reduction for robust speech recognition," *IEEE Transactions on Speech and Audio Processing*, vol. 13, no. 6, pp. 1119–1129, 2005.

[67] H. Hai, Y. Hong-Tao, and F. Xiao-Lei, "A spit detection method using voice activity analysis," vol. 2, pp. 370–373, 2009.

[68] J. W. Shin, J. H. Chang, H. S. Yun, and N. S. Kim, "Voice activity detection based on generalized gamma distribution," *IEEE International Conference on Acoustics, Speech and Signal Processing 2005 (ICASSP'05.)*, vol. 1, pp. 1781–1784, 2005.

[69] Y. Suh and H. Kim, "Multiple acoustic model-based discriminative likelihood ratio weighting for voice activity detection." *IEEE Signal Processing Letters*, vol. 19, no. 8, pp. 507–510.

[70] D. Levi and S. Ullman, "Learning model complexity in an online environment," *IEEE Canadian Conference on Computer and Robot Vision 2009 (CRV'09.)*, pp. 260–267, 2009.

[71] R. Talmon, D. Kushnir, R. R. Coifman, I. Cohen, and S. Gannot, "Parametrization of linear systems using diffusion kernels," *IEEE Transactions on Signal Processing*, vol. 60, no. 3, pp. 1159–1173, 2012.

[72] J. S. Garofolo, *Getting started with the DARPA TIMIT CD-ROM: An acoustic-phonetic continous speech database.* National Institute of Standards and Technology (NIST), 1993.

[73] "Freesound database. available: http://www.freesound.org."

[74] T. Bäck, *Evolutionary algorithms in theory and practice: evolution strategies, evolutionary programming, genetic algorithms.* Oxford university press, 1996.

[75] Z. Li, K. F. C. Yiu, and Z. Feng, "A hybrid descent method with genetic algorithm for microphone array placement design," *Applied Soft Computing*, vol. 13, no. 3, pp. 1486–1490, 2013.

תכן וניתוח של מעצב אלומה קבועה בתדר

חיבור על מחקר

לשם מילוי חלקי של הדרישות לקבלת תואר מגיסטר למדעים

בהנדסת חשמל

אורן רוזן

הוגש לסנט הטכניון- מכון טכנולוגי לישראל

אדר ה'תשע"ו חיפה פברואר 2016

תודות

המחקר נעשה בהנחיית פרופ' ישראל כהן מהפקולטה להנדסת חשמל בטכניון.

ברצוני להביע את הערכתי לפרופסור ישראל כהן על ההנחיה, התמיכה וההדרכה במהלך עבודת המחקר.

ברצוני להודות גם לפרופסור דוד מלאך על עזרתו ותמיכתו בכתיבת עבודה זו.

לבסוף, ארצה גם להודות לאבי אבי ולאשתי נטלי, על תמיכתם וסבלנותם בכל שלבי עבודתי.

עבודה זו נכתבה לזכרה של אמי, אילנה רוזן ז"ל.

תקציר

שיטות עיצוב אלומה משמשות לשיפור יחס ההספק בין אות רצוי להספק אות המוגדר כהפרעה במגוון מערכות עיבוד אות ותקשורת כגון: מכ"מ, סונאר, עיבוד אותות רפואי, תקשורת, חישה סיסמית ועוד. אחד השימושים הקלאסיים לשיטות עיצוב אלומה, לדוגמה, הינו היכולת לבצע סינון מרחבי ובכך לגרום להעברת אותות מכיוונים רצויים ולהנחתת אותות והפרעות מכיוונים אחרים. נוסף על כך, שיטות עיצוב אלומה שימושיות אף לשערוך כיוון הגעת אות, ביטול הדהודים, איכון מקור ושימושים רבים נוספים.

תכנון קלאסי של אלגוריתמי עיצוב אלומה כדוגמה אלגוריתמי ה-Delay and Sum וה-MVDR, מניבים מוצא תלוי תדר ולכן שיטות אלה מומשו תחילה עבור אפליקציות צרות סרט. שימוש ישיר בשיטות אלו עבור אפליקציות רחבות סרט, כגון אותות דיבור ואותות רפואיים, גורם לעיוות של האותות כיוון ששבח העיבוד המרחבי (Spatial processing gain) תלוי אף הוא בתדר. לאור זאת, תכנון של מעצב אלומה רחב סרט בעל תגובה קבועה בתדר ישפר משמעותית את ביצועי המערכת. בפרט, תגובת מעצב אלומה רצויה עבור אפליקציות רחבות סרט תהיה רוחב אונה ראשית קבוע בתדר עבור תחום תדרים רחב, קרי, אותות מכיוונים רצויים יועברו באופן אחיד עבור תחום התדרים הרחב.

קיימות בספרות מספר שיטות תכן עבור מעצב אלומה קבועה בתדר. עבור חלק משיטות אלו, מתקבלת ירידה בביצועי המערכת בעיקר בהיבטי רמת אונות-צד, הנחתת הפרעות ורעשים וכן רגישות לשינויים בפרמטרי מערכת נוספים. בשיטות אחרות קיימת סיבוכיות חישוב גבוהה הגורמת לחוסר יכולת מימוש עבור מערכי מיקרופונים גדולים ועקב מגבלות חומרה. למרות קיומן של שיטות עיצוב אלומה המספקות ביצועי מערכת רובוסטיים, תכן מעצב אלומה קבועה בתדר בעל רגישות נמוכה לרעש ולשינויים בפרמטרי מערכת עודנו אתגר משמעותי.

עבודה זו מציגה שיטה חדשה לתכן מעצב אלומה קבועה בתדר. שיטה זו מבצעת שימוש במסנני תגובת הלם סופית (finite impulse response filter) במוצא מערך המיקרופונים אשר בעזרתם מבוצע עיצוב האלומה תחת קריטריון של רוחב אונה ראשית קבוע בתדר. הודות ליתרונות הגאומטריים ולתצורת מערך המיקרופונים, ניתן לעצב את תגובת התדר של המסננים ובכך לשלוט ברוחב האונה הראשית של תגובת המערך. השיטה שפותחה מספקת ביצועי מערכת משופרים תוך שמירה על סיבוכיות חישוב נמוכה בהשוואה לשיטות אחרות הקיימות בספרות. ניתן להיעזר בשיטה זו גם במערכות

הדורשות כיוונון אונה (beam steering) ראשית לכיוון רצוי, כגון מערכות תקשורת מתקדמות ומערכות עקיבה אחר דובר.

שיטה נוספת לשיפור ביצועי מעצב האלומה הינה שילוב מערכת גילוי דיבור. גילוי דיבור הינו תהליך לזיהוי קטעי דיבור וקטעי רעש. בגילוי דיבור נעשה שימוש נרחב ביישומים רבים בתחום עיבוד האותות כגון ביטול רעשים, זיהוי דיבור, קידוד דיבור ותקשורת. שיטות מוקדמות לגילוי דיבור תוכננו לעבודה במתאר בעל רעשי סביבה סטציונאריים, בעבודה זו מבוצע טיפול גם ברעשי סביבה טראנזיאנטים. רעשים טרנזיאנטים הינם הפרעות קצרות זמן ובעלות אנרגיה גבוהה כגון שיעול, הקשות מקלדת ודפיקות דלת. השיטות המוקדמות מזהות רעשים אלה כאותות דיבור ולא כהפרעה. הסיבה העיקרית לזיהוי השגוי עבור שיטות אלה הינה ההנחה כי הרעש משתנה לאט ביחס לאות הדיבור.

על מנת להתמודד עם בעיית הרעשים הטראנזיאנטים, פותח אלגוריתם לגילוי דיבור המבוסס על אשכול ספקטרלי (spectral clustering) ועל גרעיני דיפוזיה (diffusion kernels). האלגוריתם מבוסס על הורדת ממד הייצוג של האות באמצעות ווקטורי תכונה, אליהם אנו מתייחסים בתור ענן דגימות. לאחר מכן, נעשה שימוש בייצוג החדש בכדי לבנות מודל סטטיסטי לסימון כלל המידע כדיבור או כאי-דיבור באמצעות מודל תמהיל גאוסי (Gaussian Mixture Model). תוצאות הניסויים מראות כי קיים שיפור משמעותי בביצועי האלגוריתם המוצע ביחס לאלגוריתם עדכני במתאר רעש סביבתי. בשיטה זו ניתן לבצע שימוש במערכות תקשורת ועקיבה אחר דובר ואף לשפר את ביצועי מיקום הדובר. לדוגמה, ניתן לשפר את ביצועי צריכת האנרגיה של מערכות תקשורת על-ידי עיבוד מידע אך ורק כאשר התגלה דיבור.